Dark Cosmology Centre
Niels Bohr Institute
University of Copenhagen

A *Spitzer* study of γ-ray burst selected star-forming galaxies

Doctoral Dissertation

José María Castro Cerón

Supervisor: **Prof. Jens Hjorth**
Co-supervisor: **Dr. Darach Watson**
External Supervisor: **Dr. Javier Gorosabel**

Copenhagen, 21st April 2008

To my wonderful wife, Ana Lucía.

I –Hassan– the son of Muhammad the weigh-master, I –Jean-Léon de Médicis– circumcised at the hand of a barber and baptised at the hand of a pope, I am now called the African, but I am not from Africa, nor from Europe, nor from Arabia. I am also called the Granadan, the Fassi, the Zayyati, but I come from no country, from no city, no tribe. I am the son of the road, my country is the caravan, my life the most unexpected of voyages.

My wrists have experienced in turn the caresses of silk, the abuses of wool, the gold of princes and the chains of slaves. My fingers have parted a thousand veils, my lips have made a thousand virgins blush, and my eyes have seen the cities die and the empires perish.

From my mouth you will hear Arabic, Turkish, Castilian, Berber, Hebrew, Latin and vulgar Italian, because all tonges and all prayers belong to me. But I belong to none of them. I belong only to God and to the Earth, and it is to them that I will one day soon return.

...

When men's minds seem narrow to you, tell yourself that the land of God is broad, and broad His hands and His heart. Never hesitate to go far away, beyond all seas, beyond all frontiers, all countries, all beliefs.

taken from "Leo Africanus", a historical fiction novel by Amin Maalouf

Contents

Somewhat of a preface... **5**

Outline and important results 5

1 Introducing and contextualising **9**

1.1 Once upon a time... a bit of history 10

1.1.1 *Vela*, *Velar*, *Velando*... 10

1.1.2 The *Arthur Holly Compton Gamma Ray Observatory* . 16

1.1.3 The *Satellite per Astronomia X Beppo* 20

1.1.4 Contemporary spacecraft 24

1.2 What is all this about? The nature of long duration GRBs . . 26

1.3 Host galaxy studies 27

1.4 Other relevant types of galaxies 30

1.4.1 Lyman Break Galaxies 31

1.4.2 Lyman Alpha Emitters 32

1.4.3 Distant Red Galaxies 33

1.4.4 Submillimetre Galaxies 34

1.5 The *Spitzer* Space Telescope 35

2 Obscured star formation and dark GRBs **43**

2.1 Dark GRBS: an introduction 43

2.1.1 The fireball model... briefly 48

2.2 The dark GRB 001109 49

2.2.1 Searching for the afterglow 49

2.2.2 Classified as dark 53

3 *Spitzer* Data analysis: reduction, photometry, errors... **57**

3.1 Accessing the archives 57

3.2 Working with PostBCDs 59

3.3 Photometry 62

3.3.1 Aperture: GAIA 62

3.3.2 Image preparation: unit conversion 65

3.3.3 Background gradient 67

3.3.4 Doing aperture photometry 70

3.3.5 Negative flux backgrounds 73

3.4 Estimating photometric errors 74

3.4.1 Uncertainty maps 74

3.4.2 New method 74

3.5 Corollary 78

4 Low $M_\star$, high specific SFRs and dust extinction **79**

4.1 Data and samples 82

4.1.1 CC06 82

4.1.2 CC08 83

4.2 Methodology 84

4.2.1 CC06: spectral energy distribution fits 84
4.2.2 CC08: interpolations 89
4.3 Star formation rates 91
4.3.1 Calculations 91
4.3.2 Discussion 93
4.4 Total stellar masses 94
4.5 Intrinsic extinction 97
4.6 Specific star formation rate 98
4.7 Physical evolution 100
4.8 Addendum 102
4.9 Discussion 103

A Paper I **119**

B Paper II **129**

C Paper III **135**

Somewhat of a preface...

The work I present in this Dissertation has been carried out in partial fulfilment of the requirements for the degree of Doctor of Philosophy (specialising in Astrophysics) in the Faculty of Science of the University of Copenhagen. It was done at the Dark Cosmology Centre, Niels Bohr Institute, and supervised by Prof. Jens Hjorth, Dr. Darach Watson and Dr. Javier Gorosabel.

Outline and important results

The main topic of my Dissertation is the nature of the galaxies that host long duration Gamma Ray Bursts (GRBs; >2 s). GRBs are intense pulses of γ-rays from sources of cosmological origins. They were serendipitously discovered in 1967. A major leap forward came 30 years after when the first longer wavelength counterparts were detected in 1997. Since then GRB science has been in a rapid state of development. Long duration GRBs are well described by a canonical model that places them within star forming galaxies, and associates them with stellar, core collapse events. So the detection of a GRB is a clear indication that its host harbours massive star formation. How host galaxies relate to other known populations of star forming galaxies is the subject of an on going debate. Multiwavelength photometry can help establish this relation, essential if we are to understand the full range of properties of star forming galaxies at high redshifts and fully exploit the potential of GRBs as probes of cosmic star formation. My research makes a contribution towards this understanding.

The Dissertation is divided into four parts.

- Chapter 1 sets the tone with a brief review of the historical developments in the field of GRBs and provides additional background information for the topics covered later in the Dissertation.

- I look at the issue of obscured star formation and extinction in Chapter 2, preparing the stage for studying the properties of GRB host galaxies; Chapter 2 is based on the following paper:

  Paper I: J. M. Castro Cerón, J. Gorosabel, A. J. Castro-Tirado, et al. "On the constraining observations of the dark GRB 001109 and the properties of a $z = 0.398$ radio selected starburst galaxy contained in its error box" 2004, *A&A*, **424**, 833–839.

  After introducing dark GRBs, and an operational definition to classify them, I bring forward the most relevant aspects of my study of GRB 001109 in Paper I, showing that it is a truly dark GRB.

- I describe how I handled Spitzer GRB host data, photometry and error analysis, which make up the core of my technical work, in Chapter 3.

- Then I concern myself with deriving host galaxy properties in Chapter 4, chiefly from mid infrared photometry obtained with the Spitzer Space

Telescope, and support my results with a multiwavelength approach. Chapter 4 is based on the following two complementary papers:

Paper II: J. M. Castro Cerón, M. J. Michałowski, J. Hjorth, et al. "Star formation rates and stellar masses in $z \sim 1$ gamma ray burst hosts." 2006, *ApJ*, **653**, L85–L88.

Paper III: J. M. Castro Cerón, M. J. Michałowski, J. Hjorth, et al. "On the distribution of stellar masses in gamma ray burst host galaxies." 2008, *ApJ*, submitted (arXiv:0803.2235v1 [astro-ph]).

I address, in the above papers, some properties of a sample of GRB host galaxies: star formation rates (SFRs), total stellar masses ($M_\star$), intrinsic extinction and physical evolution. I find them to be low mass, star forming systems. I derive the unobscured SFRs for a sample of 6 GRB hosts in Paper II ($0.4\,M_\odot\,\mathrm{yr}^{-1} < \mathrm{SFR} < 428\,M_\odot\,\mathrm{yr}^{-1}$) and the obscured SFRs for a sample of 30 host galaxies in Paper III ($0.02\,M_\odot\,\mathrm{yr}^{-1} < \mathrm{SFR} < 10\,M_\odot\,\mathrm{yr}^{-1}$. The median $M_\star$ I find it to be $10^{9.7}\,M_\odot$ for both samples. When I compare them to other types of star forming galaxies (e.g. distant red galaxies, Lyman alpha emitters, Lyman break galaxies and submillimetre galaxies), the hosts of GRBs have some of the highest specific star formation rates. My results include the most accurate and robust SFR values in a small sample of GRB host galaxies to date and, for the first time, an accurate value of $M_\star$ in those galaxies.

- I conclude summarising the research I have presented, and discussing future prospects and my immediately upcoming projects to further this line of work.

Papers I-III are included, in their full original format, in Appendices A, B and C respectively. In writing each chapter of my Dissertation I aimed to underline the main results from each paper. My readers can then dwell in the details and nuances by reading the appendices.

Chapter 1

Introducing and contextualising

My Dissertation verses about the host galaxies of Gamma Ray Bursts (GRBs). The nuclear part of my work is the derivation of the host properties, chiefly from mid infrared (MIR) data obtained from observations with the *Spitzer* Space Telescope (Werner et al. 2004). In addition I utilise a multiwavelength (including optical, near-infrared, submillimetre and radio data) approach to support my results. The work presented here is based on three papers, namely: Castro Cerón et al. (2004), Castro Cerón et al. (2006) and Castro Cerón et al. (2008). For practical purposes and reasons of brevity, throughout the manuscript, paper one will be referred to as CC04, paper two will be referred to as CC06 and paper three will be referred to as CC08. But before I delve in my humble contributions to the field I will introduce it here. A thorough analysis of all the aspects of the science of GRBs is well beyond my goals and the scope of this Dissertation. Instead I will provide some basic background and the references for the interested reader to pursue a broader treatment.

1.1 Once upon a time... a bit of history

A Long Time Ago in a Galaxy Far, Far Away... I am sure all my readers have encountered these words before. And that is really how our story begins. The time is now going on 41 years; that is longer than most of us have lived, so it was long ago. The galaxy is the host of GRB 670702, the first GRB positively detected by humankind. We don't know how far it is, but it is presumedly safe to think of it as far, far away. It used to be that virtually all papers on the subject of GRBs started their introductions stating something along the lines of: *GRBs are one of the most mysterious phenomena in the Universe*. The past decade has been comprised of many breakthrough years so astronomers no longer feel that GRBs are utter mysteries (though we still have lots to learn). But it was that way for 30 years due to the lack of key observational data. Now back to GRB 670702; it was detected by the *Vela* spacecraft (Terrell 1989).

1.1.1 *Vela*, *Velar*, *Velando*...

These were the days of the Cold War, of the good and the bad guys. So the good guys built a gadget to watch over the bad guys. This was a series of satellites named *Vela* (Figures 1.1 and 1.2). The word can be loosely translated from Spanish as *watch* or *watchman* (Real Academia Española 2001). The all too often cited translation *to watch* is incorrect because all verbs in Spanish end in either -*ar*, -*er* or -*ir*. *Vela* was a three tier project in the United States to monitor compliance with the 1963 Treaty Banning Nuclear Weapon Tests in the Atmosphere, in Outer Space and Under Wa-

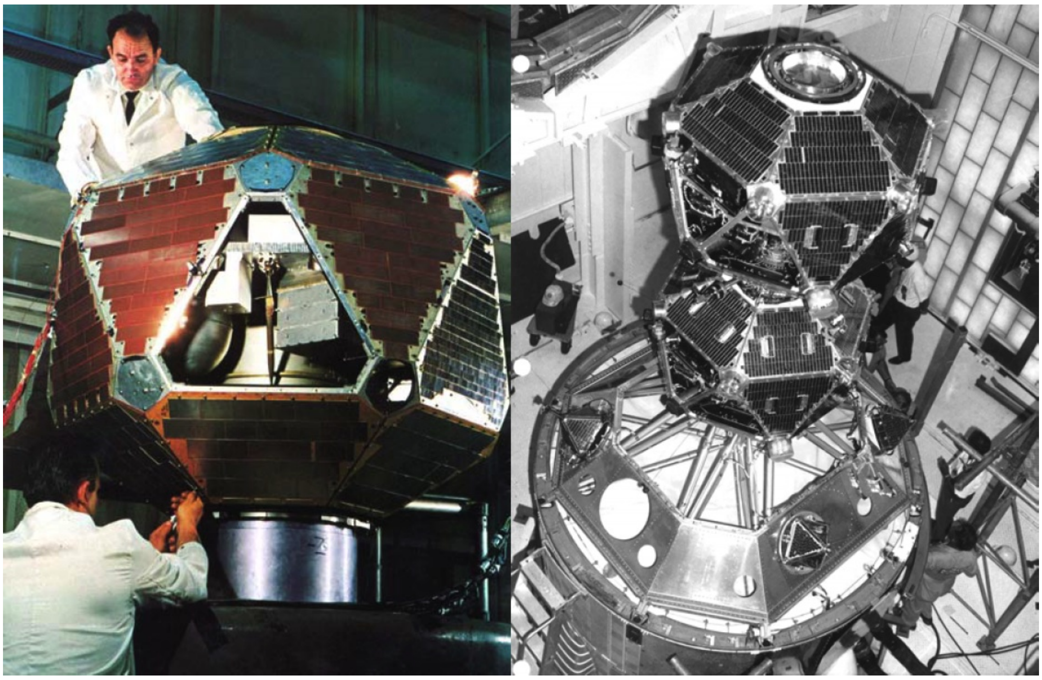

Figure 1.1: The first space system to accomplish nuclear surveillance was called *Vela-Hotel* –later, simply *Vela*. Its primary purpose was to monitor compliance with the Partial (a.k.a. Limited) Nuclear Test Ban Treaty then being negotiated in Geneva. The first pair of satellites was launched using an *Atlas Agena* on 16 October 1963, a few days after the Nuclear Test Ban Treaty went into effect, and two more pairs were launched on 16 July 1964 and 17 July 1965. Six Advanced *Vela* satellites, containing additional, more sophisticated detectors, were launched in pairs on *Titan IIIC* vehicles on 28 April 1967, 23 May 1969, and 8 April 1970. The *Vela* spacecraft successfully monitored compliance with the Nuclear Test Ban Treaty and provided scientific data on natural sources of space radiation for many years. The last of the advanced *Vela* satellites was deliberately turned off on 27 September 1984, over fifteen years after it had been launched. **Left:** A *Vela* satellite in fabrication at TRW's facility. **Right:** A pair of *Vela* satellites (*Vela 5A* and *5B*) mounted on their *Titan IIIC* launch vehicle before installation of the fairing. (*Photo: document AFD-060912-025; USAF's Space and Missile Systems Center Office of Public Affairs.*)

ter. The Treaty prohibited all test detonations of nuclear weapons except underground. It was developed both to slow the arms race (nuclear testing

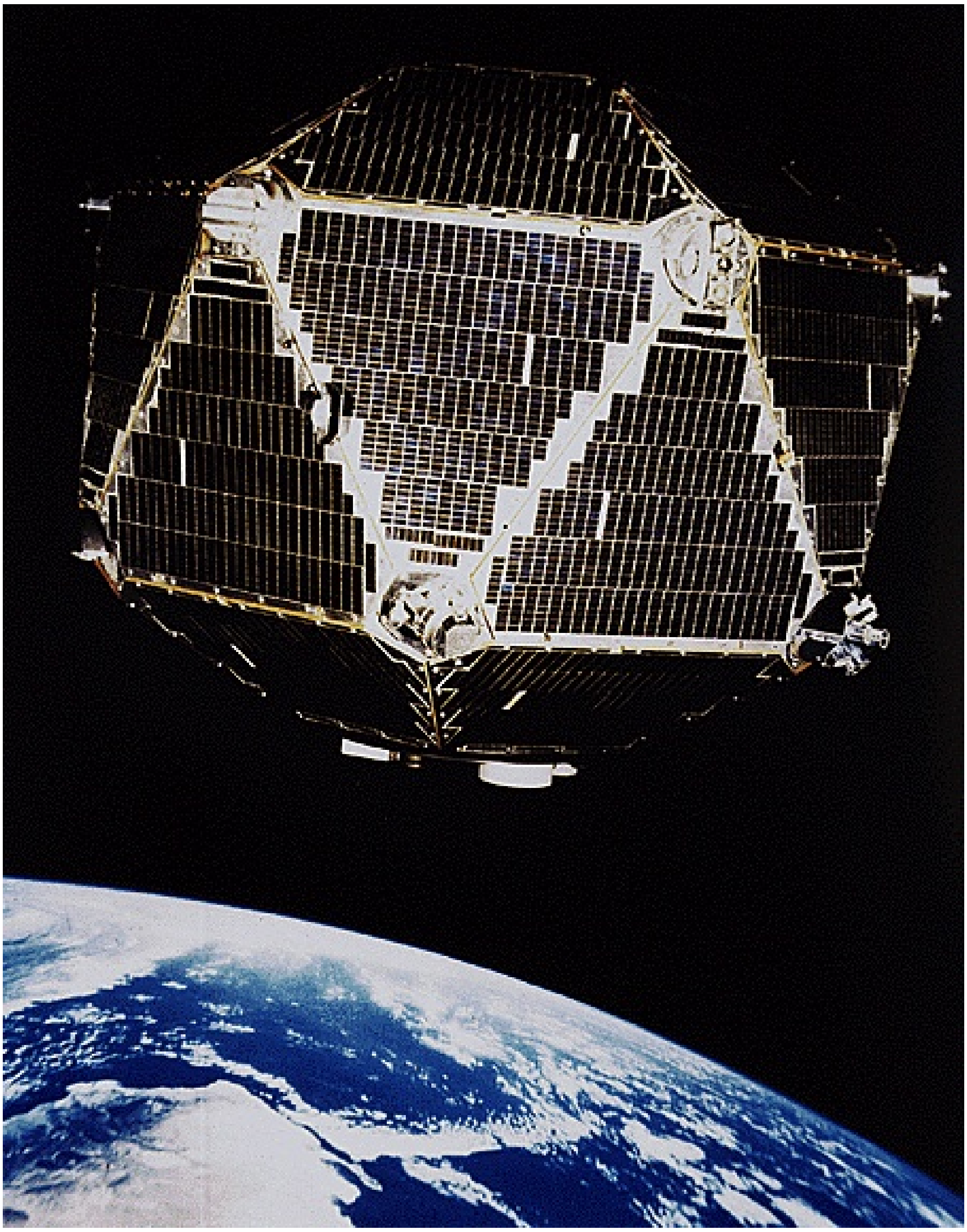

Figure 1.2: The *Vela-5B* satellite in low earth orbit. Astronomical γ-ray sources have to be detected via space-born (i.e. satellites) or air-born (i.e. high altitude ballons) instrumentation because the atmosphere is opaque to such radiation (except for TeV γ-rays, which can be detected from the ground with the Čerenkov technique). The *Vela* spacecraft made the first detections of a GRB. (*Photo: NASA's High Energy Astrophysics Science Archive Research Centre.*)

is necessary for continued nuclear weapon advancements) and to stop the excessive release of nuclear fallout into the Earth's atmosphere. The development work for *Vela* was primarily performed by the Advanced Research Projects Agency and was overseen by the Air Force (USAF). *Vela* was the most cost-efficient USAF space project and it became a model of good management, good design, and good cooperation in military space programs (Waldron 1997). It also gave birth, in a classic example of scientific serendipity, to a fascinating field in Astrophysics: GRBs.

It all started Sunday 2 July 1967, UT 14 h 19 min. *Vela 4A* and *Vela 4B* detected, simultaneously, the same event. No one noticed initially simply because no one was looking. Since 1965, with the construction and launch of the *Vela 3* satellites, Ray W. Klebesadel of Los Álamos Scientific Laboratory (now Los Álamos National Laboratory) had assumed the continuing programatic responsibility for the X-ray and γ-ray instruments. He saw to it that events which triggered the detectors but were clearly not signatures of nuclear detonations were carefully filed away for future study. In 1969, while looking back over *Vela 4* data just prior to the launch of *Vela 5*, Klebesadel and his colleague Roy A. Olson found the event recorded by *Vela 4A* and *Vela 4B* on 2 July 1967, which also triggered the still operational *Vela 3* satellites. The event appeared to be a cosmic γ-ray burst but at the time the constellation of satellites did not have sufficient timing resolution at the trigger to make a good determination of direction to the burst source. In retrospect, this event had a time history (Figure 1.3) similar in appearance to the later recognised cosmic bursts (Klebesadel et al. 1973; Strong et al. 1974). Klebesadel believes that this event represents the *first observed GRB*:

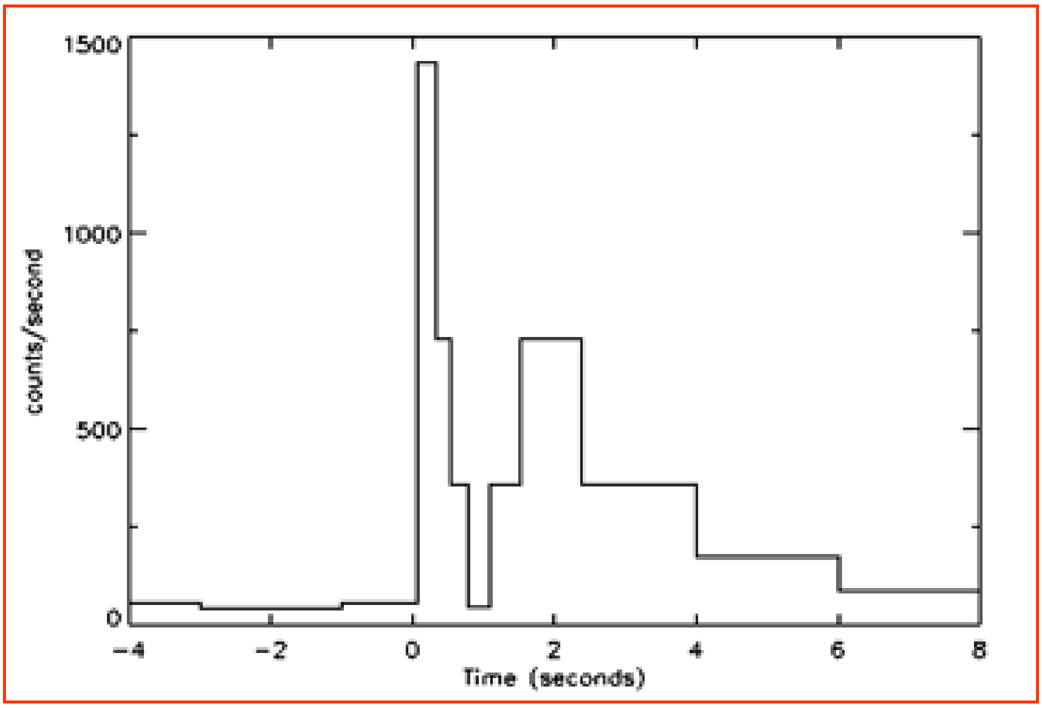

Figure 1.3: The light curve of GRB 670702, the first GRB ever detected. It exhibited a double peaked signal and lasted 6 s. A solar origin could not be completely ruled out, so GRB 670702 was not included in the discovery paper (Klebesadel et al. 1973), but it is part of the preliminary catalogue in Strong et al. (1974) and recognised now as the first GRB detected. Later on Strong & Klebesadel (1976) used the *Vela 4A* and *4B* data to construct a time history of this event. (*Adapted from Strong & Klebesadel 1976.*)

GRB 670702. In 1972, Ian B. Strong, also at Los Álamos, was asked to look at Klebesadel's files of *Vela* γ-ray events. With the timing accuracy of the later *Vela* satellites Klebesadel and Strong, along with Olson, were able to deduce the directions to the events with sufficient accuracy to rule out the Sun and Earth as sources. They concluded that the γ-ray events were *of cosmic origin*. In 1973, this discovery was announced (Klebesadel et al. 1973). Their paper discusses 16 cosmic GRBs observed by *Vela 5A*, *5B* and *Vela 6A*, *6B* between July 1969 and July 1972. Confirmation of the new phenomena from other spacecraft came forward quickly. These confirming results, published close on the heels of the original discovery, gave the whole scenario an aura of enhanced mystery. The excitement created in the astronomical Community was evidenced by a burst of publications of instrumental and theoretical papers on the newly discovered GRBs.

Contrary to popular belief, the claim that the unusual delay in publishing the first GRB results was due to military security issues is an urban myth. *Vela* data, that clearly contained no signatures of nuclear detonations, were routinely declassified in a relatively short time. This is obvious by the steady flow of papers published on other *Vela* data prior to 1973 (e.g. search ADS for *Vela satellite*). They waited so long to reveal their GRB findings because the Los Álamos scientists, who had never thought of themselves as astronomers (their leader Ray W. Klebesadel was trained as an electrical engineer), wanted to be sure that the flashes of γ-rays were coming from somewhere in space.

The *Dark Ages* of GRB Science followed. By 1990 a few hundred GRBs had been detected by a variety of high altitude balloon experiments and an array of spacecraft, including *Apollo 16*, *Helios 2*, *HEAO-1*, *International Sun Earth Explorer 3*, *Orbiting Geophysical Observatory 3* and *5*, *Orbiting Solar Observatory 6–8*, *Prognoz 6–7*, *Pioneer Venus Orbiter* (1978-1992), *Konus* and *SIGNE* on *Venera 11–12* and *Wind*, *Transient Gamma-ray Spectrometer* on *Wind*, *SIGNE 3*, *Solar Maximum Mission* (1980–1989), *Solrad 11 AB*, *MIR Space Station*, *GINGA*, *WATCH* and *SIGMA* on *GRANAT* and *EURECA*, and *Ulysses*. Performance slowly improved over time but the nature of GRBs remained almost as obscured as in the early 1970's. The enormous size of the localisation error boxes (i.e. which varied, depending on the spacecraft, from few degrees to many arcminutes) and/or the time delay to distribute them (i.e. from many days to weeks, or even months) precluded the securement of any key observational data. Meanwhile theorists were going rampant, prompting Robert J. Nemiroff to say in 1994: *Is speculation in this area becoming valueless?* (Nemiroff 1994).

1.1.2 The *Arthur Holly Compton Gamma Ray Observatory*

The launch of the *Arthur Holly Compton Gamma Ray Observatory* (*CGRO*; Figure 1.4), one of NASA's *Great Observatories*, brought online BATSE (the Burst and Transient Source Experiment; Fishman 1981), which would trigger real progress. BATSE was an all sky γ-ray monitor that would detect and localise hundreds of GRBs per year. In 1991 the general expectation of the GRB Community was that bursts would follow a distribution on the sky with a concentration towards the disk of the galaxy, similar to the already detected neutron stars which were thought to be the progenitors. Previous experiments had hinted otherwise, but the sensitivity of the earlier detectors was all too low to be able to capture the edges of any possible distribution (i.e. only the nearest GRBs would have been seen). It was believed that BATSE would be sensitive enough to show the distribution of GRBs along the Milky Way and thus close the ongoing debate on the distance scale. But right from the first observations BATSE stubbornly indicated that GRBs were isotropically distributed, even the faintest ones (Figure 1.5). This came as a shock to the vast majority of the Community.

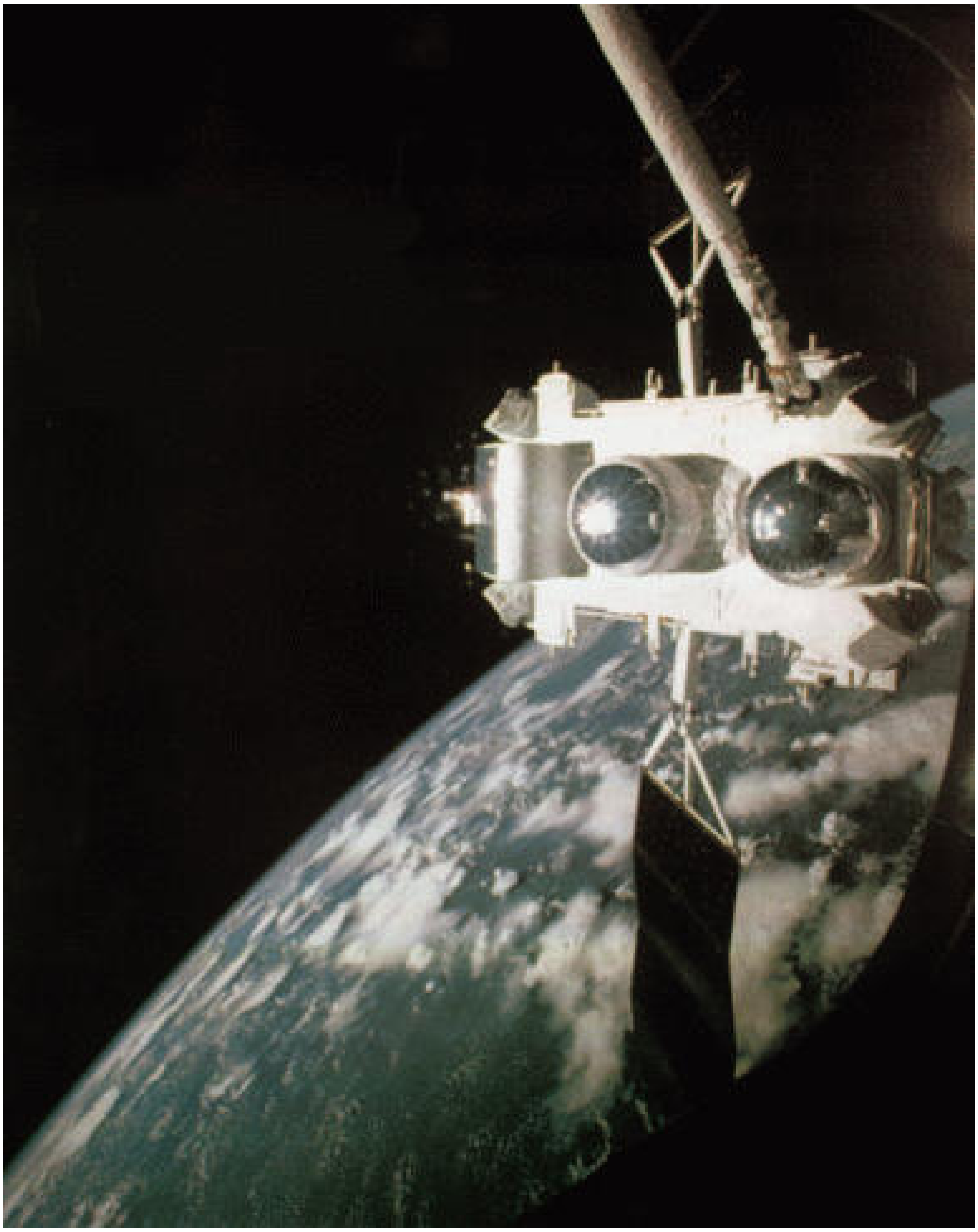

Figure 1.4: NASA's *CGRO*, the heaviest ever scientific satellite, was launched on 5 April 1991 by the *Atlantis* space shuttle. On board it carried the eight BATSE modules. In nine years of operations BATSE contributed significantly to change our understanding of GRBs. (*Photo: the Gamma Ray Astronomy Team Home Page at NASA's Marshall Space Flight Centre.*)

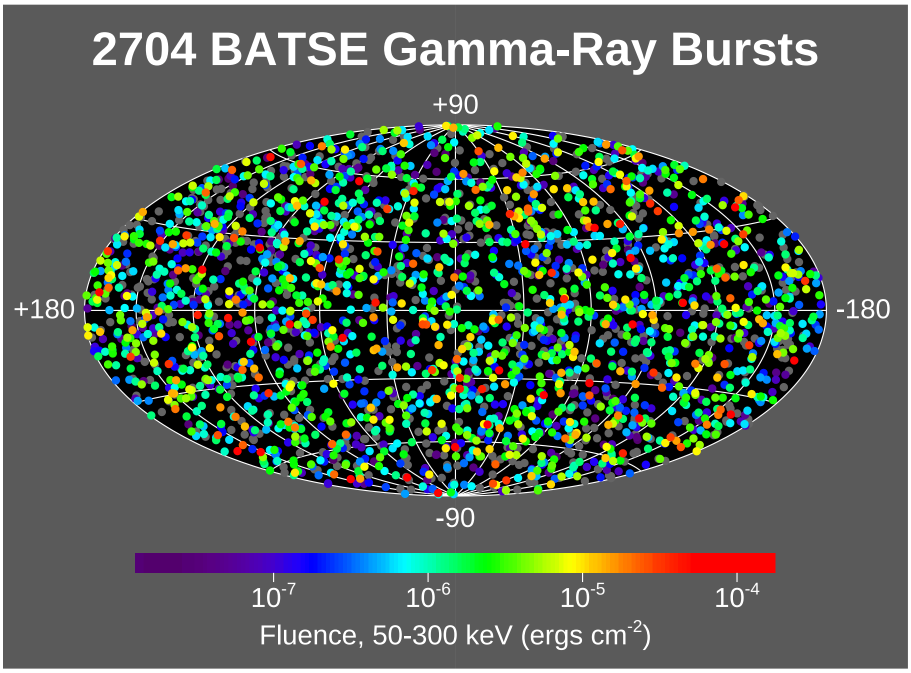

Figure 1.5: This map shows the localisation of a total of 2 704 GRBs recorded with the BATSE on board NASA's *CGRO* during its nine year mission. The projection is in Galactic coordinates; the plane of the Milky Way Galaxy is along the horizontal line at the middle of the figure. The burst locations are colour coded based on the fluence, which is the energy flux of the burst integrated over the total duration of the event. Long duration, bright bursts appear in red, and short duration, weak bursts appear in purple. Grey is used for bursts for which the fluence cannot be calculated due to incomplete data. (*Photo: the Gamma Ray Astronomy Team Home Page at NASA's Marshall Space Flight Centre.*)

The isotropy of the GRB distribution was now firmly established, but the issue of the distance scale remained. After all GRBs could be spherically distributed about the Galactic halo. BATSE yielded another surprise. The expected faint GRBs were absent or observed much more infrequently than predicted. The distribution of the sources was not homogeneous as derived from a $logN - logS$ diagram. Rather, a deficiency of weak events was present and the distribution deviated from the -3/2 slope of a the straight line for a uniform distribution in Euclidean space (Meegan et al. 1992). Again these results had been hinted by earlier experiments and BATSE made them unquestionable. The deficiency of faint bursts could be explained if they were cosmological and so the balance was tilted towards cosmological distances. Though a consensus in the Community was gaining momentum, nonetheless sources in the Galactic halo could not be completely ruled out.

Robert J. Nemiroff thought that the discussion on the distance scale of GRBs was reminiscence of the Great Debate of 1920 between Herbert Curtis and Harlow Shapley about the distance scale of the Universe. And so he organised, in the same auditorium and 75 years later, a similar debate: Don Lamb for the local origin vs. Bohdan Paczyński for the cosmological theory (Rees 1995).

Right from the beginning GRBs exhibited wide diversity: their light curves can range from smooth, fast rise and quasi exponential decay, to variable, multipeaked curves; the pulses of γ-emission can be rather complex. This motto summarises GRBs well: *When you've seen one GRB, you've seen... one GRB*. So one of the most relevant early results from BATSE was to establish a phenomenological division. Kouveliotou et al. (1993) showed the likely existence of two distinct populations. Their analysis of BATSE data suggested a bimodality in the duration of GRBs, with a clear minimum at 2 s: short duration ($t < 2$ s), hard spectrum bursts and long duration ($t > 2$ s), soft spectrum bursts. Once more we have here a case hinted at the beginning of GRB history and confirmed by BATSE. It seems appropriate at

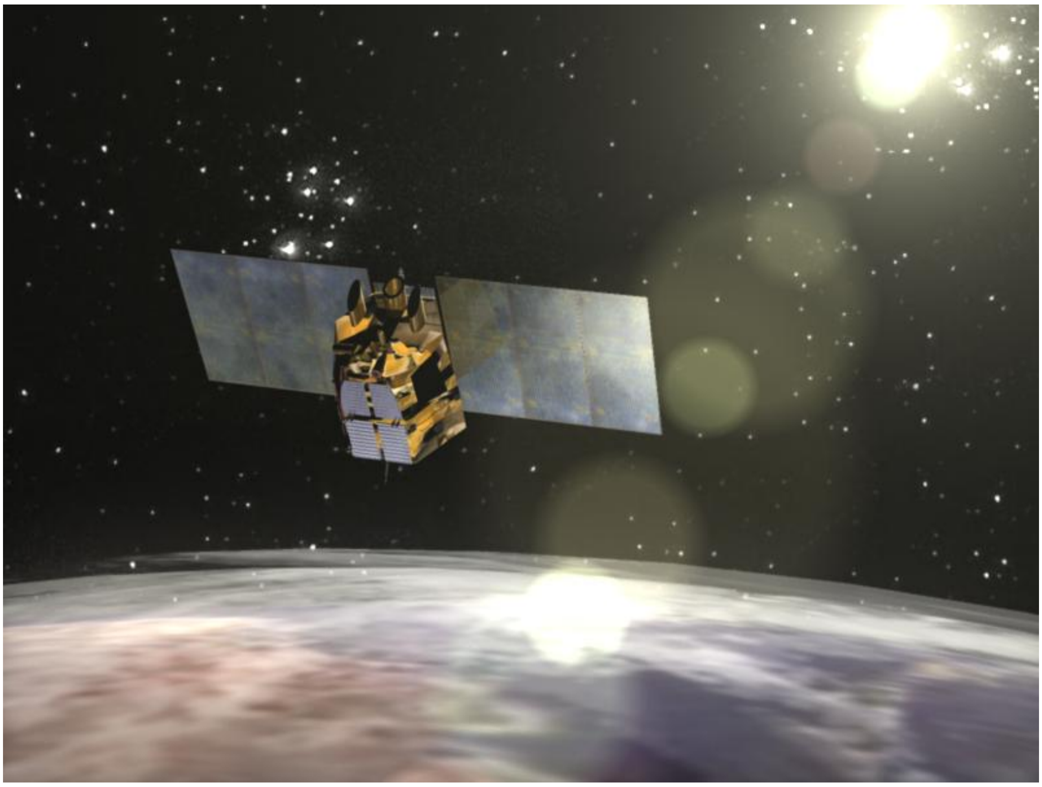

Figure 1.6: *Beppo*SAX (in honor of Italian physicist Giuseppe Occhialini, 1907–1993) was a project of the *Agenzia Spaziale Italiana* with participation of the *Nederlands Instituut voor Vliegtuigontwikkeling en Ruimtevaart*. In 1997 it revolutionised the science of GRBs by detecting the first counterpart at longer wavelengths (i.e. X-rays), which allowed for a precise localisation and was a leap forward in studying the so far elusive phenomena. (*Photo: ACS Studio.*)

this point to highlight for my readers that all the work in this Dissertation pertains only to long duration bursts.

1.1.3 The *Satellite per Astronomia X Beppo*

In 1997 a leap forward came through. The Italian-Dutch *Satellite per Astronomia X* (*Beppo*SAX, Figure 1.6; Boella et al. 1997) revolutionised our understanding of GRBs by localising them promptly and accurately on the sky, though GRBs were not its primary science goal. The main characteristic of the *Beppo*SAX mission was the wide spectral coverage, ranging from 0.1 up to 600 keV. On board it carried the Gamma Ray Burst Monitor (GRBM; 60–600 keV) and two Wide Field Cameras (WFC, 2–30 keV; Jager et al. 1997). If a burst fell serendipitously in the field of a WFC *Beppo*SAX could detect the gamma event and localise any X-ray counterpart to an uncertainty of about $5'$. These longer wavelength counterparts had been claimed to exist following few detections (e.g. first one was by *GRANAT* for GRB 920723 Terekhov et al. 1995), but speed and precision were paramount for any follow up campaign to be successful. And success was achieved 28 February 1997: GRB 970228. The Italian scientists responsible for the GRBM onboard the satellite (E. Costa, *Consiglio Nazionale delle Ricerche*, and F. Frontera, *Università degli Studi di Ferrara*), in conjunction with the Mission Scientist (L. Piro, *Consiglio Nazionale delle Ricerche*) and the Mission Director (R. C. Butler, *Agenzia Spaziale Italiana*), were able to reschedule the satellite observations and point the *Beppo*SAX narrow field X-ray telescopes (NFI) in only 8 hours at the GRB. In consequence a X-ray source never before seen was discovered and localised with an accuracy of one hundreth of a degree. The source was actually in the constellation of Orion. A second follow up was performed with the NFI after about 2 days. This second observation showed a strong drop, about 20 times lower, in the source flux (Figure 1.7; Costa et al. 1997).

I believe it is important to point out the following. Nowadays we are quite spoiled by *Swift* (see §1.1.4). An 8 hour turn around seems an eternity. But my readers need to understand the boldness of the decision to repoint a satellite with such a short time notice back in 1997. It can only be explained

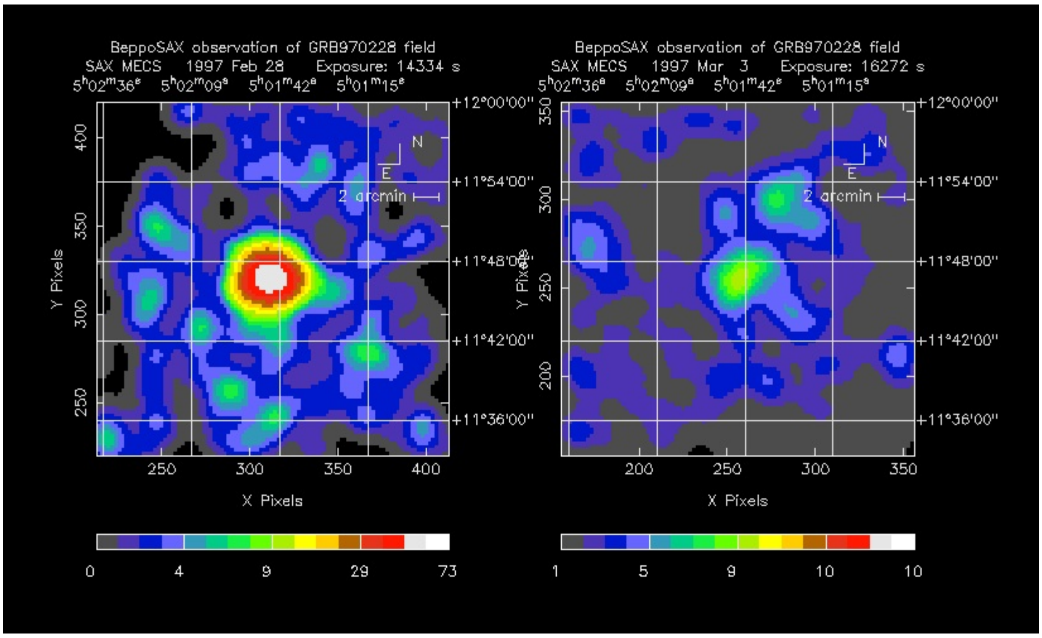

Figure 1.7: The X-ray counterpart of GRB 970228. These are false colour images of the source 1SAXJ0501.7+1146, detected in the error box of GRB 970228 with *Beppo*SAX's Medium Energy Concentrator Spectrometre (2-10 keV). White corresponds to 31 counts pixel^{-2}, green corresponds to 6 counts pixel^{-2} and grey to a background of 0?1 counts pixel^{-2}. The source faded by a factor of $\sim$20 in 3 days. From the ASCA faint sources data (Georgantopoulos et al. 1997), the probability that the source detected during the second pointing is coincident by chance with the position of 1SAXJ0501.7+1146 is of the order of 10^{-3}. **Left:** First pointing of the narrow field X-ray telescopes, 8 hours after the onset of the burst. **Right:** Second pointing of the narrow field X-ray telescopes, after about 2 days. (*Adapted from Costa et al. 1997.*)

because in those early days everyone was extremely excited about a potential breakthrough. Those were the days when the whole *Beppo*SAX Team would rush in the middle of the night, almost in pyjamas, to Telespazio's Control Centre to look at the data and discuss the best course of action (E. Costa, priv. comm.).

Following the prompt and accurate localisation of a X-ray counterpart,

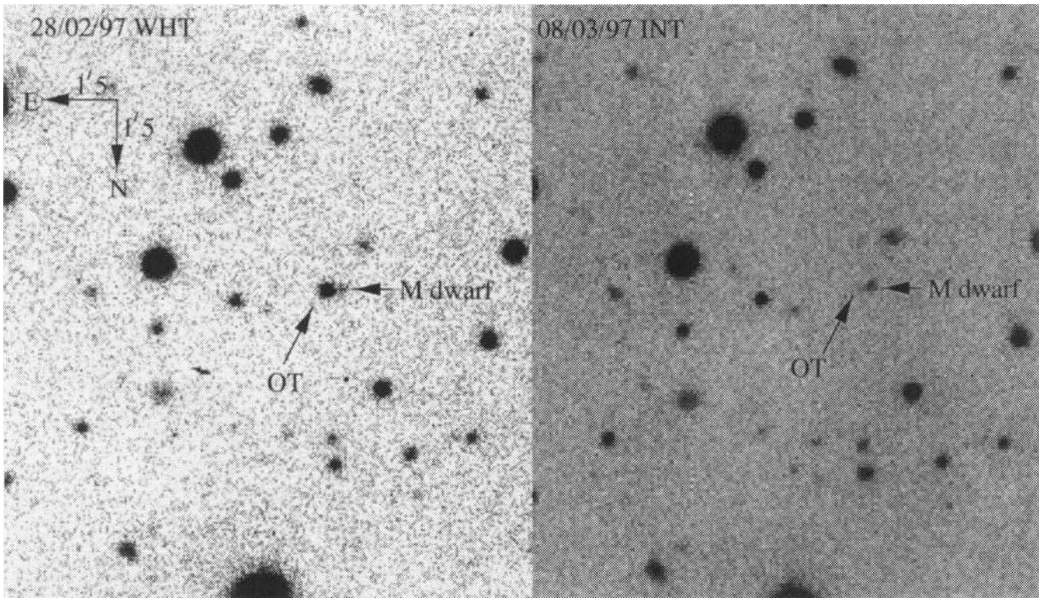

Figure 1.8: The rapid and accurate localisation of GRB 970228's X-ray counterpart by *Beppo*SAX allowed for the first identification of an optical counterpart. These are V band images of a $1.5' \times 1.5'$ region of the sky containing the position of the optical transient, marked by OT. The M dwarf, separated from the optical transient by $2.9''$, is also indicated. **Left:** Image obtained with the WHT (La Palma, Spain) on 28 February 1997, UT 23 h 48 min. **Right:** Image obtained with the INT (La Palma, Spain) on 8 March 1997, UT 20 h 42 min. (*Adapted from van Paradijs et al. 1997.*)

the much sough after optical counterpart was immediately nailed down (Figure 1.8; Groot et al. 1997b; van Paradijs et al. 1997). As the optical counterpart faded away an underlying extended object was discovered: the host galaxy that would be sheltering the burst at a cosmological distance (Groot et al. 1997a). A radio afterglow was first detected by Frail et al. (1997) for GRB 970508 using the Very Large Array. The first millimetre band counterpart came from Bremer et al. (1998) at the Plateau de Bure Interferometre, also for this burst. The issue of the distance scale was finally settled when Metzger et al. (1997) measured a redshift of 0.835 for GRB 970508. A 30 year old argument, which had prompted so much discussion, was finally settled thanks to *Beppo*SAX.

One more important contribution from *Beppo*SAX was the discovery of transient sources detected by the WFCs but not the GRBM. Similar to long duration GRBs, they have a softer spectrum and were dubbed X-Ray Flashes (XRF; Heise et al. 2001). Sakamoto et al. (2005) expanded the definition to include X-Ray Rich burts (XRR). Though their empirical definitions differ, they seem to form a continuous distribution with bursts varying smoothly from XRFs to XRRs to GRBs. *Beppo*SAX opened an era of vertiginously fast research with a wealth of exciting breakthroughs.

1.1.4 Contemporary spacecraft

Further fast accurate positions, provided by IPN (Hurley & Cline 2004), *RXTE* (Swank 1999), *HETE-2* (Ricker et al. 2003), *INTEGRAL* (Winkler et al. 2003) and specially *Swift* (Gehrels et al. 2004), with its improved sensitivity, speed and accuracy, have lead to many more identifications of GRB afterglows at longer wavelengths. Various robotic telescopes have played an important role in securing very early time optical/near infrared (NIR) observations. A wealth of data has paved the road to many mind boggling discoveries.

Among those I should highlight the discovery of the GRB/supernova connection (SNe, Figure 1.9; Galama et al. 1998; Hjorth et al. 2003; Stanek et al. 2003), the detection of the optical counterparts for short GRBs and their redshift measurements (Hjorth et al. 2005a; Fox et al. 2005; Gehrels et al. 2005;

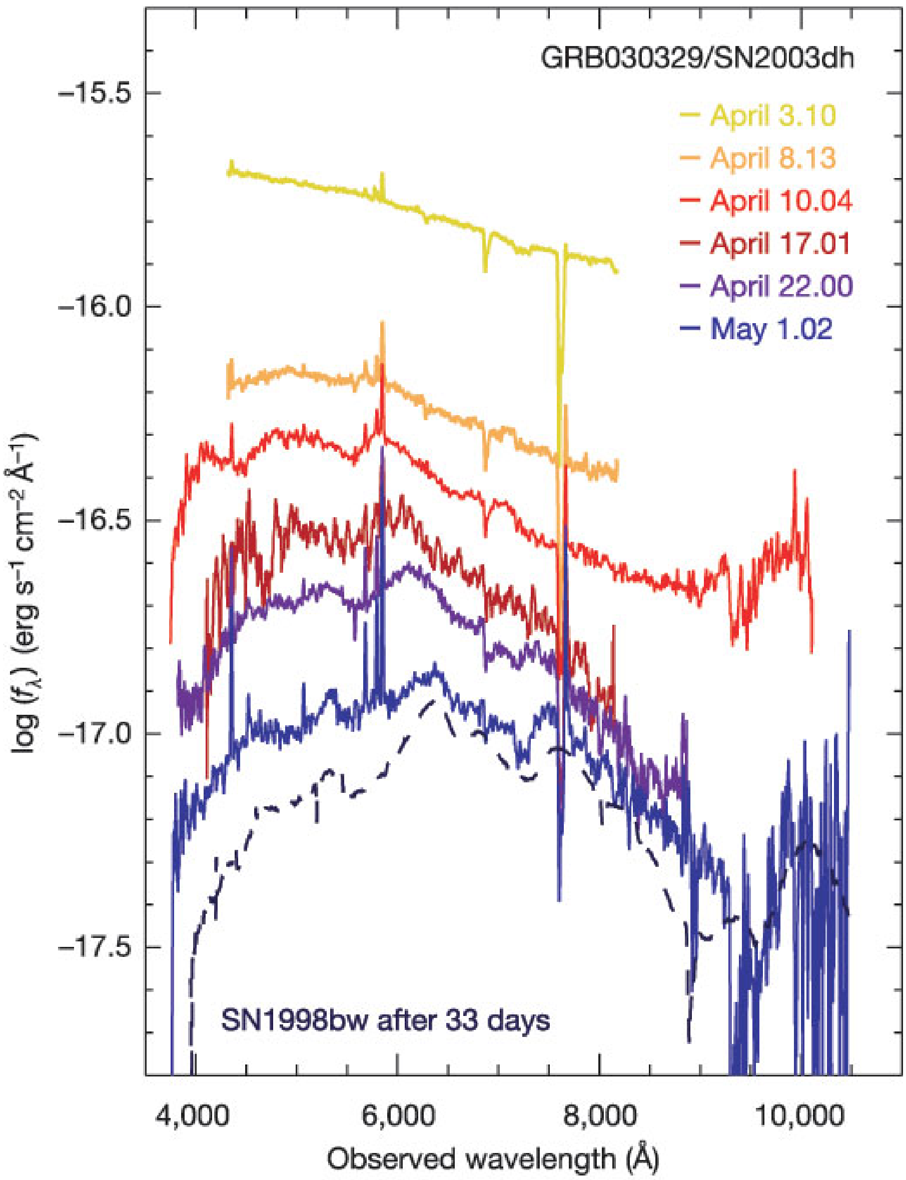

Figure 1.9: Spectral evolution of the combined optical flux density of the afterglow of GRB 030329, the associated SN 2003dh and its host galaxy. The upper spectrum is fitted by a power law, as commonly seen in afterglow spectra. The middle spectra show deviations from a power law, similar to SN 1998bw at the same phase. The lower spectra, dominated by SN 2003dh, reveal the supernova signatures. For comparison, the spectrum of SN 1998bw after 33 days is shown (dashed line) shifted to the GRB 030329 redshift. All SN 2003dh spectra are presented in observed wavelengths and no reddening correction was applied. The host galaxy is an actively star forming, low metallicity, dwarf galaxy, qualitatively very similar to the host galaxy of GRB 980425/SN 1998bw. (*Adapted from Hjorth et al. 2003.*)

Villasenor et al. 2005; Hjorth et al. 2005b; Berger et al. 2005; Gehrels & Swift Team 2005) and the recent discovery of two long duration GRBs without an associated SN (Fynbo et al. 2006; Gehrels et al. 2006; Della Valle et al. 2006; Gal-Yam et al. 2006). As of the writing of this Dissertation, a bright X-ray transient has been discovered, followed by a type Ibc SN (2008D). It suggests that a large population of bursts, currently below the detection threshold of wide field instruments, might exist (Soderberg et al. 2008).

1.2 What is all this about? The nature of long duration GRBs

Because my Dissertation work deals exclusively with long duration GRBs it seems sensible that I give here a very brief description of the physics behind them. GRBs are pulses of γ-rays from sources of cosmological origins, and are the most luminous, photon emitting events in the Universe. From an observer's point of view they are brief ($2\,\mathrm{s} \lesssim t \lesssim 10^2\,\mathrm{s}$) and very intense flashes of high energy photons ($10\,\mathrm{keV} \lesssim E \lesssim 1\,\mathrm{MeV}$) occurring at a rate of a few each day throughout the Universe. For few seconds they outshine the entire Universe in γ-rays, then they completely disappear. The afterglow that follows the burst can be observed at all wavelengths, from X-rays to radio, and lasts longer time scales (i.e. days, up to months or even years in the radio bands). A canonical model is well established for long duration GRBs: they occur in star forming regions in star forming galaxies (Bloom et al. 2002; Gorosabel et al. 2003; Christensen et al. 2004; Fruchter et al.

2006) and are associated with stellar core collapse events and hence with high mass star formation (e.g. Galama et al. 1998; Hjorth et al. 2003; Stanek et al. 2003; Zeh et al. 2004; Campana et al. 2006).

The confirmation that GRBs occur at cosmological distances had the effect of wiping out from the burst scenery most models (Nemiroff 1994). Though there are still numerous alternative models in existence, there is a standard theoretical framework named the fireball model. The details are not relevant to this Dissertation but my readers can learn more from Mészáros & Rees (1997); Sari et al. (1998). In addition there are very nice reviews by Piran (1999); van Paradijs et al. (2000); Mészáros (2002); Zhang & Mészáros (2004).

1.3 Host galaxy studies

It is central to contemporary cosmology to map the build up of cosmic structure and star formation; and we know that the detection of a GRB is an indication that its host galaxy harbors massive star formation. As tracers of star formation GRBs have fundamental advantages: dust extinction has essentially no effect in their detection at γ-ray and X-ray wavelengths; GRBs can be observed to very high redshifts; these redshifts can be measured from afterglow spectroscopy independently of the host magnitudes; and the selection of GRBs is independent of the host galaxy luminosity at any wavelength. Moreover, because GRBs fade quickly after their onset they do not have long term effects in their neighbourhood as opposed, for example, to QSOs, whose continuous luminous emission makes them a significant source of ionisation.

That is to say that GRBs are unique eyes to gainfully look at the star forming Universe. But the following critical questions should be answered in order to use GRBs as tracers of star formation: What is the level of bias in optically selected GRB host samples? And what is the intrinsic bias in the GRB star formation rate?

The study of the host galaxies became possible only after GRB localisations reached a precision of a few arcseconds (i.e. after *Beppo*SAX). Of the highest interest is that the selection mechanism of GRB hosts is not flux limited, unlike other techniques to select galaxies at high redshifts. Such techniques involve the use of deep optical and near-infrared imaging to select systems based on spectral features such as breaks o line emission, X-ray emission, submillimeter emission, or through spectroscopic and photometric redshift surveys. These techniques are all strongly biased. For instance, Lyman break selection (see §1.4.1) is continuum flux limited (Shapley et al. 2003), while Lyman alpha selection (see §1.4.2) is line flux limited (Fynbo et al. 2003). Submillimetre selection (see §1.4.4) is, in turn, severely limited by the sensitivity of current detectors (Blain et al. 2002). So the samples based in those selection techniques are possibly missing substantial populations of galaxies at high redshifts, while GRB selected galaxies can probe the faint end of the luminosity function not yet accessible to other techniques.

In practically all cases in which *Hubble Space Telescope* (HST) observed a GRB field a host galaxy has been detected at the position of the early afterglow. Most GRB host galaxies are faint and blue (Fruchter et al. 1999; Le Floc'h et al. 2003). The morphological distribution of GRB hosts includes all galaxy types (Figure 1.10) with a high fraction of hosts showing irregular

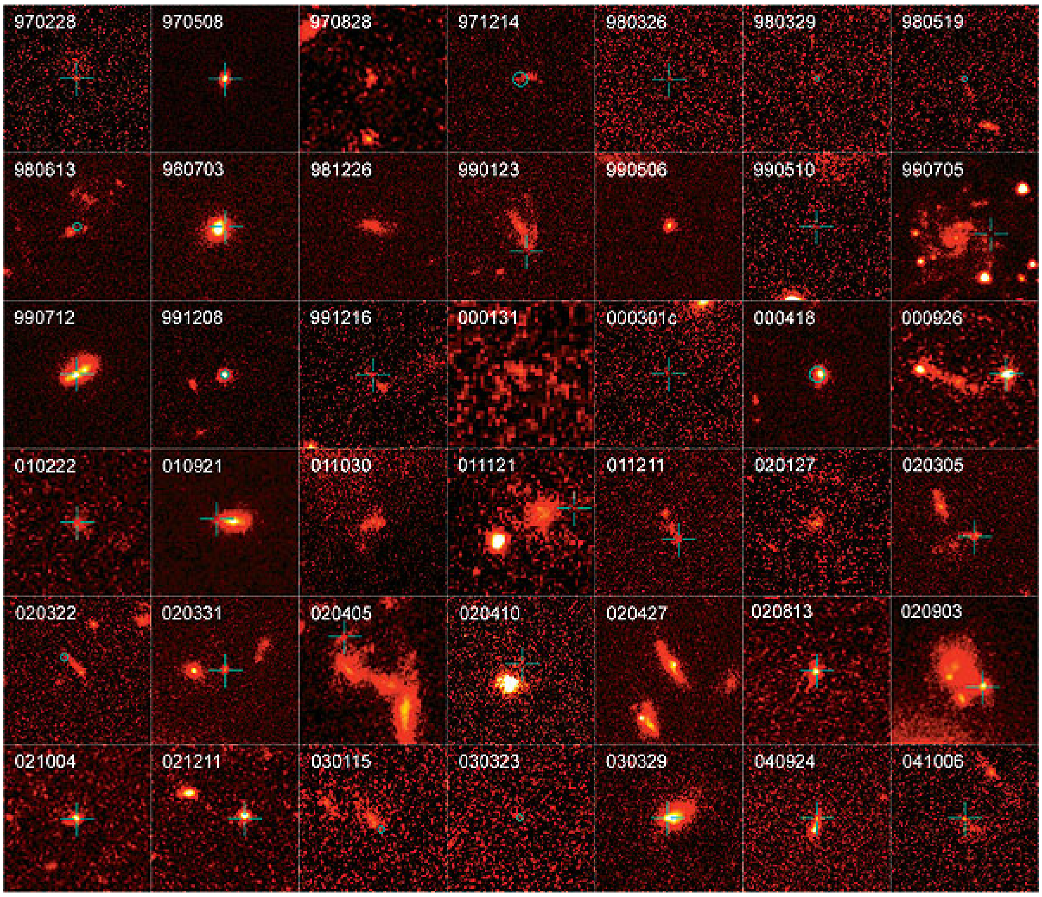

Figure 1.10: Each individual image corresponds to a square region on the sky 3.75″ on a side. These images were taken with the Space Telescope Imaging Spectrograph (STIS), the Wide Field and Planetary Camera 2 (WFPC2) and the Advanced Camera for Surveys (ACS) on *HST*. In those cases where the location of the GRB on the host is known to better than 0.15″ the position of the GRB is shown by a green mark. If the positional error is smaller than the point spread function of the image (0.07" for STIS and ACS, 0.13" for WFPC2) the position is marked by a cross-hair; otherwise the positional error is indicated by a circle. Owing to the redshifts of the hosts, these images generally correspond to blue or ultraviolet images of the hosts in their rest frame, and thus detect light largely produced by the massive stars in the hosts. The mosaic nicely compiles the wide range of luminosities and morphologies exhibited by GRB host galaxies. (*Adapted from Fruchter et al. 2006.*)

and merging or interacting morphologies (Conselice et al. 2005; Fruchter et al. 2006). Mergers are excellent sources of star formation because the gas content of the colliding galaxies falls rapidly into the combined potential well, setting off starbursts. A few hosts show tentative evidence of very high star formation rates (Chary et al. 2002; Berger et al. 2003), but their optical properties do not appear typical of the galaxies found in blind submillimetre galaxy surveys (see §1.4.4 Tanvir et al. 2004; Fruchter et al. 2006). It is currently debated how GRB hosts relate to other known populations of star forming galaxies. At redshifts around 3 the ultraviolet luminosities of host galaxies and the metallicities of GRB sightlines are consistent with the expectation if hosts are drawn from the underlying population of all star forming galaxies weighted with the total star formation density per luminosity bin (Jakobsson et al. 2005; Fynbo et al. 2008). With *Spitzer*'s (Werner et al. 2004) Infrared Array Camera (Fazio et al. 2004) MIR photometry, together with optical and NIR data, we can establish how the host galaxies relate to other star forming populations in terms of total stellar mass. This is essential if we are to understand the full range of properties of star forming galaxies at high redshifts and fully exploit the potential of GRBs as probes of cosmic star formation.

1.4 Other relevant types of galaxies

In CC06 and CC08 I derive a range of properties for GRB host galaxies. These properties are in turn checked against those of few other types of galaxies relevant for physical cosmology. So a concise explanation about these galaxy types, including their main observational characteristics, is in order. They include:

1.4.1 Lyman Break Galaxies

Observations of high redshift galaxies can test theories of galaxy and structure formation. For instance, one of the most direct tests of hierarchical galaxy formation models is the predicted decline of the abundance of massive galaxies with redshift. Some of the best known high redshift galaxies are the $z \sim 3$ galaxies discovered with the Lyman break technique (LBG; Steidel & Hamilton 1992). This technique consists of a set of colour criteria to identify star forming galaxies at high redshift through multiband imaging across the 912 Å Lyman continuum discontinuity. At high redshifts ($z \gtrsim 2.5$) the Lyman limit is shifted far enough into the optical window to be detectable with broadband photometry. By placing filters on either side of the redshifted break one can identify high redshift objects by their faintness in the U band and by an otherwise blue spectral energy distribution. Using redder passbands, the technique can be used to look for galaxies at even higher redshifts. For example, one can define similar criteria for B band dropouts which would be galaxy candidates at redshifts $3.5 \lesssim z \lesssim 4.5$ and so on.

These galaxies are forming stars rapidly and are generally thought to be massive enough to be the ancestors of today's large galaxies. Measurements have been made of their clustering properties, star formation histories, contribution to the cosmic star formation rate, rest frame optical emission lines and interaction with the intergalactic medium. See van Dokkum et al. (2004) and references there in for a summary. The masses of luminous $z \sim 3$ LBGs appear to be a factor of $\sim$10 lower than the most massive galaxies today. Such relatively low masses are qualitatively consistent with hierarchical models. LBGs in these models are "seeds" marking the highest density peaks in the early Universe and form the low mass building blocks of massive galaxies in groups and clusters.

1.4.2 Lyman Alpha Emitters

Lyman alpha (Lyα) is the transition and resulting emission line of the hydrogen atom as an electron goes from n = 2 to n = 1 (where n is the principal quantum number referring to the energy level of the electron). It is the strongest transition in the hydrogen atom and, since the most abundant element in the Universe is hydrogen, the Lyα line was early on suggested as a probe of galaxy formation in the primitive Universe. The search for Lyα emission has in recent years proven to be a powerful tool for studying the galaxy population at high redshifts (z = 2–7). Lyα emitting galaxies (LAEs) are important tracers of galaxy formation. The Lyα emission is produced by ongoing star formation in the galaxies, and the line emission enables discovery of objects that may be too faint to be seen in the continuum. LAEs offer an opportunity to probe the faint end of galaxy formation at high redshift, and may serve as building blocks of larger galaxies in a hierarchical Universe. See Lai et al. (2008) and references therein for a summary.

Because Lyα emission is easily extinguished by dust, LAEs have often been characterised as protogalaxies experiencing their first burst of star formation. However, the differing behaviour of Lyα and continuum photons encountering dust and neutral gas makes it possible for older galaxies to exhibit Lyα emission when morphology and kinematics favour the escape of these photons. Hence the LAEs could instead represent an older population with actively star forming regions. See Gawiser et al. (2006) and references therein for a summary. Although the sample of known emitters is increasingly growing, their nature (e.g. stellar masses, ages, metallicities, star formation rates) is still poorly constrained.

1.4.3 Distant Red Galaxies

The identification of star forming galaxies at $z \gtrsim 3$ by the Lyman break technique has greatly enhanced our understanding of galaxy formation and the star formation history of the Universe. However, the census of normal galaxies at $z \sim 3$ is potentially incomplete because of selection effects. It is not clear whether LBGs are the most common progenitors of today's massive galaxies. The highly successful Lyman break technique selects objects with strong ultraviolet emission, corresponding to galaxies with high star formation rates and a limited amount of obscuration of the stellar continuum. Galaxies whose light is dominated by evolved stellar populations, as well as those that are heavily obscured by dust, may be underrepresented in LBG samples.

Such "evolved" high redshift galaxies can be selected effectively in the rest frame optical, which is redshifted to NIR wavelengths for $z \gtrsim 2$. van

Dokkum et al. (2003, 2004) solved the issue by selecting high redshift galaxies by their observed NIR colours. They identified a substantial population of galaxies at $z > 2$ with comparatively red rest frame optical colours. These distant red galaxies (DRGs) are efficiently selected by the simple observed colour criterion $J_S - K_S > 2.3$. The criterion $J_S - K_S > 2.3$ is expected to isolate galaxies with prominent rest frame optical breaks. This "optical break" selection is complementary to the ultraviolet Lyman break selection. Although there is some overlap, most DRGs are too faint in the rest frame ultraviolet to be selected as LBGs in ground based surveys.

1.4.4 Submillimetre Galaxies

Direct observation of the galaxy formation process was made possible by the development of powerful new radiation detectors sensitive to wavelengths in the range $200\,\mu$m to about 1 mm: the submillimetre (submm) waveband. Deep surveys of the submm sky using the Submillimetre Common User Bolometre Array (SCUBA; Holland et al. 1999) on the James Clerk Maxwell Telescope uncovered, starting in 1998, a population of distant, dust rich galaxies (SMG). Based on the radio/submm indices, optical colours, and spectroscopic identifications, the majority of these systems are thought to lie at redshifts of $z \sim 1$–4. Identifying the counterparts of submm sources at other wavelengths has proven difficult because of the large beam size of submm instruments and the inherent faintness of the sources at all shorter wavelengths. Studies of the SMG population suggest that luminous far infrared (FIR) galaxies are likely to be associated with an early phase in the formation of massive galaxies. An in depth review of the subject is presented in Blain et al. (2002) and references there in.

SMGs have been claimed to contribute significantly to the star formation history of the Universe at $z \sim 2$–3 and to have built up a substantial fraction of the present day stellar population. SMGs are luminous ($L_{\rm IR} \sim 10^{12-14}\,L_\odot$) and cold ($T_{\rm dust} = 36 \pm 7$ K). Galaxies with similar luminosities but with higher dust temperatures ($T_{\rm dust} > 45$ K) are difficult to detect in the submm with current technology. See Chapman et al. (2005) for a summary. Five GRB hosts (980613, 980703, 000210, 000418 and 010222 — CC06; Tanvir et al. 2004; Berger et al. 2001, 2003) have been detected in submm and/or radio. They may represent the long sought hotter (and less luminous) counterparts of SMGs (Michałowski et al. 2008).

1.5 The *Spitzer* Space Telescope

The core of my Dissertation results comes from the analysis, in CC06 and CC08, of MIR data obtained with the *Spitzer* Space Telescope for a sample of GRB host galaxies. Thus it seems appropriate to close the introductory chapter with a short account of *Spitzer* and the instruments onboard.

Spitzer (formerly *SIRTF*, Space Infrared Telescope Facility) was launched into space by a Delta rocket from Cape Cañaveral, Florida (United States) on 25 August 2003. During its mission, *Spitzer* is obtaining images and spectra by detecting the IR energy, or heat, radiated by objects in space between wavelengths of 3 and 180 μm (Figure 1.11). Most of this IR radiation is blocked by the Earth's atmosphere and can not be observed from the ground.

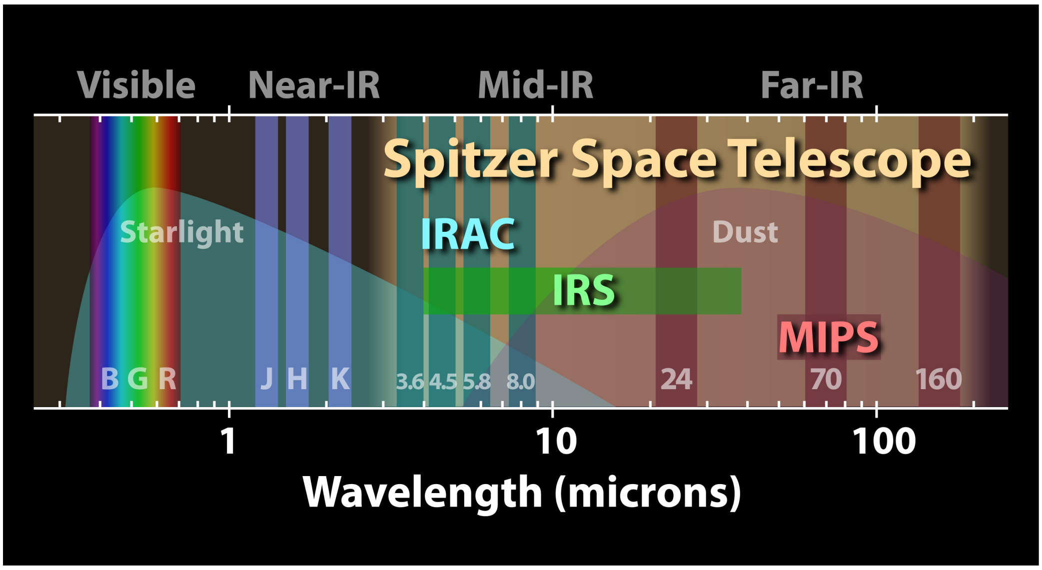

Figure 1.11: *Spitzer*'s spectrum. (*Photo: NASA/JPL-Caltech/R. Hurt (SSC).*)

Consisting of a 0.85 m telescope and three, focal plane, cryogenically cooled (superfluid helium) science instruments, *Spitzer* is the largest IR telescope ever launched into space (Figure 1.12). Its highly sensitive instruments give us a unique view of the Universe and allow us to peer into regions of space which are hidden from optical telescopes. Many areas of space are filled with vast, dense clouds of gas and dust which block our view. IR light, however can penetrate these clouds, allowing us to peer into regions of star formation, the centres of galaxies, and into newly forming planetary systems. IR also brings us information about the cooler objects in space, such as smaller stars which are too dim to be detected by their visible light, extrasolar planets, and giant molecular clouds. Also, many molecules in space, including organic molecules, have their unique signatures in the IR.

Because IR is primarily heat radiation, the telescope must be cooled to

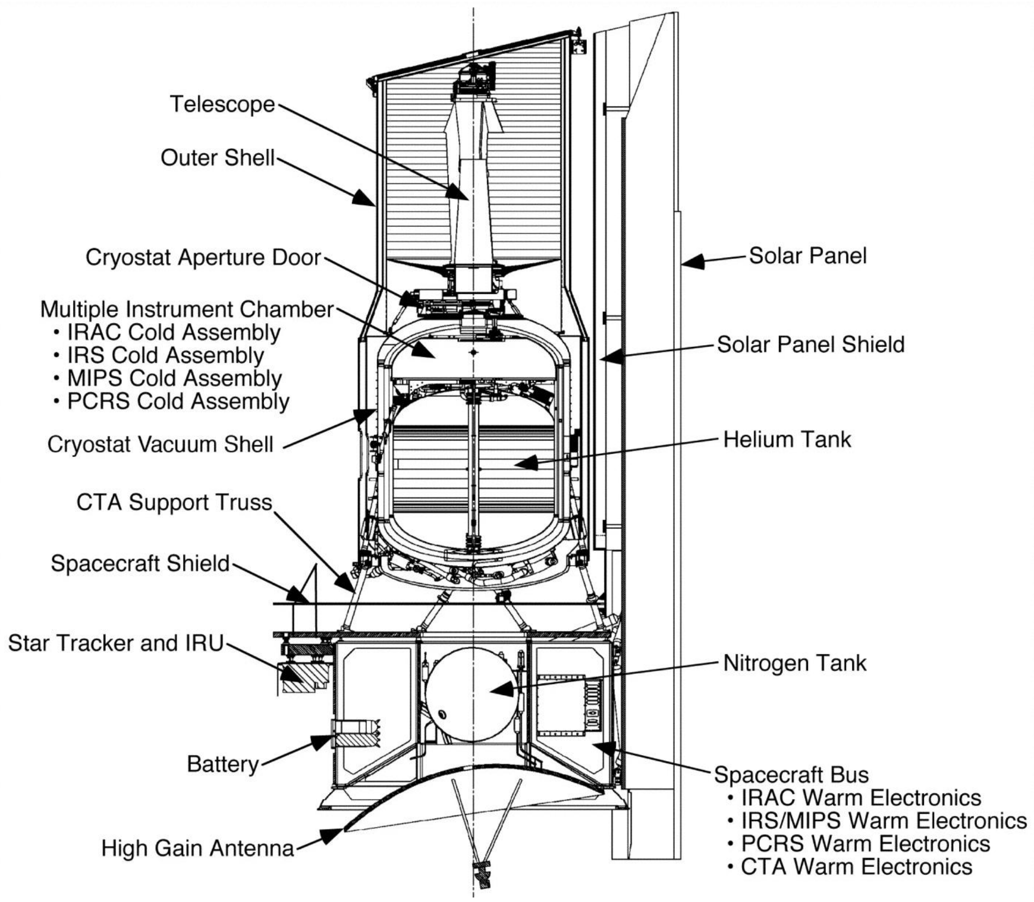

Figure 1.12: Cutaway view of the *Spitzer* flight hardware. The observatory is approximately 4.5 m high and 2.1 m in diametre. In this figure the dust cover is shown prior to its ejection approximately 5 days after launch. (*Adapted from Werner et al. 2004.*)

near absolute zero so that it can observe IR signals from space without interference from the telescope's own heat. Also, the telescope must be protected from the heat of the Sun and the IR radiation put out by the Earth. To do this, *Spitzer* carries a solar shield and was launched into an Earth trailing solar orbit. This unique orbit places *Spitzer* far enough away from the Earth to allow the telescope to cool rapidy without having to carry large amounts of cryogen (∼360 l). Such innovative approach has significantly reduced the cost of the mission. Currently the duration of the cryogenically cooled part of the mission is estimated in 5.5 yr. The cryogen is expected to be exhausted during the Spring of 2009.

Spitzer, described a the seminal paper by Werner et al. (2004), will be the final mission in NASA's Great Observatories Program – a family of four orbiting observatories, each observing the Universe in a different kind of light (visible, γ-rays, X-rays and IR). Other missions in this program include the *HST*, the *CGRO* and the *Chandra X-Ray Observatory*. *Spitzer* is also a part of NASA's Astronomical Search for Origins Program, designed to provide information which will help us understand our cosmic roots, and how galaxies, stars and planets develop and form.

Most of the data used in this Dissertation has been obtained with the Infrared Array Camera (IRAC; Figure 1.13). This is a 4 channel camera that provides simultaneous $5.12' \times 5.12'$ images at $3.6\,\mu$m, $4.5\,\mu$m, $5.8\,\mu$m and $8\,\mu$m. The pixel size is $1.2''$ in all bands. Two adjacent fields of view in the focal plane are viewed by the 4 channels in pairs ($3.6\,\mu$m and $5.8\,\mu$m; $4.5\,\mu$m and $8.0\,\mu$m). All 4 detector arrays in the camera are 256 pixels $\times$ 256 pixels in size, with the two short wavelength channels using InSb and the two longer wavelength channels using Si:As IBC detectors. The IRAC point source sensitivity requirements (5σ, 200 s) at $3.6\,\mu$m, $4.5\,\mu$m, $5.8\,\mu$m and $8.0\,\mu$m are $6\,\mu$Jy, $7\,\mu$Jy, $36\,\mu$Jy and $54\,\mu$Jy, respectively.

The IRAC instrument is addressing the four major scientific objectives defining the *Spitzer* mission: to study the early universe, to search for and study brown dwarfs and superplanets, to study ultraluminous galaxies and active galactic nuclei, and to discover and study protoplanetary and planetary

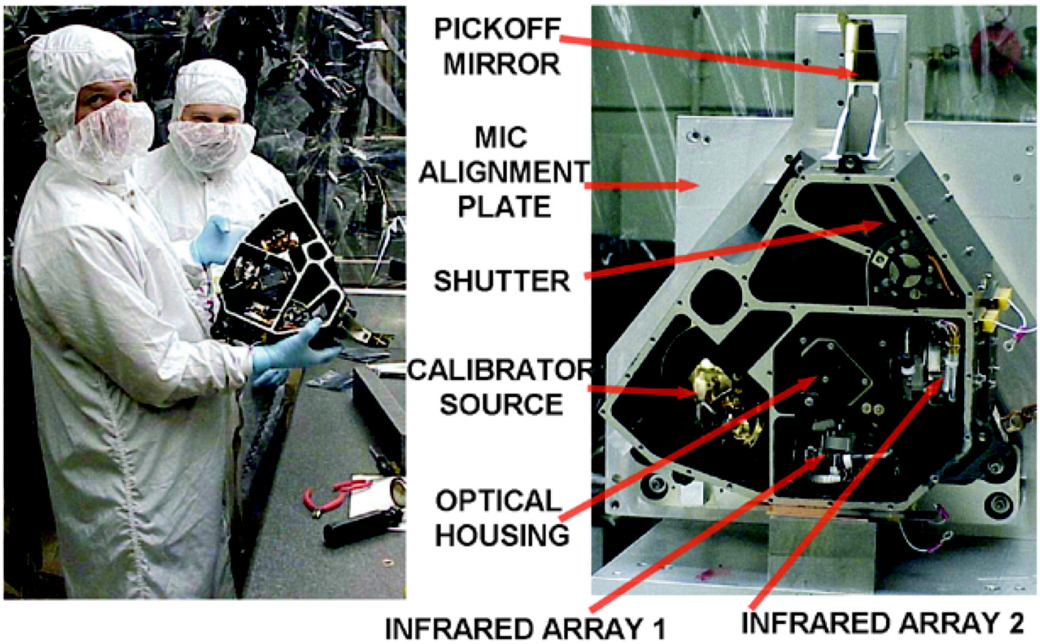

Figure 1.13: IRAC Cryogenic Assembly at NASA's Goddard Space Flight Centre, with the top cover removed to show the inner components. The multiple instrument chamber alignment plate was used only for testing. The parts marked IR Array 1 and 2 are the IRAC channel 4 and 2 focal plane assemblies, respectively. (*Adapted from Fazio et al. 2004.*)

debris disks. In addition, IRAC is a general purpose camera that is being used by observers for a wide variety of astronomical research programmes. IRAC is described in a seminal paper by Fazio et al. (2004).

In CCO06 I have also utilised some data obtained with the Multiband Imaging Photometer for *SIRTF* (MIPS; Figure 1.14). This instrument is designed to provide very deep imaging and mapping at 24 μm, 70 μm and 160 μm. In integrations of 2 000 s, it reaches a 5σ detection limits at these wavelengths of 0.2 μJy, 0.5 μJy and 8 μJy, respectively (the latter one is limited by confusion noise). In addition it has low resolution spectroscopic capabilities (R = 15–25) between 50 μm and 100 μm).

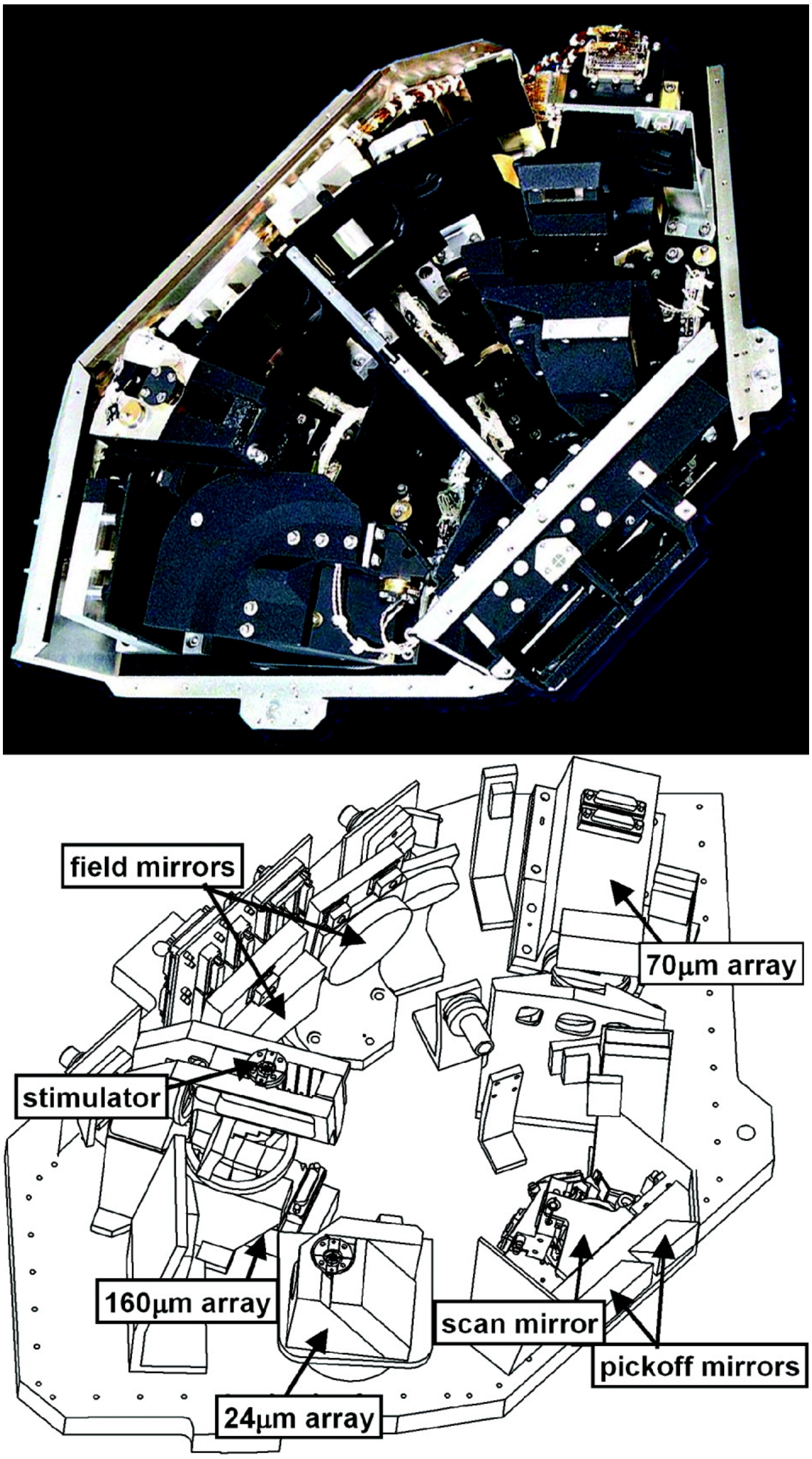

Figure 1.14: The instrument baseplate is about 30 cm × 40 cm in size, and the instrument mass is 18 kg. **Top:** MIPS instrument. **Bottom:** Cutaway drawing. (*Adapted from Rieke et al. 2004.*)

MIPS has 3 detector arrays: A 128 pixels $\times$ 128 pixels arsenic doped silicon (Si:As) array, operating at a wavelength of 24 μm and with a $5'$ field; a 32 pixels $\times$ 32 pixels gallium doped germanium (Ge:Ga) array for 70 μm microns and a $5'$ field; and a 2 pixels $\times$ 20 pixels Ge:Ga array, mechanically stressed to extend its photoconductive response to 200 μm, and with a field of $0.5' \times 5'$. Onboard calibrators are provided for each array. Additionally, it has a scan mirror to provide mapping with a very efficient use of the telescope time. MIPS is described in a seminal paper by Rieke et al. (2004).

In addition to IRAC and MIPS *Spitzer* carries onboard an Infrared Spectrograph (IRS), from which I have not used any data. IRS consists of four separate instruments which take fingerprints of the IR radiation emitted by distant objects. Pairs of modules work respectively in the NIR and MIR. Each pair contains a low resolution instrument and a high resolution instrument, optimised for objects of different brightness and for different types of scientific observations. IRS is described in a seminal paper by Houck et al. (2004).

Chapter 2

Obscured star formation and dark GRBs

This chapter is based on CC04, which has been included as part of my Dissertation in Appendix A. The purpose of this chapter is to highlight the most relevant aspects of the work done in CC04. In that paper I studied the dark GRB 001109. Here I will also touch on the subject of dark GRBs and obscured star formation, which is relevant for the work I present later on the properties of GRB host galaxies as derived from *Spitzer* observations.

2.1 Dark GRBS: an introduction

Shortly after the discovery of the first optical counterpart to a GRB (970228; see §1.1.3) it became obvious that such were not to be the case for every single burst. Within a few months there were several GRBs localised in small error boxes that lacked any optical counterpart despite deep, rapid searches.

GRB 970828 is a good example (Djorgovski et al. 2001). Even in the *Swift* era, with a dedicated satellite that has been designed for fast, multiwavelength observations of every GRB detected, not all bursts exhibit an optical counterpart. GRBs with no detected counterpart for reasons other than observational constraints or delays fall into the category of *dark bursts*. Few scenarios have been proposed to account for their existence (see Jakobsson et al. 2004 and references therein for a summary):

- *Obscuration:* the GRB afterglow would be extinguished by molecular gas or dust, whether in the circumburst medium, in our own Galaxy, or elsewhere in between. The prompt (high energy) radiation from the GRB can destroy the dust in a radius of a few tens of parsecs. Yet dust within the host at longer distances might still obscure the afterglow.

- *High redshift:* For GRBs with $z \gtrsim 5$ the ultraviolet light, which is severely extinguished by absorption in the Lyα forest, into the R band. The choice of the R band here is motivated by the fact that, typically, afterglow searching is done in the R band.

- *Intrinsically dark:* Should the relativistic ejecta of the of the GRB encounter a low density ambient medium, the afterglow will be optically faint.

But just what fraction of the GRBs detected in γ-rays are really (intrinsically) dark? For years the answer to this question remained rather uncertain because the Community did not agree on a standard physical definition. In the period spanning 1997–2001, approximately only one third of all GRBs with well determined coordinates have had successful searches for optical counterparts (Fynbo et al. 2001; Lazzati et al. 2002). This often resulted in GRBs being classified as dark when an optical afterglow was not found, irrespective of how inefficient the search was (Fynbo et al. 2001). Statistical samples built this way were far from uniform due to differences in localisation accuracy for various bursts, delays since their onset, observation strategies and conditions. Yet they were some times the basis of far reaching conclusions. For example, the estimated fraction of dark GRBs can constrain obscured star formation in the Universe (Djorgovski et al. 2001; Ramirez-Ruiz et al. 2002).

A popular definition often employed was a brightness threshold as a function of time: a magnitude $R > 23$ one day after the onset of the burst (Djorgovski et al. 2001). Though arbitrary by necessity such a definition exemplified the reaction time and depth of common searching efforts. Motivated by the results that faint bursts do not by themselves belong to a separate class, Jakobsson et al. (2004) proposed an operational definition for classifying dark GRBs: being subluminous with respect to the fireball model (for a description of this model see Mészáros & Rees 1997, see also §2.1.1). In other words, having an optical to X-ray spectral index $\beta_{\rm OX}$ of less than 0.5. It can be written like this:

$$\beta_{\rm OX} = \frac{\log F_\nu(\nu_{\rm optical}) - \log F_\nu(\nu_{\rm X-ray})}{\log \nu_{\rm X-ray} - \log \nu_{\rm optical}}, \tag{2.1}$$

where $F_\nu(\nu_{\rm optical})$ and $F_\nu(\nu_{\rm X-ray})$ must be synchronised to the same time reference. De Pasquale et al. (2003) found that optically faint GRBs are

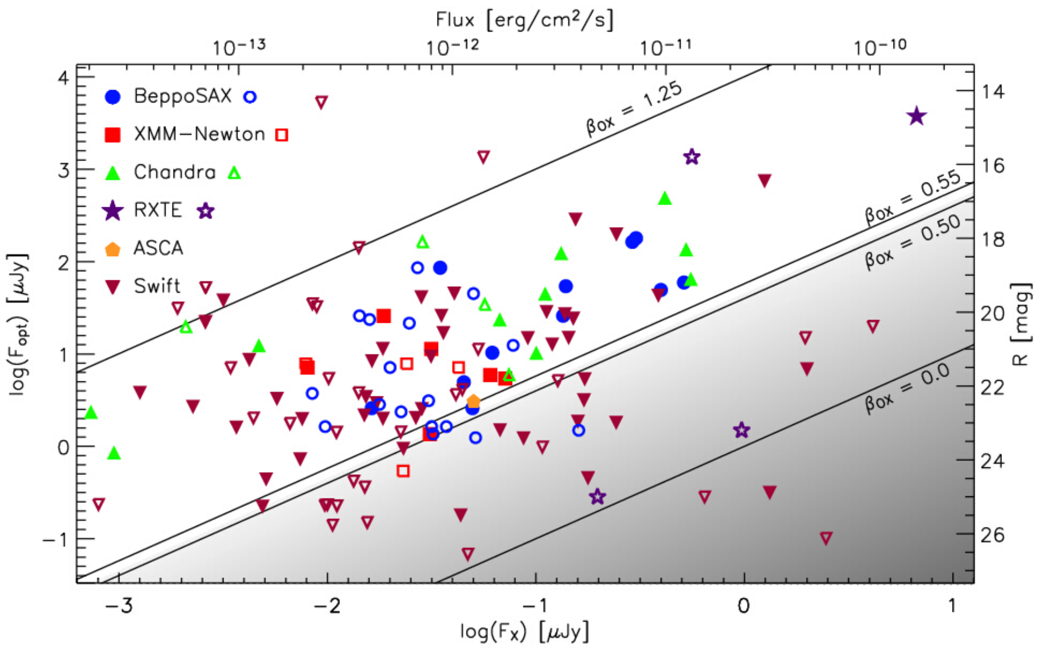

Figure 2.1: Diagram of optical flux densities vs. X-ray flux for 135 bursts (last update was 5 April 2006). The optical flux densities, the corresponding R band magnitudes shown on the right hand ordinate, and the X-ray flux densities all have been either interpolated or extrapolated to 11 hr after the onset. The magnitudes have been corrected for Galactic extinction. Filled symbols indicate optical detections, while open symbols are upper limits. Lines of constant $\beta_{\rm OX}$ are shown along with the corresponding value. Dark bursts are defined as those that have $\beta_{\rm OX} < 0.5$. The current sample contains 28 dark GRBs or ∼20%. (*The original diagram was first published by Jakobsson et al. 2004; this one is an updated version taken from* `http://astro.ku.dk/~pallja/dark.html`.)

also X-ray faint. In this context the $\beta_{\rm OX} < 0.5$ definition of dark bursts has the advantage that it does not consider as dark those GRBs which may be optically faint simply because they are intrinsically faint.

Figure 2.1 displays a sample of 135 bursts (both *Swift* and pre-*Swift*) classified according to the operational definition in Jakobsson et al. (2004). 28 out of the 135 (∼20%) GRBs fall in the dark burst category. The lines of

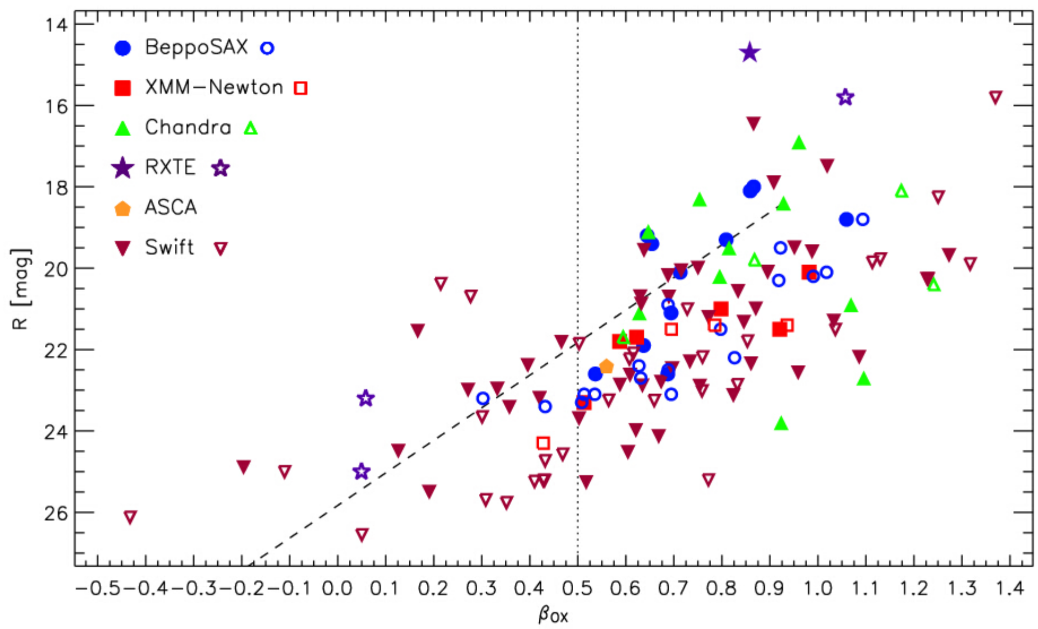

Figure 2.2: An equivalent representation of Figure 2.1. Here the optical flux density is plotted against $\beta_{\rm OX}$. The dashed line shows the effect of including the host extinction for GRB 021004. (*Taken from* `http://astro.ku.dk/~pallja/dark.html`.)

constant $\beta_{\rm OX}$ shown make the diagram a quick, simple diagnostic tool to identify dark GRBs from the limited information that is typically distributed early in a follow up campaign. Figure 2.2 is equivalent to Figure 2.1: optical flux density vs. $\beta_{\rm OX}$.

There are a few caveats though. The sample includes upper limits, which means that the calculated fraction of dark GRBs is a lower limit. Only about 20% of the bursts have limits deep enough to allow them to be classified as dark. On the other hand, the detections above the $\beta_{\rm OX} = 0.5$ marks the corresponding upper limit; for this sample no more than $\sim$50% could be classified as dark. Obviously, the definition is only operational. One can not derive from it the cause of the darkness in a given GRB, that requires detail modelling. The potential capability of GRB afterglows to destroy dust in their immediate surroundings, coupled with particular geometries in their hosts (i.e. a relatively dust line of sight), might put a burst which occurred in dusty host galaxy as non dark.

2.1.1 The fireball model... briefly

My readers will grant me some latitude as I digress momentarily to briefly describe the simplest fireball model. This way the choice of $\beta_{\rm OX} < 0.5$ will become immediately clear. The generic emission process for both the GRB and the afterglow is synchrotron. It is commonly assumed that the emitting electrons have a power law energy distribution. The spectral index, β ($F_\nu \propto \nu^{-\beta}$), depends on the energy distribution of the electrons, p, and the location of the synchrotron cooling break, ν_c, beyond which the electron cooling time becomes short compared to the expansion time (Sari et al. 1998):

$$\beta = \begin{cases} (p-1)/2, & \nu < \nu_c, \\ p/2, & \nu > \nu_c. \end{cases} \tag{2.2}$$

This result is not affected by the outflow collimation, nor the density profile of the environment in which the expansion takes place. For GRB afterglows the cooling break is commonly found to occur as $\sim 10^{14}$ Hz $< \nu_c <$ $\sim 10^{18}$ Hz. So there is a break in the spectra distribution somewhere between the optical and the X-ray regimes (though there are cases when the break can be located outside this bracket). The power law index of the energy distribution of the electrons is usually between 2 and 2.5. Furthermore, a power law energy distribution with $p < 2$ would imply an infinite electron distribution total energy. And so our simple model yields 0.5 ($p = 2$, $\nu_c > 10^{18}$ Hz) $> \beta_{\mathrm{OX}_{\mathrm{average}}} > 1.25$ ($p = 2.5$, $\nu_c < 10^{14}$ Hz). That is why a value of $\beta_{\mathrm{OX}} < 0.5$ implies that a burst is optically subluminous respect to the fireball model.

2.2 The dark GRB 001109

In CC04 I studied the dark GRB 001109. I presented optical and NIR follow up observations of GRB 001109 from 1 to 300 days after the burst. No transient emission was found at these wavelengths within this GRB's 50″ radius *Beppo*SAX error box. There are two main parts to this paper. The first one is the search that ruled out association between the GRB and the sources found in the error box. The second one is its classification as a dark burst.

2.2.1 Searching for the afterglow

GRB 001109 was detected by *Beppo*SAX's WFCs with a refined uncertainty of 2.5′ (Gandolfi 2000). A NFI follow up observation detected a new X-ray source inside the 2.5′ radius WFC error box (Amati et al. 2000). The VLA found a radio source within the NFI error box (Taylor et al. 2000, Figure 2.3). This source did not decay so it was ruled out as the radio afterglow. My collaborators and I started target of opportunity observations 9 hr after the onset of the burst. We attempted to detect the afterglow in the optical ($UBVRI$) and NIR (JHK) bands. I reduced the data in the standard way and performed aperture photometry with SExtractor (Bertin & Arnouts

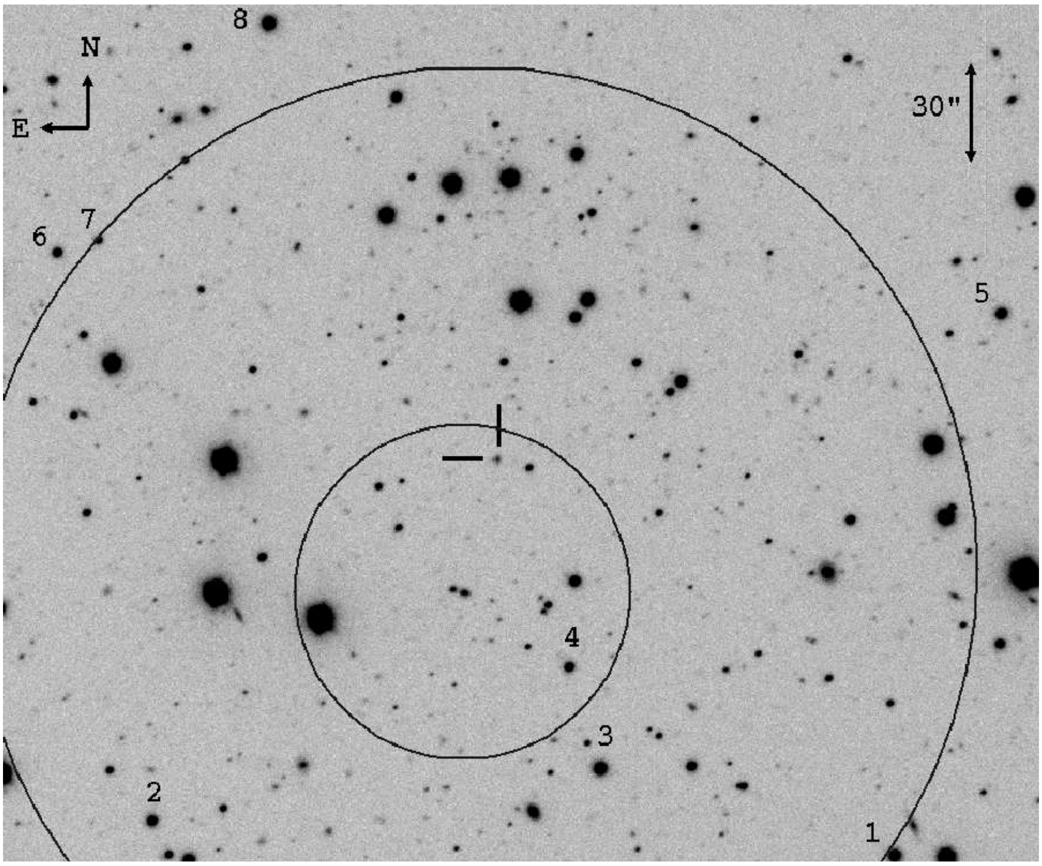

Figure 2.3: The contents of the *Beppo*SAX error box for the GRB 001109 field. This R band image was taken with the 2.56 m NOT (+ALFOSC) on 14.0524–14.0734 UT August 2001. The source in between ticks is the galaxy coincident with VLA J1830+5518 and consistent with the position of the X-ray afterglow. The numbered stars are the secondary standards indicated in Table 2. The large circle represents the refined WFC error box (Gandolfi 2000) and the small one the NFI error circle (Amati et al. 2000). The field of view covered by the figure is $5.1' \times 4.3'$. North is upwards and East is leftwards. (*Adapted from CC04.*)

1996). Spectroscopic observations were made at the 6.05 SAO telescope (12 s $\times$ 600 s exposures; with SCORPIO and a 300 lines/mm grating. The spectral resolution (FWHM) obtained was $\sim$20 Å and the effective wavelength coverage was 3500–9500 Å(Afanasiev et al. 2001).

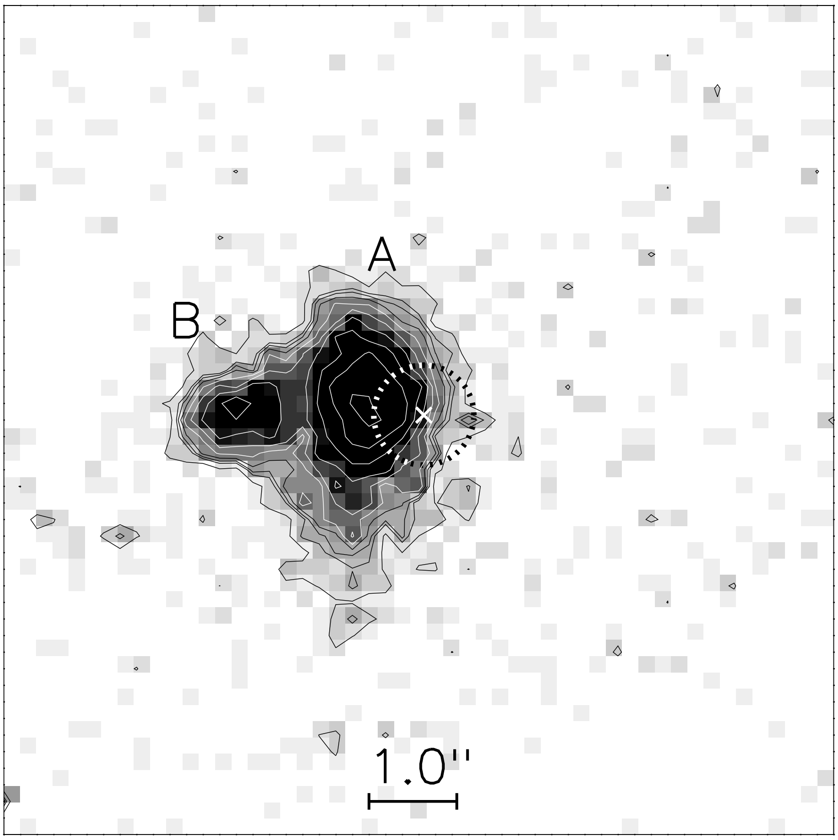

Figure 2.4: Contour plot displaying the galaxy coincident with VLA J1830+5518. The figure shows the coadded I band image taken with the 2.56 m NOT (+ALFOSC) (17.0720–17.1148 August 2001) of the source coincident with VLA J1830+5518. A seeing of $0.8''$ allowed me to separate the two components, objects A and B. The centre of the circle marks the position of the radio source (Taylor et al. 2000), RA(J2000) = $18^h30^m06.51^s$, Dec(J2000) = $55°18'35.7''$. The radius of the circle is $0.57''$. The contours show the detection confidence level above the background in a logarithmic scale. North is upwards and East is leftwards. (*Adapted from CC04.*)

I found neither an optical nor a NIR afterglow. Strong limits come from the deep NIR observations. I derived the following upper limits: for an optical afterglow $R > 20.9\,$mag $10.2\,$hr after the onset and $I > 22.9\,$mag 11.4 hr after the onset; for a NIR afterglow $K' > 19.9\,$mag, $H > 20.7\,$mag and $J > 21.3\,$mag, all of them $\sim$10 hr after the onset with a 3σ confidence level. Careful astrometry lead me to discover a complex system composed of two objects (dubbed A and B in CC04; Figure 2.4) $1.25''$ apart; one of these objects was coincident with the VLA radio source. Strictly speaking the astrometry reveals the registration of the optical image, and has nothing to do with the location of the VLA radio source which was determined absolutely in the International Coordinate Reference Frame. The SCORPIO spectrum indicated that the alignment of the two objects in this complex system was a chance projection.

Object A, coincident with the VLA radio source, was modelled to be a dusty galaxy at $z = 0.381$ with $A_V = 1.4\,$mag and an episode of star formation, which dominates the optical continuum, triggered 0.25 Gyr ago. Could object A be the host galaxy of GRB 001109? In that case the redshift of GRB 001109 would be $z = 0.381$. And could the VLA radio source be related to GRB 001109? I could not establish these connections with certainty.

I calculated the probability to find a radio source with the brightness of the one coincident with object A in an error box with a radius of $50''$ (NFI). Following Fomalont et al. (2002) the density of radio sources detected at 8.4 GHz above a flux density S in μJy is given by:

$$N = (0.099 \pm 0.010) \left(\frac{S}{40}\right)^{-1.11 \pm 0.13} \text{arcmin}^{-2}. \tag{2.3}$$

So I concluded that the chance probability of having a source brighter than 238 μJy $\pm$ 31 μJy inside the NFI error box is 3$\pm$0.9% and thus, considered that the probability is not low enough to establish a physical relationship between the location of this radio source inside the GRB error box and the occurrence of the γ-ray event.

Although the radio emission from object A is not related to the afterglow of the GRB, object A could still be the host galaxy of the burst. To further constrain this suggestion I calculated the number of galaxies, with magnitude $B < 22.96$ (reddened), to be found inside a circular area with a $50''$ radius. Using the Millennium Galaxy Catalogue (Liske et al. 2003) I estimated a count of $\sim$3 galaxies (the B passband flux density was dereddened of Galactic extinction). Thus a connection between object A and GRB 001109 can not be established with certainty.

2.2.2 Classified as dark

My optical/NIR observations are consistent with a connection between the VLA radio source and object A. On the other hand, I could not establish a connection between object A and GRB 001109.

Figure 2.5 displays selected detections and upper limits associated with GRB 001109 (to keep the figure legible I have only plotted the most constraining measurement for each of the optical and NIR bands). I shifted all plotted measurements to a common epoch ($t = t_0 + 0.4$ days; epoch of the radio detection) assuming a power law decay index $\alpha = 1.27$ (suggested by the X-ray observations reported in Amati et al. 2003). As shown, the most constraining upper limit corresponds to the 2.56 m NOT I band image. This

I band measurement allowed me to impose an upper limit on the afterglow's optical to X-ray spectral index: $\beta_{\rm OX} < 0.33 \pm 0.02$. The corresponding $\beta_{\rm OX}$ upper limits for the full *Beppo*SAX's NFI dark burst sample can be worked out from the limits on the optical to X-ray flux density ratio[1] ($f_{\rm OX}$ from Table 1 in De Pasquale et al. 2003):

$$f_{\rm OX} = \frac{\nu_{\rm optical}^{-\beta}}{\nu_{\rm X}^{-\beta}}, \tag{2.4}$$

where β is the power law index of the specific flux; see §2.1.1. GRB 001109 has the strongest limit in this sample, where the $\beta_{\rm OX}$ upper limit values span from 0.33 to 0.55.

If we define a dark GRB as one with no counterpart brighter than $R <$ 23 mag at 24 hr from the onset, then GRB 001109 is clearly a dark GRB, given the $I > 22.9$ limit imposed by the 2.56 m NOT observations 0.47 days after the γ-ray event. I have used my 2.56 m NOT $I > 22.9$ upper limit to further constrain the luminosity of GRB 001109 within the context of the *Beppo*SAX's NFI dark burst sample De Pasquale et al. (see upper limits for dark bursts in Table 1 of 2003). To do so I have (following the methodology described in De Pasquale et al. 2003, and in agreement with the operational definition by Jakobsson et al. 2004) calculated the R band upper limit 11 hr after the GRB, from the 2.56 m NOT I band constraint. First, I calculated the R band flux density associated with the I band limit using the spectral index $\beta_{\rm OX} = 0.33 \pm 0.02$ (see above). Then, the R band flux density was

[1]The optical to X-ray flux density ratio ($f_{\rm OX}$) is defined as the R band flux density (or upper limit), in units of μJy, divided by the 1.6–10 keV X-ray flux density, in units of 10^{-13} cg (De Pasquale et al. 2003).

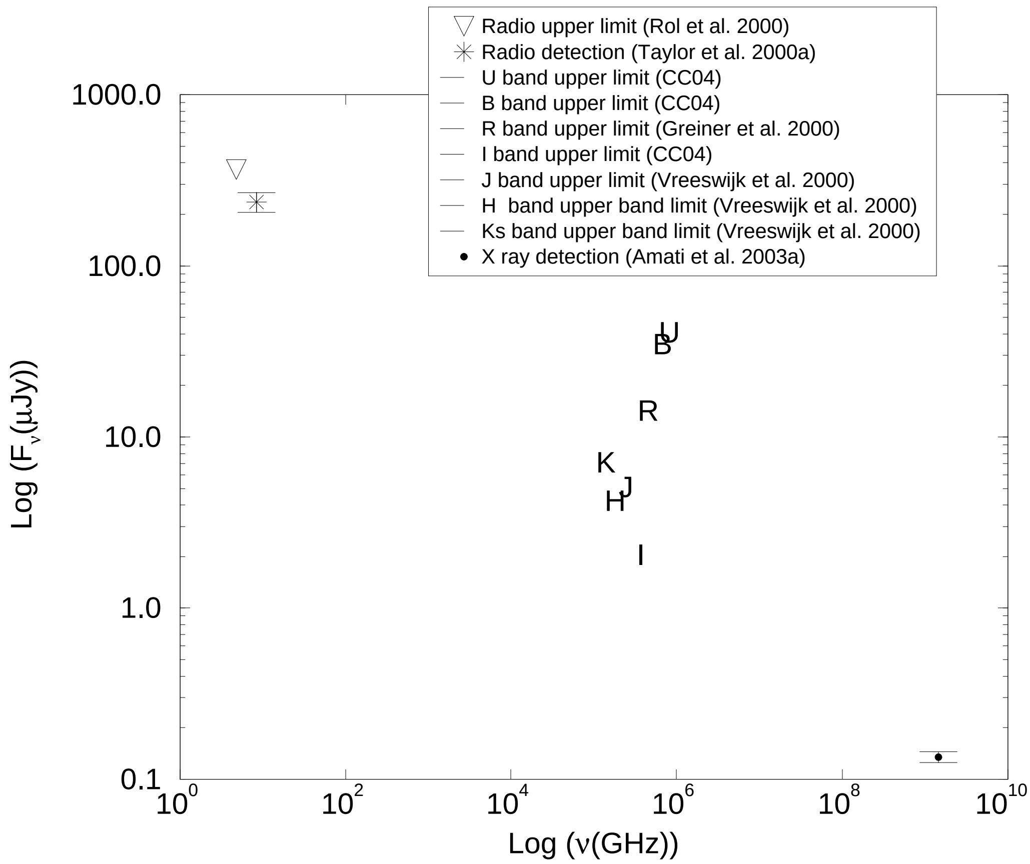

Figure 2.5: Selected detections (X-ray) and upper limits ($UBVRIJHK_S$) associated with GRB 001109. The most constraining upper limit corresponds to the 2.56 m NOT I band measurement. (*Adapted from CC04; for reasons of brevity and economy of space the references in this figure have not been included in the Bibliography, rather they can be found at CC04, which is included in Appendix A.*)

rescaled from $t - t_0 = 11.3624$ hr (9.8646 UT November 2000; mean 2.56 m NOT observing time) to $t - t_0 = 11$ hr (assuming a power law decay index $\alpha = 1.15$, adopted by De Pasquale et al. 2003). Further, the R band flux density upper limit was corrected for Galactic extinction using a $E(B-V)$ = 0.04 value (Schlegel et al. 1998). As a result I derived an dereddened R band flux density upper limit of 1.80 μJy 11 hr after the γ-ray event. My new

R band flux density upper limit is approximately 7 times deeper than the one reported previously (11.81 μJy in De Pasquale et al. 2003). Moreover, my I band image lowers the $f_{\rm OX}$ from 0.59 (De Pasquale et al. 2003) to 0.09 (CC04), making GRB 001109, by far, the darkest *Beppo*SAX NFI GRB.

GRB 001109 belongs to the subsample of darkest *Beppo*SAX NFI bursts ($\sim$25% of the total *Beppo*SAX NFI dark GRB sample) which show $f_{\rm OX}$ values incompatible (at a 2.6σ level) with GRBs with detected optical transients (De Pasquale et al. 2003). For those objects the spectral index $\beta_{\rm OX} \leq 0.62$, so GRB 001109 is clearly in this group, which is composed by GRBs 981226, 990704, 990806 and 000210.

It is important to highlight that GRB 001109 exhibited the brightest X-ray afteglow among the dark *Beppo*SAX NFI bursts (De Pasquale et al. 2003). On the other hand it showed the lowest N_H reported for the dark *Beppo*SAX NFI GRBs (De Pasquale et al. 2003). In fact, GRB 001109 N_H value is consistent with the ones measured for GRBs with detected optical transients. Thus, the bright X-ray afterglow of GRB 001109, its low N_H value (in comparison to the rest of the dark BeppoSAX NFI GRB sample) and the constraining optical limits imposed in the present work, might indicate that GRB 001109 showed a spectrum intrinsically different from GRBs with detected optical transients.

Chapter 3

Spitzer Data analysis: reduction, photometry, errors...

The bulk of my Dissertation was inspired by the existence of unpublished *Spitzer* archival data on GRB host galaxies. In this chapter I describe how I operated with these data. I have tried to justify my choices, based on information from the *Spitzer* Observer's Manual (SOM; Spitzer Science Centre 2007b) and the IRAC and MIPS Data Handbooks (IDH and MDH respectively; Spitzer Science Centre 2006, 2007a). Additional information may be found at the *Spitzer* Science Centre web site[1] (referred from here on as SSC).

3.1 Accessing the archives

The best way to access the *Spitzer* archives is to use *Leopard*, which is the archival tool provided at the SSC. Its basic use is straight forward and for

[1] `http://ssc.spitzer.caltech.edu/`

some juicy details I advise to read the manual. There is just one thing I should like to mention here: *Leopard* has a very nice preview feature, it allows a sneak peak of any image in the archives before downloading. Great as a quick diagnostic tool to check for detections, though experience has taught me not to trust it for faint images.

The following basic types of data are available for download from the *Spitzer* archives:

- *Raw data:* the name says it all. Raw data are wholly unprocessed except for those steps necessary to render them into a readable FITS format. I once looked at them and immediately lost any desire to do so ever again. Most observers are unlikely to use these data, yet they are supplied in the event that someone might wish to reprocess the data in a different manner from the official pipeline.

- *Basic Calibrated Data:* BCDs are exposure level data after having passed through the pipeline. Instrumental signatures have been removed and the BCDs are absolutely calibrated into physical units of surface brightness (more about this later).

- *PostBCDs:* More advanced processing of many individual IRAC frames, including refinement of the telescope pointing, corrections for residual bias variations and the production of mosaiced images. I have chosen to work directly with PostBCDs in all cases.

- *Calibration Files:* For each BCD, the pipeline calibration server generates several estimates of the current detector characteristics.

If any of my readers is retrieving public data out of the *Spitzer* archives here is a tip that might be useful. *Spot* is a companion software to *Leopard*. Its primary purpose is a tool for planning observations. But one can use Spot to download the actual Astronomical Observation Request (AOR) file that was used for the observation. This is extremely helpful to gain a proper understanding of how the downloaded images came to be.

3.2 Working with PostBCDs

I will start by clarifying that when I refer to the official pipeline I imply only the processing of raw data from IRAC and MIPS at 24 μm. Those are the data I use in my Dissertation.

The BCD pipeline is designed to take a single raw image from a single detector and produce a flux calibrated image which has had all well understood instrumental signatures removed. There are pipelines for science and for calibration data: the data reduction software modules and the calibration server. The individual modules each correct a single instrumental signature. These include corrections for dark current (both first frame effect and sky darks), multiplexer bleeding, saturation nonlinearity, flat fielding, cosmic ray detection, flux calibration, detector wraparound, latency and droop (MIPS), internal scattered light and pointing refinements. Detail descriptions of all these instrumental signatures may be found in the IDH and the MDH. A raw image is thus passed between successive modules, and at each step becomes closer to a finished, fully reduced image. The actual BCD pipeline has not been released, due in large part to the degree to which it is tied to *Spitzer*

Science Operations Database. Extensive descriptions of all the algorithms are available at the SSC.

The output at this stage is a single FITS file per exposure with standard keywords, distortion coefficients, flux calibrated and containing an astrometrical solution. The PostBCD pipeline will use these files as input. Further processing will match the background brightnesses of overlapping images, outlier rejection, take care of column pulldown, correct for multiplexer bleeding again, correct for banding, remove cosmic rays and generate mosaics from all the images in an AOR. All these issues have remained fairly stable during the course of the cold part of the *Spitzer* mission (i.e. until the cryogen is exhausted, expected to happen in less than a year now).

In many cases one can start to do science directly with the PostBCD products. I assert this to be the case for my data. They have characteristics that minimise a number of instrumental signatures. For instance, my sources are not extremely bright, and there is only one source per observed field, it is always located in the centre of the arrays, plus the data is well dithered. Plus careful examination of all my fields revealed that the pipelines did a good job removing instrumental signatures. In 3 cases certain signatures were not completely removed (muxbleeding and column pulldown), yet these happened away from my source so the immediate vicinity was clean. Further, my sources are located a priori with $\sim 0.5''$ accuracy and I am only interested in measuring their fluxes, hence the classical confusion limit is not relevant. In addition, because GRB host galaxies have spectra described by a power law and are seen by *Spitzer* as red point sources (i.e. with SEDs that rise toward the longer wavelength wavebands for those sources with detections in all wavebands) photometric corrections for colour and array location are negligible.

A brief digression here is in order to highlight *Spitzer*'s excellent pointing capabilities. The 1σ blind pointing accuracy is $<0.5''$ ($1.2''$ for MIPS 24 μm). The offsetting accuracy is in the range $0.1''$–$0.2''$. An additional pointing error comes from the gyro drift which can accumulate over the 30 min period between attitude resets. This error is typically $\approx 2''$ for a *worst case* frame just before a reset. The 1σ relative astrometric uncertainty is less than $\sim 0.3''$ in the IRAC and MIPS data. My experience has been that every time I had difficulty recognising the field and thought it was due to inaccurate pointing I was proven wrong. In these cases in which I did not recognise the field, I overlaid a comparison image observed elsewhere, with the target host clearly detected, on the *Spitzer* science image. The match with the previously marked position from astrometry was invariably correct. In any case, host extraction was always visually confirmed with optical and/or NIR comparison images from the literature.

Last, but not least, a 10% accuracy in the photometry is perfectly acceptable for this work (and often I achieved better than that). I do not require precision photometry since my results are dominated by systematic uncertainties (i.e. how well the templates represent the actual SEDs, the luminosity to SFR conversion, or a factor of 2 from the choice of initial mass function; see Chapter 4 and Appendices B and C).

Nonetheless, as a sanity check, in CC06 I carefully verified the PostBCDs of six GRB hosts with my own reductions. I used the MOPEX software provided by the SSC with a range of parameters. Upon doing photometry on the the PostBCD images and the ones I reduced myself the results came to be the same. Figure 3.1 shows a randomly selected area from one of my IRAC fields. It exemplifies how reprocessing the images did not affect the photometry at the level of precision I am interested.

3.3 Photometry

3.3.1 Aperture: GAIA

Following the recommendations made at the SSC, and because of the undersampled nature of the data, I performed aperture photometry. GRB 980425 is the only host galaxy resolved by *Spitzer* and I obtained its photometry from the literature (Le Floc'h et al. 2006). None of the other GRB host galaxies in my samples are spatially resolved and so their flux densities can be estimated using small circular aperture photometry. For this work my favourite software was Starlink's *GAIA:SkyCat* (Figure 3.2), because of its nifty and very flexible graphical interface. GAIA is an image display and analysis tool whose capabilities fall roughly into three areas: the usual facilities of image display tools; those more astronomically useful ones provided for the analysis of images such as aperture and optimal photometry, contouring, source detection, surface photometry, arbitrary region analysis, celestial coordinate readout, calibration and modification, grid overlays, blink comparison and defect patching; and those for querying on-line resources (catalogues of images and data).

The former[2] Particle Physics and Astronomy Research Council (PPARC)'s

[2] On 1 April 2007 the PPARC merged with the Council for the Central Laboratory of

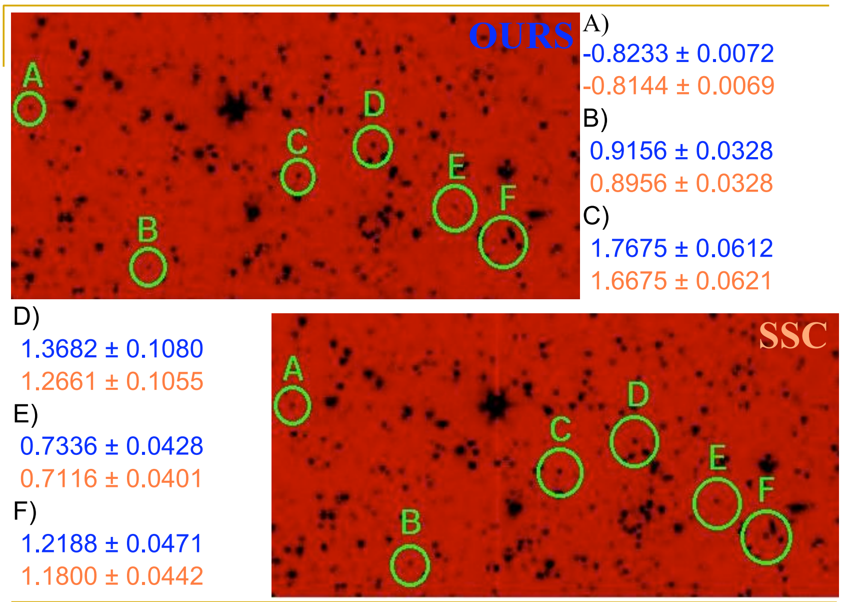

Figure 3.1: Randomly selected area from the field of one of the GRB host galaxies in CC06. Aperture photometry was performed on six field sources with SExtractor. Results presented are fluxes in instrumental units of surface brightness, and turned out to be identical (within errors). Note the column pulldown effect on the brightest object in the image. It was eliminated after reprocessing, but it did not affect the outcome of the photometry on the other sources. **OURS:** My reduced image using the MOPEX software. **SSC:** Official pipeline PostBCD.

Review of Astronomical Software, chaired by Paul Hewett, reported to the Science Committee at the end of April 2005. The Review recommended, amongst other things, that support for core infrastructure and strategic software should continue. The Science Committee declined to accept that recommendation. One consequence of this decision was that Starlink ceased to exist 30 June 2005. The Starlink programming team was disbanded and pro-

---

the Research Councils to form the STFC.

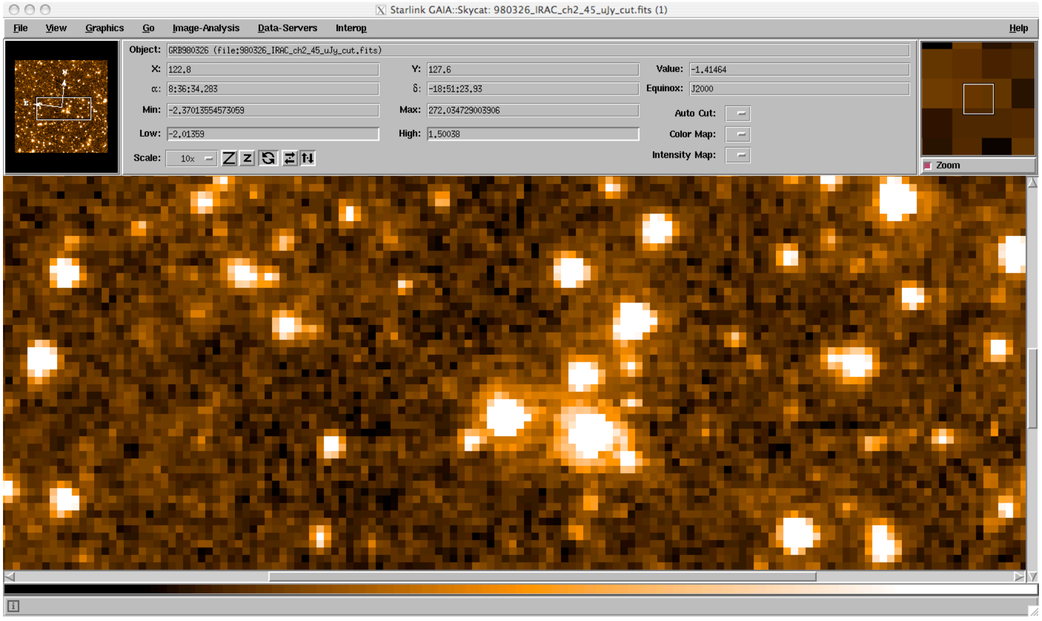

Figure 3.2: Starlink's *GAIA:SkyCat* displaying a region of about $3' \times 1'$ centred around GRB 980326, as seen by IRAC channel 2 (4.5 μm). North is up and East is to the left.

grammer contracts finished at that time. A subset of Starlink software (which includes most of what was being previously distributed) continues to be maintained, with support from the Science and Technology Facilities Council (STFC), for the benefit of the users of the Joint Astronomy Centre (JAC), where Starlink software plays a vital role in its telescopes' data reduction pipelines. Support for non JAC users is provided on a best efforts basis by volunteers and development is open source. The most current version of Starlink can be downloaded from the JAC web site[3]. For the time being it is still possible to access online documentation at the former Starlink web site[4] and at Peter Draper's Home Page[5] (a former Starlink programmer).

[3] `http://starlink.jach.hawaii.edu/`
[4] `http://www.starlink.ac.uk/`
[5] `http://star-www.dur.ac.uk/ pdraper/`

3.3.2 Image preparation: unit conversion

The original images are the PopstBCD FITS mosaics as downloaded from the archive. IRAC can expose all channels simultaneously. They are grouped in pairs: 1 (3.6 μm) and 3 (5.8 μm), 2 (4.5 μm) and 4 (8.0 μ m). Hence, at any given time, channels 1 and 3 will be observing a sky region adjacent to channels 2 and 4. For my data only one pair of channels was exposed for each object so, next to the exposed science images, the FITS contain blank areas corresponding to the unexposed channels. This issue does not apply to the MIPS images.

Images have been cut and extracted with IRAF's *imcopy* (imcopy original_image[X1:X2,Y1:Y2] cut_image.fits) from the original, official pipeline, FITS mosaics, to contain only the science image exposure. Each one is a perfect square (jagged edges have been trimmed). This implies that all the pixels contained in the cut images have been exposed an equal number of times (i.e. observed by all BCD frames used to produce the official pipeline mosaic).

For IRAC, channels 1 and 3, it is a 251 pixels $\times$ 251 pixels [physical coordinates are 91:341,97:347]. For IRAC, channels 2 and 4, it is 251 pixels $\times$ 251 pixels [physical coordinates are 432:682,89:339]. For MIPS, channel 1, it is 176 pixels $\times$ 176 pixels [physical coordinates are 44:219,50:225].

Here are some useful numbers I always keep handy when working with the data:

- All IRAC channels (PostBCD) have square pixels of side $1.2''$ that imply a FoV of $5.02' \times 5.02'$ in my trimmed images.

- IRAC ch 1 (3.550 μm; bandwidth = 0.750 μm), mean FWHM (point source) = 1.66″, gain = 3.3 e-/DN.

- IRAC ch 2 (4.493 μm; bandwidth = 1.015 μm), mean FWHM (point source) = 1.72″, gain = 3.71 e-/DN.

- IRAC ch 3 (5.731 μm; bandwidth = 1.425 μm), mean FWHM (point source) = 1.88″, gain = 3.8 e-/DN.

- IRAC ch 4 (7.872 μm; bandwidth = 2.905 μm), mean FWHM (point source) = 1.98″, gain = 3.8 e-/DN.

- MIPS channel 1 (PostBCD) has square pixels of side 2.45″ that imply a FoV of 6.98′ × 6.98′.

- MIPS ch 1 (23.68/21.9 μm; bandwidth = 4.7 μm). mean FWHM (point source) = 5.9″, gain = 5 e-/DN.

All processed *Spitzer* data are flux calibrated by applying a flux conversion factor derived from observations of calibrator sources. BCD and PopstBCD images are calibrated in physical units of surface brightness (FITS keyword BUNIT = 'MJy/sr' / Units of image data) when downloaded from the archive. To simplify photometry I have changed that to μJy/pixel. I have done so following this procedure:

$$\frac{1\,\mathrm{MJy}}{1\,\mathrm{sr}} \times \frac{1\,\mathrm{sr}}{\mathrm{X\,pixel}} \times \frac{10^{12}\,\mu\mathrm{Jy}}{1\,\mathrm{MJy}}, \tag{3.1}$$

where $1\,\mathrm{MJy} = 10^{12}\,\mu\mathrm{Jy}$; $1''^2 = 2.3504 \times 10^{-11}$ sr; and $1\,\mathrm{sr} = 1/2.350 \times 10^{-11}$ $= 4.255 \times 10^{10''^2}$. Then I calculate the number of pixels per stereoradian in each channel and compute a conversion factor to go from MJy/sr to μJy/pixel:

- For all IRAC channels with PostBCD pixel size = 1.200″; square pixel = 1.440p$''^2$; then $1\,\mathrm{sr} = 4.255 \times 10^{10}/1.440 = 2.955 \times 10^{10}$ pixel. And the CONVERSION_FACTOR = $10 \times 10^{12}/2.955 \times 10^{10} = 33.846$.

- For MIPS channel 1 with PostBCD pixel size = 2.450″; square pixel = 6.003$''^2$; then $1\,\mathrm{sr} = 4.255 \times 10^{10}/6.003 = 7.088 \times 10^{9}$ pixel. And the CONVERSION_FACTOR = $10 \times 10^{12}/7.088 \times 10^{9} = 141.083$.

Finally using IRAF's *imarith*, imarith MJy/sr_image × CONVERSION_FACTOR Jy/pixel_image, yields the imaged flux calibrated in μJy/pixel.

The SSC posted a memo[6] which describes an identical procedure about 2 or 3 months after I developed this section. The SSC memo and this section have essentially the same contents, but were developed independently.

3.3.3 Background gradient

In a few cases (chiefly MIPS images) the pipeline had a less than ideal performance when matching the background brightness of overlapping images. As a result the mosaiced FITS PopstBCD had a significant background gradient which made proper background subtraction for point sources with either a concentric annulus or an off source region problematic (i.e. if the background is irregular and a suitable region to compute the sky value can not be found). For those cases I modelled and subtracted the background from the entire

[6] http://ssc.spitzer.caltech.edu/archanaly/quick.phot

image to remove the gradient. This is done with the subprogramme *Extractor* contained within GAIA (a clone of the Source Extractor software package, SExtractor; Bertin & Arnouts 1996). As a general rule, the fainter the source to be measured, the more one should resist subtracting the background.

How to background subtract with GAIA:

1. From menu *image analysis* click *object detection*, then the *background* tab and select *mesh based*.

2. Typical mesh sizes are 64, 32, 20... the less uniform the background is the smaller you want your mesh size to be, but one is limited by the average object size, as the mesh has to be larger than the average object size. In my case 20 worked well for all the objects in the data at hand.

3. Go to the *checkimage* tab and initially set the checkimage type to *full res. background* to ensure that a suitable background image is produced. Should it be impossible to fit the background because this is very clumpy with sudden variations, i.e. chip gaps, a trick is to cut out those parts of the images which aren't needed.

4. Set the checkimage type to *background subtracted*.

5. Give an appropriate name in check image name (it will show up in the directory from which GAIA was launched).

6. Anything else stays as per the defaults.

I did the following sanity checks to fully understand the process of modelling the background:

- I checked that the noise map (i.e. full res. noise background) contains sigma values (i.e. standard deviation) and must be squared to have variance values that can be added.

- An interpolated model of the background is obtained by setting the checkimage type to *full res. background*.

The likely procedure that Extractor follows is:

1. Subtract objects and produce a background image with holes.

2. Interpolate the background image with holes and produce an interpolated model of the background.

3. During the interpolation produce a noise map by calculating the standard deviation.

I tested this the following way:

1. In an arbitrary sky region (no sources) of an arbitrary image, for 5 pixels adjacent to each other I subtracted (one by one) the background map value from the science image value.

2. Then I calculated the mean.

3. I found that it was approximately the same as the values for those pixels in the noise map.

I repeated the procedure few times. In other words, I assumed, then verified for $n = 5$ that:

$$\sqrt{\frac{\sum_{i=1}^{n}(x_{\mathrm{science}_i} - x_{\mathrm{background}_i})}{n}} \sim x_{\mathrm{noise}_i}, \tag{3.2}$$

for any i that represents a sky pixel in a smoothly varying background. In conclusion, the Extractor noise maps only include uncertainties from the sky, not from the sources. I will not be able to use them later for error estimation because uncertainties would be underestimated.

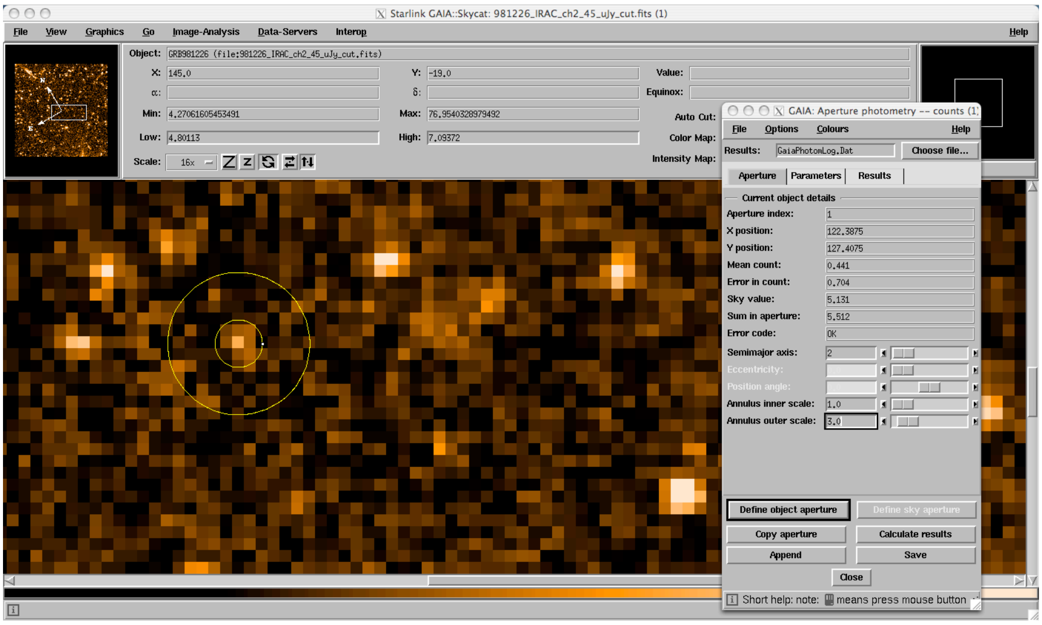

Figure 3.3: Aperture photometry with GAIA's *aperture photometry* tool in data counts on the host galaxy of GRB 981226. The image was obtained by IRAC channel 2 (4.5 μm). North is up and East is to the left.

3.3.4 Doing aperture photometry

I performed aperture photometry on the science images using GAIA's *aperture photometry* tool in data counts (Figure 3.3). This tool estimates noise directly from the data assuming Poisson noise; that means I will later have to convert the mosaic into electron units, so as to calculate the uncertainty due to source shot noise and background correctly. I proceeded as follows:

1. From menu *aperture photometry* I click *results in data counts.*

2. In the *options* submenu I click on the top three options.

3. In the *parameters* tab I click off *perform centroiding* when automatic centroiding fails because the source is too faint; I set "measurement errors use" to *photon statistics* and sky estimator to *mode* (highest degree of rejec-

tion) or *clipped mean* (2^{nd} highest), so when the background annulus is chosen intelligently, i.e. most of it contains no bright pixels, any stars or bright pixels within will be ignored. My choice of photon statistics assumes purely Poissonian errors; a detailed description of GAIA's handling of Poissonian errors may be found in the documentation[7].

4. Finally select the *aperture* tab and perform aperture photometry on an object in the image choosing for the aperture a value from the IDH and MDH aperture correction tables (the larger the better).

To interpret the results correctly one must keep in mind GAIA's awkward labels in the aperture photometry tool. I have found no documentation on this issue and it took me significant effort to *crack* the code, so I will make a record of them here:

1. Mean count = the average for the count value of all pixels within the chosen aperture (for my images this value is in μJy).

2. Error in count = the error for this average, so this is the error of the sum in aperture divided by the number of pixels in the aperture and can not be taken as the error for one pixel (for my images this value is in μJy).

3. Sum in aperture = this one is obvious and dividing this by the mean count yields the number of pixels in the chosen aperture (remember that GAIA can include fractional pixels in an aperture; for my images this value is in μJy).

In other words, get the flux from *sum in aperture* and the error from this twisted operation: error_in_count × (sum_in_aperture / mean_count).

[7]http://www.starlink.rl.ac.uk/star/docs/sun45.htx/node18.html, http://www.starlink.rl.ac.uk/star/docs/sun45.htx/node19.html and http://www.starlink.rl.ac.uk/star/docs/sun45.htx/node38.html

The absolute calibration of *Spitzer* data (IRAC, MIPS 24 μm) uses aperture photometry on a set of stars. In almost all cases these calibration apertures were too large to be fitted in my target fields. For instance, IRAC uses (in all channels) an aperture of radius $12''$ with a background annulus of $24''$, while MIPS utilises (for channel 1, 24 μm) an aperture of radius $35''$ with a background annulus of $50''$. Additionally, these larger apertures do not work well for faint sources. Hence much smaller on source apertures were needed and aperture corrections had to be applied to account for the extended size of the PSF and match the absolute calibration. I employed the aperture correction tables given in the IDH and the MDH. Because I was working on mosaics, in order to be safe I derived sufficient aperture corrections using my own data in CC06, to verify that the accuracy of these tables was acceptable (i.e. the noise introduced was not dominating).

I measured the flux densities over smaller circled areas, typically with a radius of $2''$ for IRAC data and $3''$ for MIPS data. In most cases this allowed me to recover the emission of the host while avoiding contamination from other field sources located nearby. But in a few instances I was suspicious that the nearby field sources might be contaminating my host galaxy photometry. As a sanity check I subtracted those field sources and redid the photometry. Field source subtraction was performed using the detection output image given by SExtracor, where the detected sources were replaced by background noise. The photometry on the field source subtracted images was always consistent with the original aperture photometry.

When a concentric annulus could not be applied (i.e. crowded field, nearby object) to subtract the background, the aperture photometry tool has the capability to do an off source subtraction somewhere else in the image by choosing *define sky aperture* after the option *use annular sky regions* has been ticked off under the menu *options*.

Because the PostCD files are flux calibrated the detector's gain is already accounted for in the photometry. But both the gain and the readout noise are relevant to infer the correct Poissonian error. For the details my readers should see §3.4.2.

3.3.5 Negative flux backgrounds

In a few instances I have encountered PostBCD mosaics with negative fluxes in all their background pixels. It appears as if the reference level for these images, rather than zero, were a negative number. With information from *Spitzer*'s Helpdesk[8] I figured out that what was happening here was that the skydark subtraction removed most of the background. For a source at high Ecliptic latitude, the background at the position of the target is comparable to the zodiacal emission at the position of the subtracted skydark. It could be due to the first frame effect and Fowler sampling as well, especially because the data I use has been taken with repeats.

A reasonable course of action was to add in the zodiacal emission contribution from the skydark to the data, given by the BCD header keyword SKYDRKZB. I did this. An alternative method, which I did not utilise, is to calculate the median of the image, then add a positive number to all the pixels corresponding to this (presumably negative) median to set the background to zero.

[8] help@spitzer.caltech.edu

3.4 Estimating photometric errors

3.4.1 Uncertainty maps

In CC06 I estimated my photometric errors by making use of the uncertainty maps. The PopstBCD uncertainty maps are rough uncertainty estimations and do not include all of the systematic effects associated with the detectors, nor do they include the absolute flux uncertainty. These uncertainty images are generated in the official pipeline as follows. They begin as an estimate of the readout noise (one number in electrons for the whole image) and the shot noise due to the sky (proportional to the square root of the number of electrons in the image). Then each pipeline module propagates the uncertainty image forward, including the uncertainties in dark and flat calibration files. The pipeline modules use the uncertainty image as a way to quantitatively estimate the quality of the sky estimate given by the value of a pixel. In the end, the uncertainty images overestimate the formal uncertainty of the image, because the net propagated uncertainty is much higher than the observed pixel to pixel fluctuations in the images. As a result, my errors are clearly overestimated (this can be easily verified by comparing Table 1 in CC06 and Le Floc'h et al. 2006). The situation was corrected in CC08 devising a new method to estimate the errors.

3.4.2 New method

In CC08 I developed a new method to estimate the photometric errors, based on information recently posted (at that time) in the SSC[9]. As mentioned in

[9] `http://ssc.spitzer.caltech.edu/documents/irac_memo.txt`

§3.3.4 I performed aperture photometry on the science images using GAIA's *aperture photometry* tool in data counts. Because this tool estimates noise directly from the data assuming Poisson noise and my images are μJy/pixel, I need to convert them into electron units, so as to calculate the uncertainty due to source shot noise and background correctly.

In the following lines I derive a correction factor, S, to be applied to the error estimates (assuming a purely Poisson error) given by GAIA (photon statistics) on flux calibrated (μJy/pixel) *Spitzer* images. According to the SOM, the PostBCD mosaics are the result of averaging several individual BCDs. In such setting effective readout noise and gain values must be accounted for:

- **effective RONOISE** = $\sqrt{N}$ × RONOISE,
- **effective GAIN** = N × GAIN.

In other words, one must enter the correct number of frames. The derivation of the correction factor S follows:

1.- $electrons_{source}$ = $electrons_{aperture}$ - $aperture_{fraction}$ x $electrons_{annulus}$

2.- $electrons_{aperture}$ = $flux_{aperture}$ x S

3.- $(\Delta electrons_{source})^2 = (\Delta electrons_{aperture})^2 + (aperture_{fraction} \times \Delta electrons_{annulus})^2$

(since I assumed a Poisson error, for any term: electrons = $\Delta electrons^2$)

4.- $(\Delta electrons_{source})^2$ = $electrons_{aperture}$ + $aperture_{fraction}^2$ x $electrons_{annulus}$ =
= $flux_{aperture}$ x S + $aperture_{fraction}^2$ x $flux_{annulus}$ x S =
= ($flux_{aperture}$ + $aperture_{fraction}^2$ x $flux_{annulus}$) x S

5.- $\Delta electrons_{source}$ = $\sqrt{S}$ x $\sqrt{flux_{aperture} + aperture_{fraction}^2 \times flux_{annulus}}$

6.- $\Delta flux_{source}$ = $\frac{\Delta electrons_{source}}{S}$ = $\frac{1}{\sqrt{S}}$ x $\sqrt{flux_{aperture} + aperture_{fraction}^2 \times flux_{annulus}}$

(where $\sqrt{flux_{aperture} + aperture_{fraction}^2 \times flux_{annulus}}$ = error_in_count x $\left(\frac{sum\_in\_aperture}{mean\_count}\right)$,

using GAIA's notation)

Here is proof that one con go from step 5. To step 6.:

(first an useful reminder: photons = electrons; $\frac{electrons}{gain}$ = counts)

1.- electrons = gain x counts

2.- Δelectrons = $\sqrt{electrons}$ = $\sqrt{gain \times counts}$ (assuming a purely Poissonian error)

3.- Δelectrons = $\sqrt{\left(\frac{\partial electrons}{\partial counts} \times \Delta counts\right)^2}$ = gain x Δcounts (get error from derivatives)

Now equate 2. And 3.:

4.- $\sqrt{gain \times counts}$ = gain x Δcounts ➔ Δcounts = $\sqrt{\frac{counts}{gain}}$

5.- $\frac{\Delta electrons_{source}}{S} = \Delta flux_{source}$ Q.E.D.

And so the final error estimate is given by:

$$\sqrt{\left[\frac{\sqrt{TOTALBCD \times AREA \times RONOISE^2}}{TOTAL\_FRAMTIME \times S}\right]^2 + \left[\frac{ERROR\_IN\_COUNT \times \left(\frac{SUM\_IN\_APERTURE}{MEAN\_COUNT}\right)}{\sqrt{TOTAL\_FRAMTIME \times S}}\right]^2}$$
$$\times APERTURE\_CORRECTION \times SYSTEMATICS$$

where:

TOTALBCD = number of BCD frames used in the mosaic (PBCD header keyword; dimensionless)

AREA = sum of the areas of the aperture and the annulus used for the photometry (πR^2 with R in pixels; units = pixels)

RONOISE = read out noise (BCD header keyword or SOM ; units = e)

TOTAL_FRAMTIME = FRAMTIME multiplied by TOTALBCD (units = s)

FRAMTIME = exposure time of one BCD frame (BCD header keyword or Spot AOR; unit = s)

S = GAIN / (SCALE × FLUXCONV) (units = e/μJy*s)

GAIN = (PBCD header keyword or SOM ; units = e/DN)

SCALE = my calculations to go from MJy/sr to μJy/pixel (homepage; units = sr*μJy/pixel*MJy)

FLUXCONV = conversion factor to go from DN/s to MJy/sr (PBCD header keyword or IDH and MDH; units = MJy/sr / DN/s)

ERROR_IN_COUNT = given by GAIA

SUM_IN_APERTURE = given by GAIA

MEAN_COUNT= given by GAIA

APERTURE_CORRECTION = (IDH and MDH)

SYSTEMATICS = to account for systematics multiply by 1.3 – 1.5 (dimensionless)

3.5 Corollary

To close this chapter I should add that I rechecked some of my photometric results with SExtractor. I also recalculated others by hand using GAIA's *image regions* tool. This tool allows to perform statistical calculations on arbitrarily defined regions in an image, and I could effectively mimic the aperture photometry tool. Finally, the photometry in CC06 has been published independently by Le Floc'h et al. (2006). Consistency was the norm, as I was able to reproduce their numbers. So I consider my photometry very well validated.

Chapter 4

Low $M_\star$, high specific SFRs and dust extinction

This chapter is based on CC06 and CC08, two complementary papers which have been included as part of my Dissertation in Appendices B and C respectively. The purpose of this chapter is to highlight the most relevant aspects of the work done in CC06 and CC08. In those papers I studied the properties (i.e. total stellar mass, obscured and unobscured star formation rate and extinction) of GRB host galaxies using MIR observations. I found that GRB hosts have low total stellar masses, high specific star formation rates and, at least a fraction of them, are extinguished by dust.

Today it is central for cosmology to map the build up of cosmic structure and star formation. And it is currently debated how GRB hosts relate to other populations of star forming galaxies. Using *Spitzer*'s IRAC and MIPS data, together with optical, NIR, submm and radio observations, I am contributing to establish the relationship of GRB hosts with several star

TABLE 4.1— Hosts: flux densities, star formation rates, dust and stellar masses

GRB Host	Redshift z	Redshift Ref.	$f_{4.5\,\mu m}$[a] (μJy)	$f_{8.0\,\mu m}$[a] (μJy)	$f_{24\,\mu m}$[a] (μJy)	SFR[b] ($M_\odot\,yr^{-1}$) UV$_{cont}$	SFR Ref.	SFR L_{8-1000}	M_{dust} ($10^7 M_\odot$)	$M_\star$ ($10^9 M_\odot$)
970508	0.83	1	<3.1	<17	<82	2.5[c]	7	0.4–26	0.3–1.1	1.5
970828	0.96	2	3.9 ± 1.1	<18	94 ± 17	1.1[d]	2	30 ± 8	1.3	2.5
980613	1.10	3	37 ± 1	33 ± 8	169 ± 36	70[c]	7	428 ± 51	19	31
980703	0.97	4	11 ± 2	<24	<85	30[c]	7	3.8–226	2.7–10	7.2
981226	1.11	5	4.5 ± 1.4	<31	<87	1.2[d]	5	1.0–84	0.7–3.7	3.9
990705	0.84	6	19 ± 1	<18	159 ± 31	∼5[d]	6	4.5–173	3.2–7.7	9.2

References. — (1) Bloom et al. 1998; (2) Djorgovski et al. 2001; (3) Djorgovski, Bloom & Kulkarni 2003; (4) Djorgovski et al. 1998; (5) Christensen et al. 2005; (6) Le Floc'h et al. 2002; (7) Chary et al. 2002; for reasons of brevity and economy of space the references in this table have not been included in the Bibliography, rather they can be found at CC06, which is included in Appendix B.

[a] Upper limits are quoted at the 3σ level, while errors are 1σ.
[b] We have corrected all the SFRs quoted to account for differences in their IMF scales with respect to our choice of a Salpeter IMF (0.1–100 $M_\odot$; Salpeter 1955).
[c] Corrected using the β slope technique (Chary et al. 2002, and references therein), typically larger than the Balmer lines decrement correction.
[d] Uncorrected for internal extinction; Christensen et al. 2005 argue for no extinction in the host of GRB 981226.

forming galaxy populations. In CC06 I analysed 4.5, 8 and 24 μm band *Spitzer* images of a small sample of GRB host galaxies at redshifts close to 1. I constrained their unobscured star formation rates (SFRs) based on the entire available spectral energy distributions (SEDs) and estimated their total stellar masses ($M_\star$) based on rest frame K band luminosities (see Table 4.1). In CC08 I analysed IRAC images for a larger GRB host sample with a range of redshifts. I estimated their obscured SFRs based on the rest frame UV continuua and determined their $M_\star$ by interpolating the rest frame K band luminosities (see Table 4.2). Throughout the chapter I have assumed an $\Omega_m = 0.3$, $\Omega_\Lambda = 0.7$ cosmology with $H_0 = 70\,\mathrm{km\ s^{-1}\ Mpc^{-1}}$.

SFRs ranged from a fraction of a $M_\odot\,\mathrm{yr}^{-1}$ to tens in CC08 (obscured) and hundreds (unobscured) in CC06. Similarly, the span of $M_\star$ in CC08 was $10^7\,M_\odot < M_\star < 10^{11}\,M_\odot$, and a bit shorter in CC06 owed to the smaller sample.

TABLE 4.2— Hosts: flux densities, total stellar masses, and star formation rates

GRB Host	Redshift		IRAC		$K_{\rm rest}$ (21 980 Å)		$M_{\star(K)}$	UV$_{\rm rest}$ (2 800 Å)		SFR$_{\rm (UV)}$
	z	Ref.	f_ν (μJy)	Ch.	f_ν (μJy)	Refs.	($10^9\,M_\odot$)	f_ν (μJy)	Refs.	($M_\odot$ yr^{-1})
(1)	(2)		(3)		(4)		(5)	(6)		(7)
970228	0.70	1	<3.7	1	<4.2	‡, 30	<5.7	0.34 ± 0.16	48	0.60 ± 0.28
970508	0.83	2	<2.1[a]	2	<1.8	31, 30	<3.5	0.28 ± 0.15	48	0.71 ± 0.38
970828	0.96	3	3.9 ± 0.3[a]	2	3.7 ± 0.3	31, 3	9.5 ± 0.9	<0.44	34	<1.5
980326	∼1.0	4	<2.7	2	<2.6	‡, 30	<7.1	<0.015	49	<0.056
980425	0.0085	5	2 977 ± 101	2	6 389 ± 395	‡[b], 32	1.1 ± 0.1	1 748 ± 173	‡[c], 50	0.39 ± 0.04
980613	1.10	6	38 ± 1[a]	2	42 ± 1	31, 6	142 ± 3	0.83 ± 0.11	6, 30	3.6 ± 0.5
980703	0.97	7	11 ± 1[a]	2	11 ± 1	31, 33	29 ± 2	3.2 ± 0.1	48	10.9 ± 0.3
981226	1.11	8	4.5 ± 0.5[a]	2	4.6 ± 0.5	31, 8	16 ± 2	0.27 ± 0.03	8	1.2 ± 0.1
990506	1.31	9	2.0 ± 0.7	2	2.0 ± 0.8	‡, 34	9.3 ± 3.8	0.20 ± 0.04	34	1.2 ± 0.2
990705	0.84	10	19 ± 1[a]	2	18 ± 1	31, 10	36 ± 2	∼1.8 ± 0.3	10	∼4.7 ± 0.8
000210	0.85	11	3.3 ± 2.0	2	3.2 ± 1.8	‡, 35	6.4 ± 3.6	0.79 ± 0.07	48	2.1 ± 0.2
000418	1.12	9	4.8 ± 1.8	2	5.0 ± 1.9	‡, 36	17 ± 7	1.33 ± 0.04	48	6.1 ± 0.2
000911	1.06	12	<4.3	2	<4.3	‡, 37	<13	0.33 ± 0.08	37	1.4 ± 0.3
010921	0.45	13	11 ± 2	1	12 ± 2	‡, 13	6.5 ± 0.9	2.2 ± 0.1	48	1.6 ± 0.1
020405	0.69	14	<5.4	1	<5.3	‡, 38	<7.0	2.1 ± 0.1	38	3.7 ± 0.2
020813	1.26	15	<2.5	2	<2.6	‡, 38	<11	0.41 ± 0.08	34, 38	2.3 ± 0.5
020819B	0.41	16	97 ± 2	1	104 ± 7	‡, 16	47 ± 3	4.3 ± 2.6	16	2.6 ± 1.5
021211	1.01	17	<2.2	2	<2.2	‡, 38	<6.1	0.20 ± 0.04	38	0.72 ± 0.15
030328	1.52	18	<29	3	<27	‡, 39	<170	0.56 ± 0.08	39	4.6 ± 0.6
030329	0.17	19	<4.9	1	<5.1	‡, 40[d]	<0.37	1.5 ± 0.2	40	0.14 ± 0.02
030429[e]	2.66	20	<7.0	4	<7.3	‡, 20	<124	<0.060	20	<1.3
030528[e]	0.78	21	<4.6	1	<3.8	‡, 41	<6.5	7.2 ± 1.4	41	16 ± 3
031203	0.11	22	216 ± 3[f]	1	192 ± 13[f]	‡, 42	5.3 ± 0.4	119 ± 39[f]	51	4.3 ± 1.4
040924	0.86	23	<2.9	1	<3.2	‡, 38	<6.5	<1.1	38	<2.9
041006	0.72	24	<2.9	1	<3.1	‡, 38	<4.4	<0.98	38	<1.8
050223	0.58	25	18 ± 2	1	18 ± 2	‡, 25	17 ± 1	<8.1	25	<10
050525A	0.61	26	<1.6	1	<1.6	‡, 43	<1.6	<0.48	43	<0.64
060218[e]	0.03	27	· · ·	· · ·	20 ± 6	44	0.052 ± 0.015	15 ± 3	52	0.053 ± 0.010
060505	0.09[g]	28	· · ·	· · ·	298 ± 10	45	5.8 ± 0.2	75 ± 6	‡[c], 45	1.9 ± 0.2
060614	0.13	29	· · ·	· · ·	3.8 ± 0.7	46, 47	0.15 ± 0.03	0.37 ± 0.13	53	0.019 ± 0.006

References. — ‡ This Dissertation; (1) Bloom et al. 2001; (2) Bloom et al. 1998; (3) Djorgovski et al. 2001; (4) Bloom et al. 1999; (5) Tinney et al. 1998; (6) Djorgovski et al. 2003; (7) Djorgovski et al. 1998; (8) Christensen et al. 2005; (9) Bloom et al. 2003; (10) Le Floc'h et al. 2002; (11) Piro et al. 2002; (12) Price et al. 2002a; (13) Price et al. 2002b; (14) Price et al. 2003; (15) Barth et al. 2003; (16) Jakobsson et al. 2005b; (17) Vreeswijk et al. 2003; (18) Maiorano et al. 2006; (19) Hjorth et al. 2003; (20) Jakobsson et al. 2004; (21) Rau et al. 2005; (22) Prochaska et al. 2004; (23) Wiersema et al. 2004; (24) Soderberg et al. 2006; (25) Pellizza et al. 2006; (26) Foley et al. 2005; (27) Pian et al. 2006; (28) Colless et al. 2001; (29) Della Valle et al. 2006a; (30) Chary et al. 2002; (31) Castro Cerón et al. 2006; (32) Le Floc'h et al. 2006; (33) Vreeswijk et al. 1999; (34) Le Floc'h et al. 2003; (35) Gorosabel et al. 2003a; (36) Gorosabel et al. 2003b; (37) Masetti et al. 2005; (38) Wainwright et al. 2007; (39) Gorosabel et al. 2005a; (40) Gorosabel et al. 2005b; (41) Rau et al. 2004; (42) Malesani et al. 2004; (43) Della Valle et al. 2006b; (44) Kocevski et al. 2007; (45) Thöne et al. 2008; (46) J. Hjorth 2008, priv. comm.; (47) Cobb et al. 2006; (48) Christensen et al. 2004; (49) Bloom et al. 2002; (50) Michałowski et al. 2008, in prep.; (51) Margutti et al. 2007; (52) Sollerman et al. 2006; (53) Mangano et al. 2007; for reasons of brevity and economy of space the references in this table have not been included in the Bibliography, rather they can be found at CC08, which is included in Appendix C.

Note. — Because host positions are well determined from previous broadband imaging, I quote upper limits at the 2σ level, while errors are 1σ. I have corrected all (UV, optical, NIR, and MIR) flux densities and magnitudes in this table (including those in the table notes) for foreground Galactic dust extinction. To correct the IRAC wavebands I follow Lutz (1999). For the UV, optical and NIR passbands I use the DIRBE/IRAS dust maps (Schlegel et al. 1998). I adopt a Galactic dust extinction curve A_λ/A_V, parameterized by $R_V \equiv A_V/E(B-V)$, with $R_V = 3.1$ (Cardelli et al. 1989). Col. (3): My photometry of *Spitzer*'s IRAC, publicly available, archival data. Channel 1 = 3.6 μm; channel 2 = 4.5 μm; channel 3 = 5.8 μm; channel 4 = 8.0 μm. Col. (4): Interpolated flux densities for the rest frame K band. The data used were obtained from these references. Col. (5): $M_\star$ derived from the rest frame K band flux densities listed in column (4), with $M_\star/L_{K_{\rm rest}} = 0.4\,M_\odot/L_\odot$. Col. (6): Interpolated flux densities for the rest frame UV continuum. The data used were obtained from these references. Col. (7): Unobscured SFRs derived from the rest frame UV continuum flux densities listed in column (6).

[a] Flux density values are taken from Castro Cerón et al. (2006); I refine their error estimates.
[b] My photometry of 2MASS XSC Final Release (Two Micron All Sky Survey Extended Source Catalog; released 25 March 2003; Jarrett et al. 2000; `http://www.ipac.caltech.edu/2mass/`), NIR ($K_{\rm S}$ band) archival data for galaxy ESO 184-G082 ($f_{21\,739\,\text{Å}}$ = 6 510 μJy ± 406 μJy).
[c] My photometry of *GALEX* (Galaxy Evolution Explorer; Martin et al. 2003, 2005; `http://galex.stsci.edu/`), UV archival data for the host galaxies of GRBs 980425 ($f_{2\,267\,\text{Å}}$ = 1 592 μJy ± 162 μJy) and 060505 ($f_{2\,267\,\text{Å}}$ = 72 μJy ± 10 μJy).
[d] K band is the closest passband, blueward of IRAC, for which this host has data available in the literature. It is a poorly constrained upper limit. I make use of it nevertheless, for methodological consistency. But I note that in this particular case, given the low redshift of the host, a much closer representation of reality is provided by the lower limit $M_\star = 6.4 \times 10^7\,M_\odot$ (extrapolated from J band and H band data). This value is fully consistent with those cited by Thöne et al. (2007) and references therein.
[e] X-ray flash.
[f] Because of the low Galactic latitude ($b = -4.6°$) of this host I correct for dust extinction overestimates. Following the recommendation by Dutra et al. (2003) I scale the Schlegel et al. (1998) reddening value multiplying by 0.75 and adopt $E_{\rm MW}(B-V)$ = 0.78 mag. The UV flux density error (column 6) contains the additional 25% uncertainty estimated by Margutti et al. (2007).
[g] Redshift of the 2dFGRS Public Database (Two Degree Field Galaxy Redshift Survey; `http://magnum.anu.edu.au/~TDFgg/`), archival data for galaxy TGS173Z112.

4.1 Data and samples

I initiated this project motivated by the existence of unpublished *Spitzer* archival data on GRB host galaxies (at least two IRAC channels for each host plus MIPS 24 μm). The data I analysed in CC06 was published as well by Le Floc'h et al. (2006), as part of a larger dataset. The data I analysed in CC08 comes from several programmes and it is, as of this writing, unpublished.

4.1.1 CC06

The study of the host galaxies of GRBs helps our understanding of massive star formation, as well as gives us clues to the nature of the GRB progenitors. With this idea in mind I selected, among the 16 GRB hosts available in the archive at that time those with redshifts close to 1. The rationale was two fold: it has been argued that the global SFR peaks about this redshift (Madau et al. 1998); and at $z \sim 1$ the observed 4.5 μm waveband maps directly onto the rest frame K passband, which is closely related to a galaxy's $M_\star$ and thus a reliable estimator (Glazebrook et al. 2004). Given the small size of the sample available it was easy to discriminate those close to $z \sim 1$ (it resulted in a subsample of 6) from those not. The range of redshifts spanned was $z = 1^{+0.11}_{-0.17}$. Each of my selected hosts was imaged with both IRAC and MIPS. IRAC observations were in channel 2 (4.5 μm; 300 s per host) and channel 4 (8.0 μm; 300 s per host). MIPS observations were in channel 1 (24 μm; 420 s per host).

As noted in §3.2 I used official *Spitzer* PostBCD, carefully verified with my own reductions. Host extraction was based on archival imagery world coordinate system calibration and visually confirmed with optical and or NIR comparison images from the literature. The median separation between the host centroid in each *Spitzer* image and the best set of coordinates published was less than $1''$. This separation was good enough to identify each host without confusion issues. I measured the flux densities over a circled area of radius 2 pixels in IRAC and 3 pixels in MIPS. Aperture corrections were then applied to account for the extended size of the PSF (see §3.3.4). My photometry (see Table 4.1) is consistent with Le Floc'h et al. (2006).

4.1.2 CC08

Here the sample was enlarged to 30 GRBs. It benefited from the increased number of public data as the *Spitzer* mission progressed (up to and including October 2007). This larger sample allowed me for a more robust statistical analysis, as well as to probe the distribution of $M_\star$ in redshift space. To select the sample I required each host to be included in the sample to have rest frame K band data available (for the purposes of this work I define $K \equiv 2.2\,\mu\mathrm{m} \pm 0.3\,\mu\mathrm{m}$); thus the $M_\star$ estimator is well calibrated (Glazebrook et al. 2004). Out of the 30, 24 hosts were included because they had been observed with IRAC, while other 6 very low redshift ones where included because they had ground based K band observations. The availability of the redshift was also necessary for a host to be included. The sample is presented in Table 4.2, with the flux density measurements and upper limits given in column (3). I find that, of those hosts in the sample observed with channel 1, about 36% are detected. For channel 2 the rate is about 64%. This is roughly of the same order as the detection rate by Le Floc'h et al. (2006) with IRAC channel 2 (44%).

Because hosts in this sample come from different programmes, exposure times varied, yet a majority was observed in a series of 12 thirty second exposures. Astrometric and photometric procedures in CC08 where just as described for CC06 in §4.1.1.

4.2 Methodology

4.2.1 CC06: spectral energy distribution fits

In CC06 the sample SEDs were fitted[1] with observational templates. Photometry included my *Spitzer* flux densities and data points from the literature, spanning from optical to radio wavelengths (see the caption in Figure 4.1). The observational templates used to scale the SED data included: Arp 220, an archetypal ultraluminous IR galaxy (ULIRG); NGC 6946, a well characterised, blue, star forming galaxy (both Silva et al. 1998); and 64 SED templates ranging from starbursts to quiescent ones (Dale et al. 2001; Dale & Helou 2002). The spectral width of the different bandpass filters was taken into account. Fitting was evaluated by means of a weighted least squares method.

Figures 4.1 through 4.6 show the models. Each figure caption describes the details of the fit. The Dale et al. (2001) and Dale & Helou (2002) templates yielded SFR values between those of the Arp 220 and NGC 6946 mo-

[1]My coauthor M.J. Michałowski did the fitting of the sample SEDs with observational templates. A description of the procedure is included here only for the sake of completion.

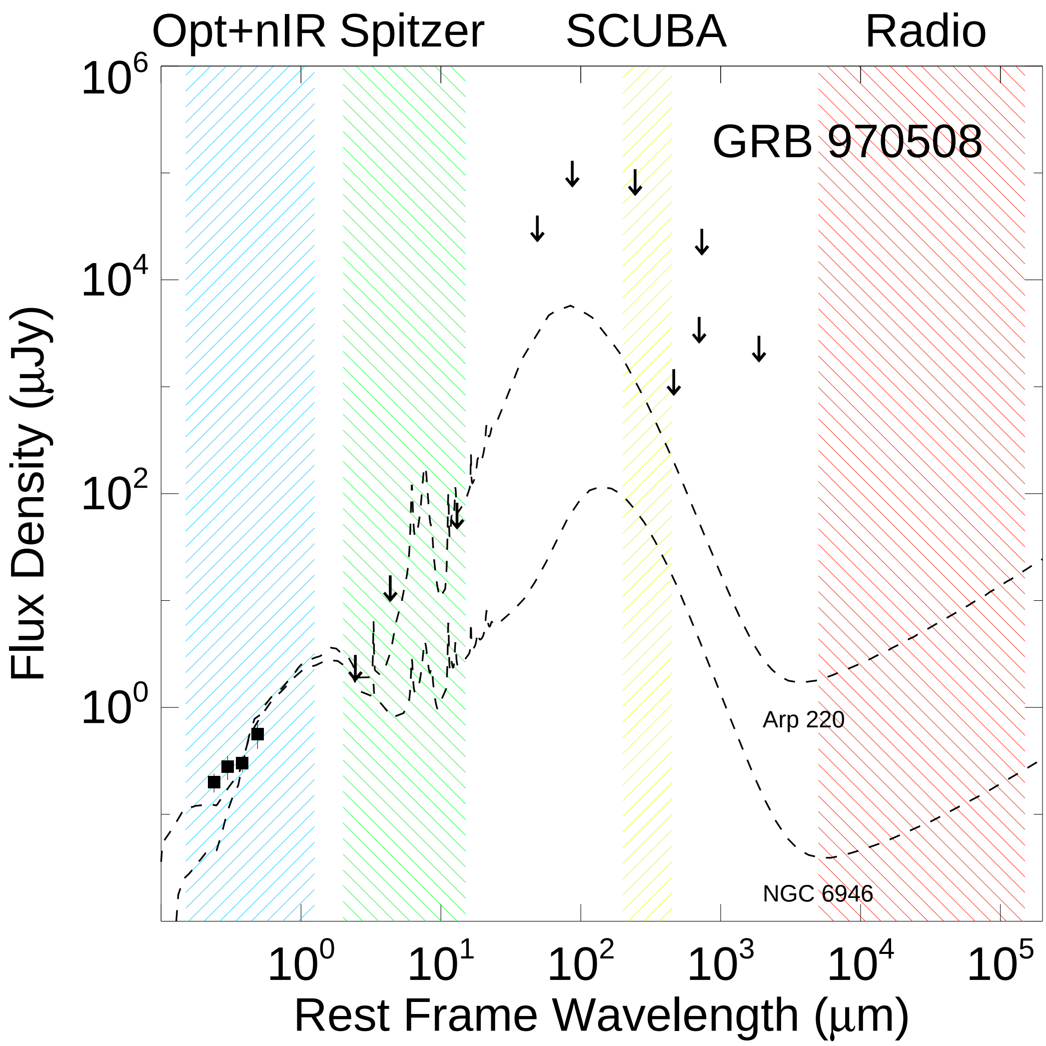

Figure 4.1: SED fits of the host of GRB 970508. Results were inconclusive as I could not discriminate a best fitting SED template. Model degeneracy was expected because I only have optical/IR data available. Filled squares: Detections (error bars within the squares). Arrows: 3σ upper limits (value marked by the base of the arrow). For each host in my sample I plotted the fit to the template that yielded the highest (Arp 220) and the lowest (NGC 6946) star formation rate value. For Figures 4.1 through 4.6: solid lines = best fit; dashed lines = fits I could not discriminate between; dotted lines = fits inconsistent with the data, shown for illustrative purposes. Data points: Optical/near-IR from Vreeswijk et al. (1999), Sokolov et al. (2001), Djorgovski et al. (2001), Le Floc'h et al. (2002), and Christensen et al. (2005). Thermal IR from my photometry of *Spitzer* archival data. FIR from Hanlon et al. (2000). Submillimeter from Smith et al. (1999), Tanvir et al. (2004), and our photometry of SCUBA archival data. Radio from Bremer et al. (1998), Shepherd et al. (1998), Berger et al. (2001), Djorgovski et al. (2001), and Berger et al. (2003). (*Adapted from CC06; for reasons of brevity and economy of space the references in this figure have not been included in the Bibliography, rather they can be found at CC06, which is included in Appendix B.*)

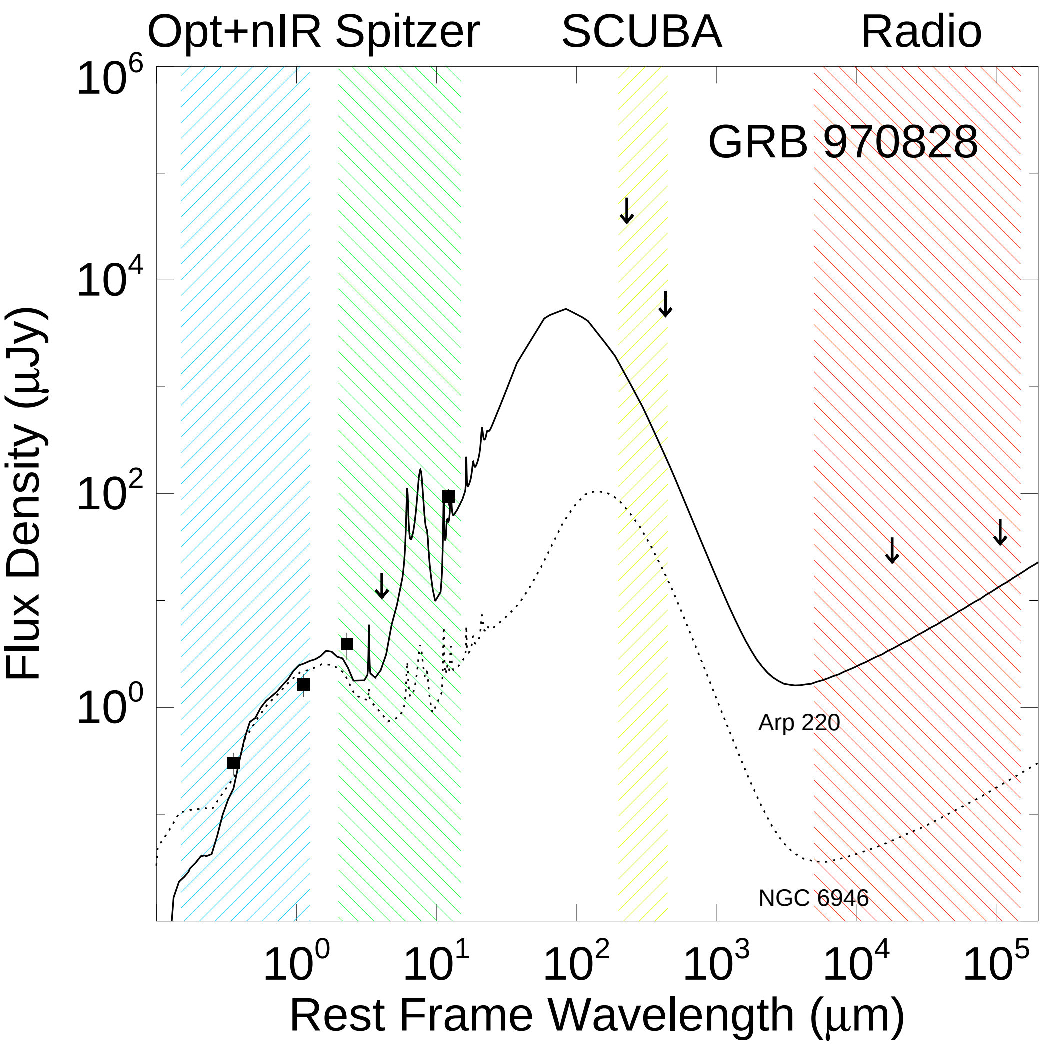

Figure 4.2: SED fits of the host of GRB 970828. Arp 220 was the best fitting SED template. This is a galaxy with a moderate star formation rate (Le Floc'h et al. 2006). (*Symbols, SED templates and references are the same as in Figure 4.1.*)

dels for all the hosts in the CC06 sample. For each host we may be fitting subcomponents that differ in their properties (Charmandaris et al. 2004). For instance, for GRB 980613 some components detected in the optical/near IR bands (Hjorth et al. 2002; Djorgovski et al. 2003) are offset by >2.5″ from the *Spitzer* centroid (Le Floc'h et al. 2006). While such effects might induce

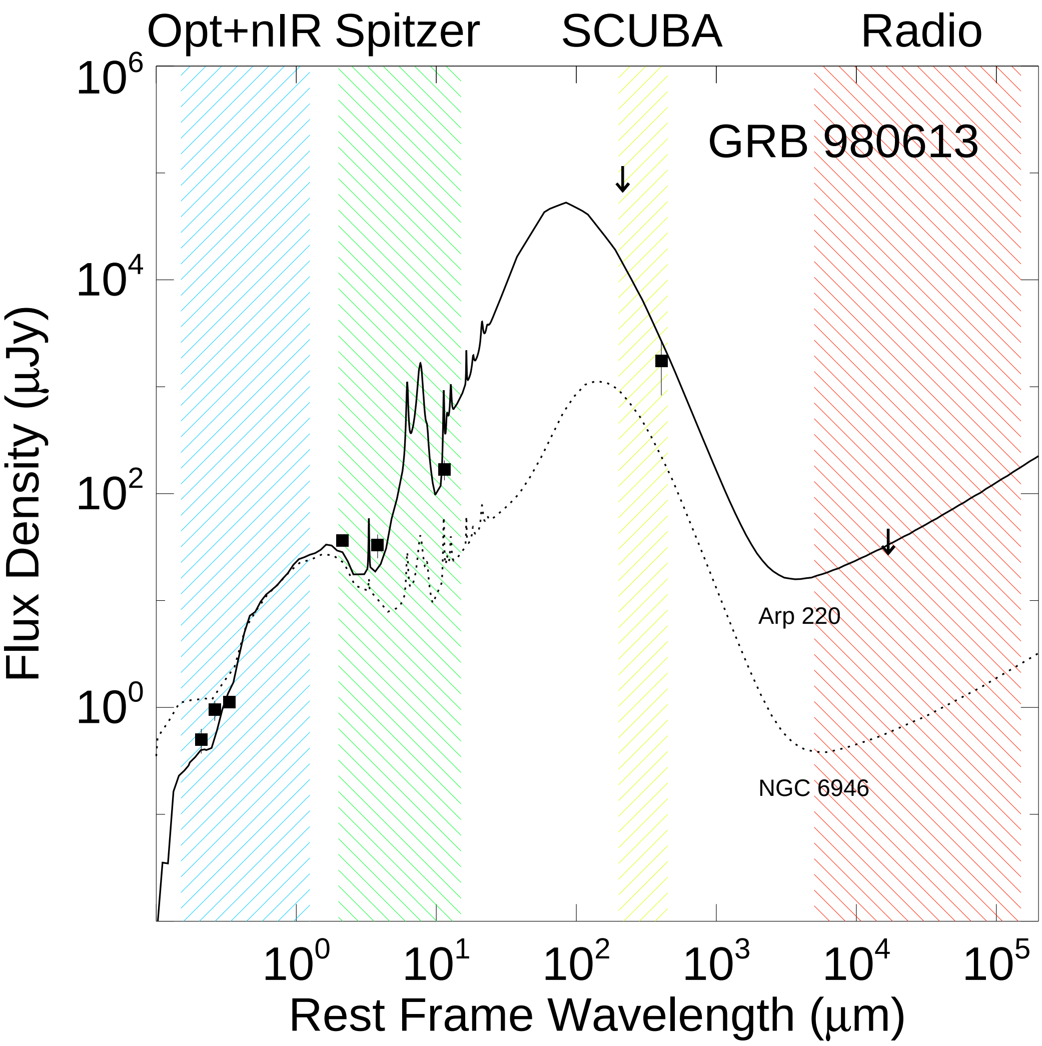

Figure 4.3: SED fits of the host of GRB 980613. Arp 220 was the best fitting SED template. This is a galaxy with a high star formation rate; the value I derive is ∼5 times higher than the one given by Le Floc'h et al. (2006). (*Symbols, SED templates and references are the same as in Figure 4.1.*)

some scatter in the SEDs we can still utilise the SED templates as powerful diagnostic tools for the SFRs of the sample.

I should note here that at the time CC06 was finished my coauthors and I were convinced that the SFR upper limits in GRBs 980703 (Figure 4.4) and 990705 (Figure 4.6) were a close representation of reality, and that all that

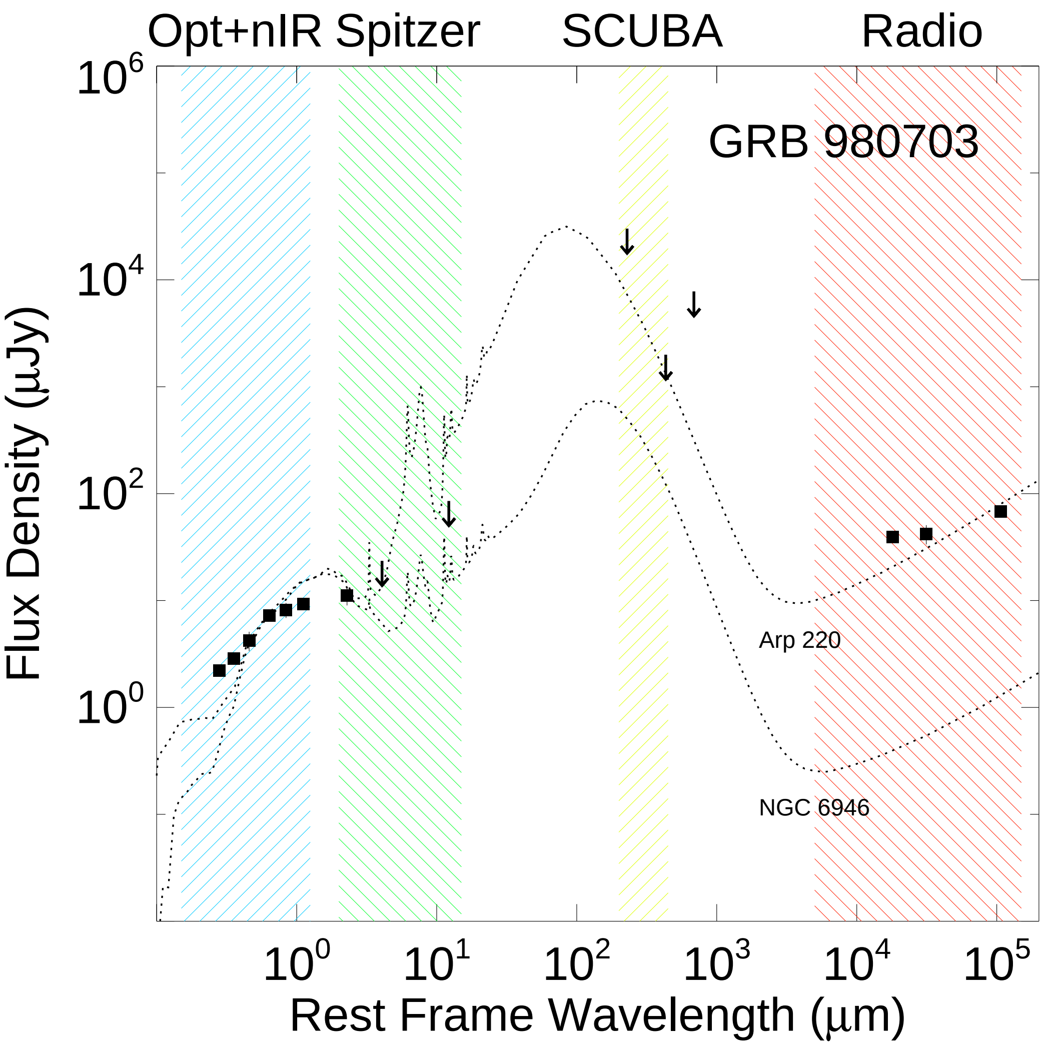

Figure 4.4: SED fits of the host of GRB 980703. None of the SED templates used could be fitted. Arp 220 approximates well the radio flux density, but it is inconsistent with the upper limit at 24 μm. In turn, NGC 6946 fits the upper limit at 24 μm, but it underestimates the radio flux density. Reproducing the SEDs of these galaxy is problematic and may require dust with properties different from those in the CC06 templates. (*Symbols, SED templates and references are the same as in Figure 4.1.*)

was required for a proper fit were more sophisticated modelling which tweaked the dust properties. Now we have evidence of this to be the case for GRB 980703. Michałowski et al. (2008) modelled the SED of this burst and obtai-

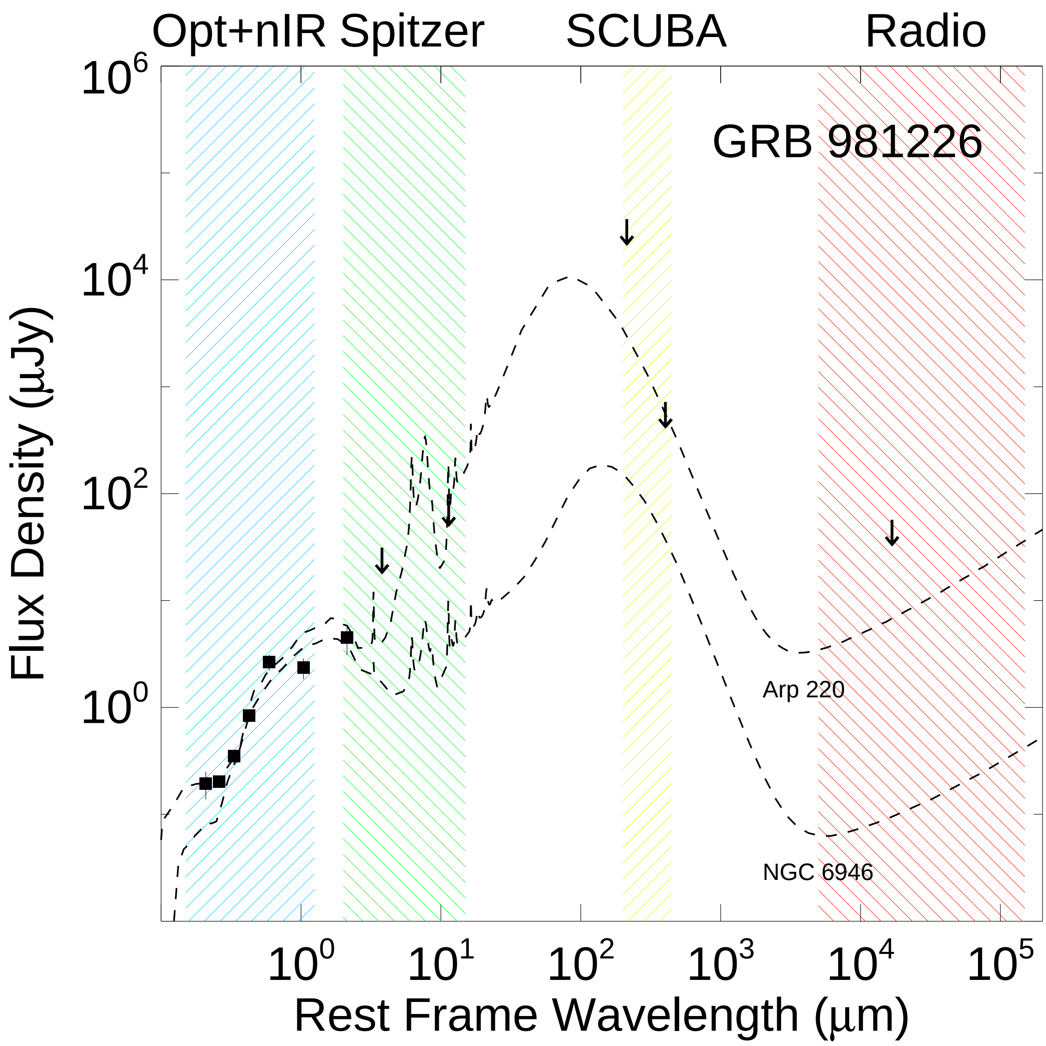

Figure 4.5: SED fits of the host of GRB 981226. Results were inconclusive as I could not discriminate a best fitting SED template. Model degeneracy was expected because I only have optical/IR data available. (*Symbols, SED templates and references are the same as in Figure 4.1.*)

ned $M_\star = 212\,M_\odot\,\mathrm{yr}^{-1}$, a remarkable agreement with our upper limit SFR.

4.2.2 CC08: interpolations

In CC06 I applied a relaxed criterion to the rest frame K band flux densities,

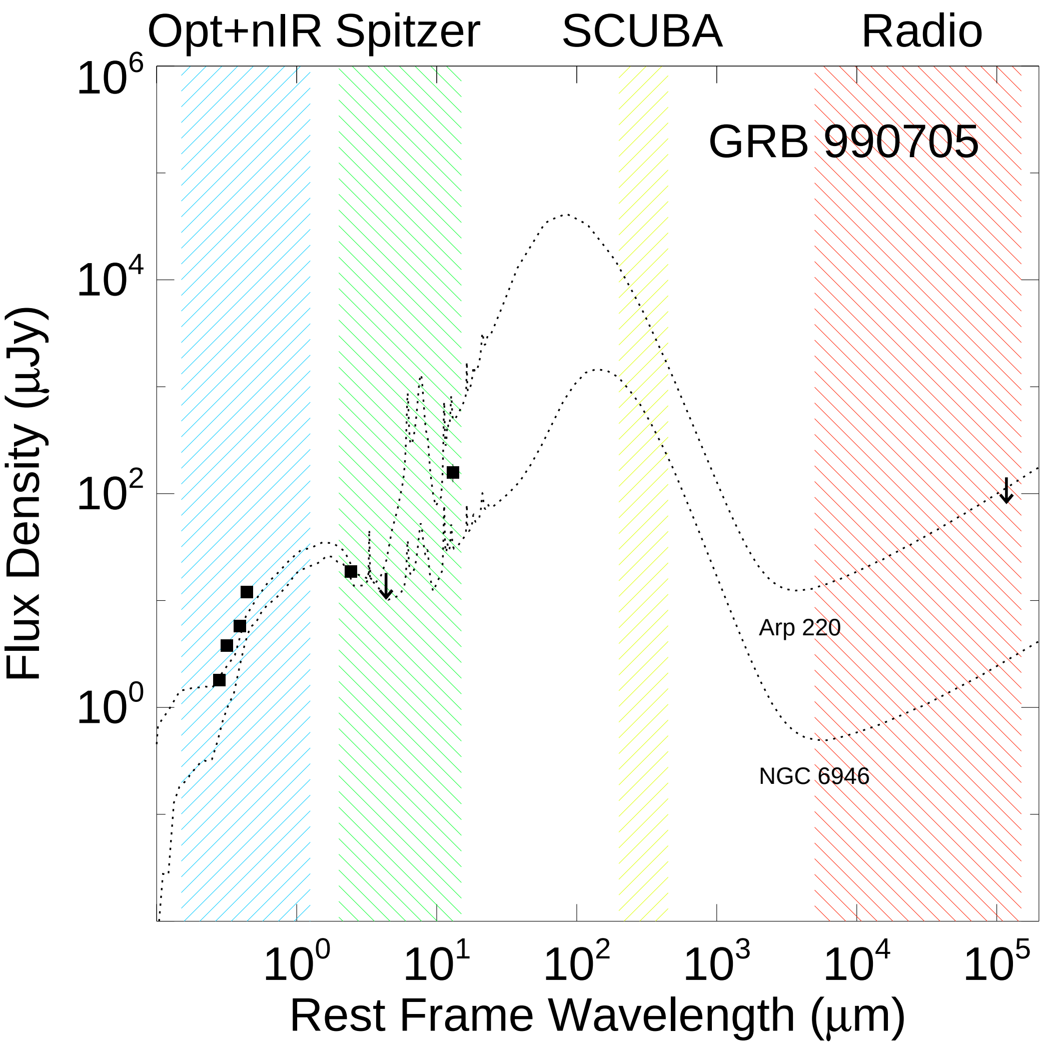

Figure 4.6: SED fits of the host of GRB 990705. None of the SED templates used could be fitted. Arp 220 overestimates the flux density at 24 μm and it is inconsistent with the upper limit at 8 μm. In turn, NGC 6946 underestimates the flux density at 24 μm. Reproducing the SEDs of these galaxy is problematic and may require dust with properties different from those in the CC06 templates. (*Symbols, SED templates and references are the same as in Figure 4.1.*)

allowing the mapped wavelengths to span a range proportional to the redshifts. This yielded acceptable results because all redshifts in the sample were near 1. Given the larger redshift range in CC08 I applied a more strict criteron. For each GRB host I computed the flux density at the central wavelength (§4.1.2) of the rest frame K band by linearly interpolating in log space. I interpolated between the IRAC channel and the closest passband, blueward of IRAC, for which data are available. In a few cases the IRAC waveband corresponds to a rest frame wavelength shorter than K band, then I extrapolated. The rest frame K band flux densities are shown in Table 4.2, column (4). The references where I obtained the optical/NIR data from are given along. In the same fashion I computed, for each host, the rest frame UV continuum (2 800 Å; Kennicutt 1998) flux density. I either interpolate between the two closest passbands, with data available, that bracket the rest frame UV continuum or, when all available data falls redward of 2 800 Å, I extrapolated. These results are shown in Table 4.2, column (6). For the cases with upper limits to $M_\star$ I estimated a conservative lower limit, by extrapolating a flat spectrum ($f_\nu \propto \nu^0$) from the reddest NIR/optical detection available (references in Table 4.2, column 4; see Figures 4.7 and 4.8).

Flux densities in CC06 were not corrected for extinction. In CC08 all flux densities are corrected for foreground Galactic dust extinction (see Table 4.2 notes for the details).

4.3 Star formation rates

4.3.1 Calculations

In CC06 the SED fitting models were utilised to calculate the unobscured SFRs for each GRB host, based on the hosts IR luminosities. I converted the host flux densities into luminosity densities by means of applying Hogg et al. (2002):

$$L_\nu(\nu_{\rm rest}) = \frac{4\pi D_L^2 f_\nu(\nu_{\rm observed})}{1+z}, \tag{4.1}$$

where D_L is the luminosity distance. Then the SED templates were scaled to match the data points. IR luminosities (L_{8-1000}) were obtained integrating under the scaled SED templates from 8 to 1 000 μm (rest frame). This wavelength range was chosen so the SFRs could be computed using Kennicutt (1998):

$$SFR(M_\odot\,{\rm yr}^{-1}) = 4.5\times10^{-44} L_{\rm IR}\,{\rm erg\,s^{-1}}. \tag{4.2}$$

The results are summarised in Table 4.1. Errors quoted are statistical and assume the template is a good representation of the data. In addition there may be significant systematic errors related, for example, to how well the template represents the actual SED (Michałowski et al. 2008), the L_{8-1000} to SFR conversion (Kennicutt 1998) (both of the same order, ∼30%), or a factor of two from the choice of initial mass function (IMF; Erb et al. 2006).

In CC08 I followed the same procedure, except that I used the UV continuua flux densities to calculate the obscured SFRs. I fed them to equation 4.1, then applied this other diagnostic, also from Kennicutt (1998):

$$SFR(M_\odot\,{\rm yr}^{-1}) = 1.4\times10^{-28} L_{\rm UV}\,{\rm erg\,s^{-1}}. \tag{4.3}$$

The results are summarised in Table 4.2, column (7). Errors quoted are statistical. In addition there are systematic errors of order 30% (Kennicutt 1998).

4.3.2 Discussion

Fitting full (optical to radio) SEDs in CC06 allowed us to calculate the most accurate and robust values for the SFR in a small sample of GRB host galaxies to date. For the hosts of GRBs 970508, 980703, 981226 and 990705, the lower ends of their SFR ranges in CC06 indicate low star formation, consistent with the estimates from the UV continuum (CC08) and, in the case of GRB 981226, with no internal extinction (Christensen et al. 2005). The host of GRB 970828 is a moderately star forming galaxy, in good agreement with Le Floc'h et al. (2006). The host of GRB 980613 is characterised by high star formation activity. Our SFR value for this host is ∼5 times higher than the one obtained by Le Floc'h et al. (2006) with a lower uncertainty, because we have fitted the entire SED, as opposed to only the flux density at 24 μm. We verified that calculating exclusively with the 24 μm flux densities we reproduce the results in Le Floc'h et al. (2006) for all hosts in CC06.

We find that our CC06 SFR values are significantly higher (up to a factor of 30) than the lower limits from the rest frame UV continuum emission (CC08) and higher (by a factor of 6) than those corrected with the β slope technique (Chary et al. 2002). GRBs 970828, 980613 and 980703 illustrate how even the best estimates of dust extinction in a galaxy from the UV slope may fall short, not only for ULIRGs (Chary & Elbaz 2001), but also for LIRGs (i.e. $10^{12}\,L_{\odot} > L_{8-1000} \geq 10^{11}\,L_{\odot}$).

4.4 Total stellar masses

The procedure I followed to calculate $M_\star$ in CC06 and CC08 is basically the same, with the exception noted in §4.2.2: the flux density at the central wavelength of the rest frame K band was interpolated in CC08 but not in CC06 where all redshifts in the sample were close to 1.

I inferred $M_\star$ for my GRB host galaxies from rest frame K band flux densities. In order to obtain $M_\star$ I apply:

$$M_\star(M_\odot) = 3.74 \times 10^{-11} \times \frac{4\pi D_L^2 f_\nu(\nu_{\rm obs})}{1+z} \times \frac{M_\star}{L_{K_{\rm rest}}}, \qquad (4.4)$$

where for any given object, D_L is its luminosity distance in cm; $f_\nu(\nu_{\rm obs})$ is its flux density at the observed wavelength in μJy; observations should have been made at wavelengths $1.9\,\mu$m $< \nu_{\rm obs}/(1+z) <$ $2.5\,\mu$m; and the factor of 3.74 $\times$ 10^{-11} converts the first term in equation 4.4 to units of solar luminosity density. The second term in equation 4.4, $M_\star/L_{K_{\rm rest}}$, also in solar units, must be estimated separately for each object.

$M_\star/L_{K_{\rm rest}}$ depends to some extent on the composition of the stellar population (Portinari et al. 2004). According to Labbé et al. (2005), who used Bruzual & Charlot (2003) with a Salpeter IMF (Salpeter 1955), it depends on the rest frame $U-V$ colour, the age, and $M_\star$. GRB host galaxies are usually blue, young, and faint (§1.3). In CC06 I assumed $M_\star/L_{K_{\rm rest}}$ to be $\sim$0.1 $M_\odot/L_\odot$ (this value being based on the lowest detection in Labbé et al. 2005) to obtain robust lower limits. With new data in hand for CC08 I computed $M_\star/L_{K_{\rm rest}}$ for three GRBs: 980703, 000210 and 000418, utilising the rest frame K band flux densities from Table 4.2, column (4) and the

$M_\star$ values derived from stellar population model SED fitting (Michałowski et al. 2008), and obtained the following results: $0.29\,M_\odot/L_\odot$ for GRB 980703, $0.63\,M_\odot/L_\odot$ for GRB 000210 and $0.43\,M_\odot/L_\odot$ for GRB 000418. These results yield a mean $M_\star/L_{K_{\rm rest}} = 0.45\,M_\odot/L_\odot$, which fully consistent with the average value in Courty et al. (2007), and among the lowest ratios presented by Portinari et al. (2004) for a Salpeter IMF (Salpeter 1955). It is sensible to calculate an average $M_\star/L_{K_{\rm rest}}$ with values from different galaxies because this ratio is nearly constant, with very little dependence on any previous star formation history. In fact, $M_\star/L_{K_{\rm rest}}$ varies only by a factor of two between extremely young and extremely old galaxy stellar populations (Glazebrook et al. 2004). So I estimated a conservative $0.4\,M_\odot/L_\odot$ in the calculations of $M_\star$ for my CC08 host galaxy sample. Table 4.2, column (5) summarises my $M_\star$ estimates. Errors quoted are statistical. I present a histogram of the distribution of $M_\star$ in log space for my CC08 GRB host sample in Figure 4.7. van der Wel et al. (2006) examined the redshift dependent systematic errors in determining $M_\star$ from broad band SEDs. They found no significant bias when Bruzual & Charlot (2003) models where used with a Salpeter IMF (Salpeter 1955).

My $M_\star$ are always lower than those of the normal $0.4 < z < 2$ galaxies from the Gemini Deep Deep Survey (GDDS; Abraham et al. 2004). The GDDS is a deep optical/NIR ($K < 20.6$) survey complete, for the already mentioned redshift range, down to $M_\star = 10^{10.8}\,M_\odot$ for all galaxies and to $M_\star = 10^{10.1}\,M_\odot$ for star-forming galaxies. At least 70% of my galaxies have $M_\star < 10^{10.1}\,M_\odot$. This comparison clearly highlights the efficiency of the GRB selection technique, against that of traditional high redshift surveys, to pick

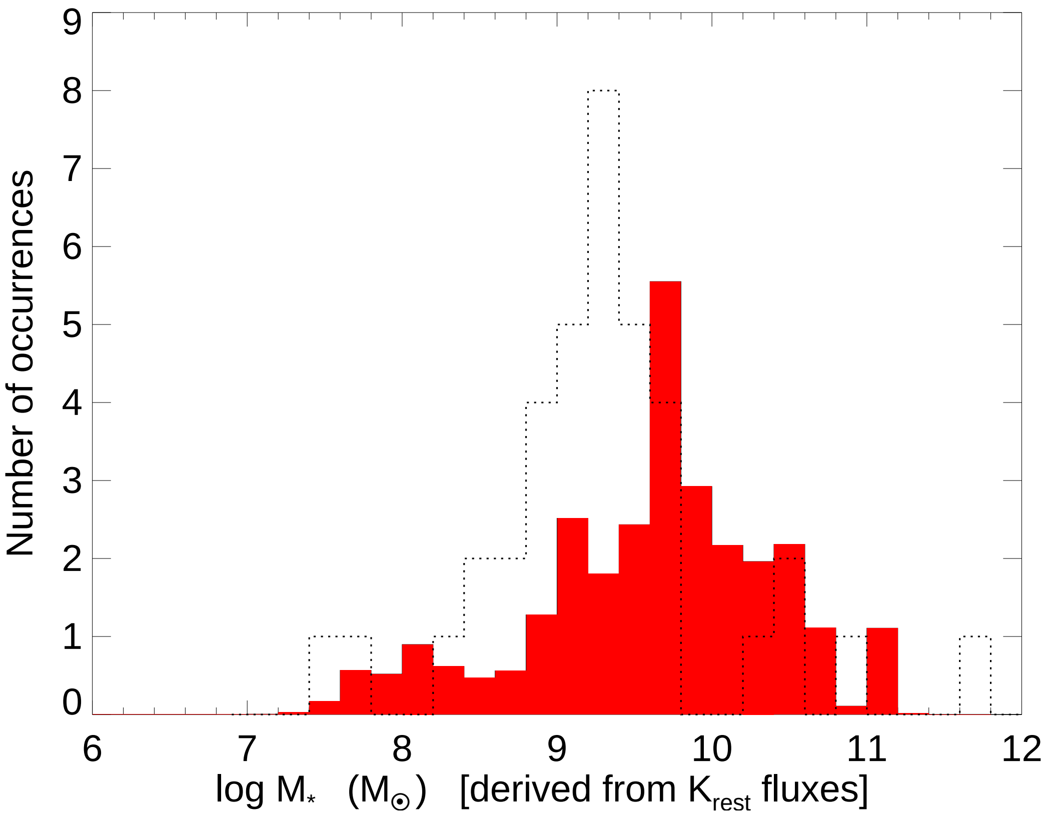

Figure 4.7: Distribution of $M_\star$ in GRB host galaxies. *Filled histogram*: 29 out of the 30 hosts in the CC08 sample, spanning a redshift interval $0 < z < 1.5$. I note that GRB 030429 has been excluded from the histogram above and the calculation of the median $M_\star$. This is because its host was never detected at any wavelength and, consequently, no lower limit to $M_\star$ can be estimated. The horizontal axis shows the inferred host $M_\star$, derived from interpolated rest frame K band flux densities. The median $M_\star$ of the sample is $\langle M_\star \rangle = 10^{9.7}\, M_\odot$. For those host galaxies for which I have upper limits I estimate a conservative lower limit by extrapolating a flat spectrum ($f_\nu \propto \nu^0$) from the reddest NIR/optical detection (references in Table 4.2, column 4); then I split an area normalised to unit among the bins bracketed by the limits. For each GRB host for which I have detections I assume a normalized Gaussian distribution of the error bars in linear space. Then I allocate $M_\star$ in proportion to the area of the Gaussian in each bin. *Open histogram*: Figure 2 from Savaglio et al. (2007) is shown for comparison. (*Adapted from CC08.*)

low $M_\star$ galaxies at high redshifts. GRBs are an efficient tool to probe the low end of the $M_\star$ distribution in high redshift galaxies.

4.5 Intrinsic extinction

At least part of my GRB host galaxy sample is extinguished by dust. A comparison of my data with the literature indicate that six GRB hosts, 970828, 980613 and 990705 (Le Floc'h et al. 2006, 24 μm flux densities; CC06, SED fitting), as well as 980703, 000210 and 000418 (CC06, SED fitting for GRB 980307; Michałowski et al. 2008, SED modelling), have highly obscured SFRs.

Additionally several authors have argued for dust extinction in the host of GRB 031203 (e.g., Prochaska et al. 2004; Margutti et al. 2007). Applying the SED fitting recipe in CC06 (§4.2.1 and §4.3.1) to this host galaxy's MIR photometry ($f_{3.6\,\mu\mathrm{m}} = 216\,\mu\mathrm{Jy} \pm 3\,\mu\mathrm{Jy}$; $f_{5.8\,\mu\mathrm{m}} = 390\,\mu\mathrm{Jy} \pm 16\,\mu\mathrm{Jy}$; $f_{24\,\mu\mathrm{m}} = 13\,103\,\mu\mathrm{Jy} \pm 41\,\mu\mathrm{Jy}$; flux densities corrected for foreground Galactic dust-extinction, Lutz 1999; Dutra et al. 2003) we obtain a $\mathrm{SFR}_{L_{8-1000}} = 13\,M_\odot\,\mathrm{yr}^{-1}$. That brings the total number of extinguished hosts to at least 7 out of 30, and allows me to crudely estimate that >25% of the sample in my Dissertation suffer significant dust extinction ($A_V \gtrsim 1\,\mathrm{mag}$). Neither my host galaxy sample, nor those others cited in this work, are bias-free. The searches for the GRBs in such samples have been carried out mostly following the localization of an optical afterglow, implicitly biasing the sample against dust-extincted systems (Chapter 2). Such potential bias strengthens my statement on dust extinction in GRB host galaxies. Parenthetically, I note that GRBs 970828, 980613, 980703 and 990705 make up two thirds of the redshift $z{\sim}1$ selected, small subsample in CC06. They hint at the possibility that even a higher fraction of hosts are affected by dust extinction, though with the caveat of low number statistics.

4.6 Specific star formation rate

The specific SFR, which for the purpose of this work may be defined as $\phi \equiv \mathrm{SFR}/M_\star$, gives an indication of how intensely star forming a galaxy is. It provides a way to compare the star formation in galaxies with very different sizes. In Figure 4.8 I plotted ϕ versus $M_\star$ for my CC08 GRB host galaxy sample. The absence of host galaxies in the lower left corner can be explained as a combination of selection effects and low number statistics. A host galaxy in this region of the plot has both a low $M_\star$ and a low SFR, making its detection difficult unless it is detected at very low redshifts. As the sampled comoving volume becomes smaller because of the lower redshift required to make such a detection, the chance of finding a GRB (and of course its host galaxy) decreases accordingly. Given the size of our sample, it is reasonable to expect no detections in this area of the plot. The four GRB host galaxies with the lowest $M_\star$ (GRBs 060218, 060614, 030329 and 980425) are all at very low redshifts and UV bright. I also note that my GRB sample, largely from the pre-*Swift* era, may be biased against low SFR hosts, since many redshifts have been measured from emission lines, which requires a relatively bright host.

On the other hand, the non detection of any GRB host in the upper right corner of Figure 4.8 should not be due to a selection effect. Such hosts either do not exist or their afterglows were significantly obscured by dust, hence preventing their localisation. The host sample I have compiled offers some indication as to the former posibility. My two host galaxies with the highest $M_\star$ (GRBs 030328 and 980613) would require a dust extinction of $A_V \sim$

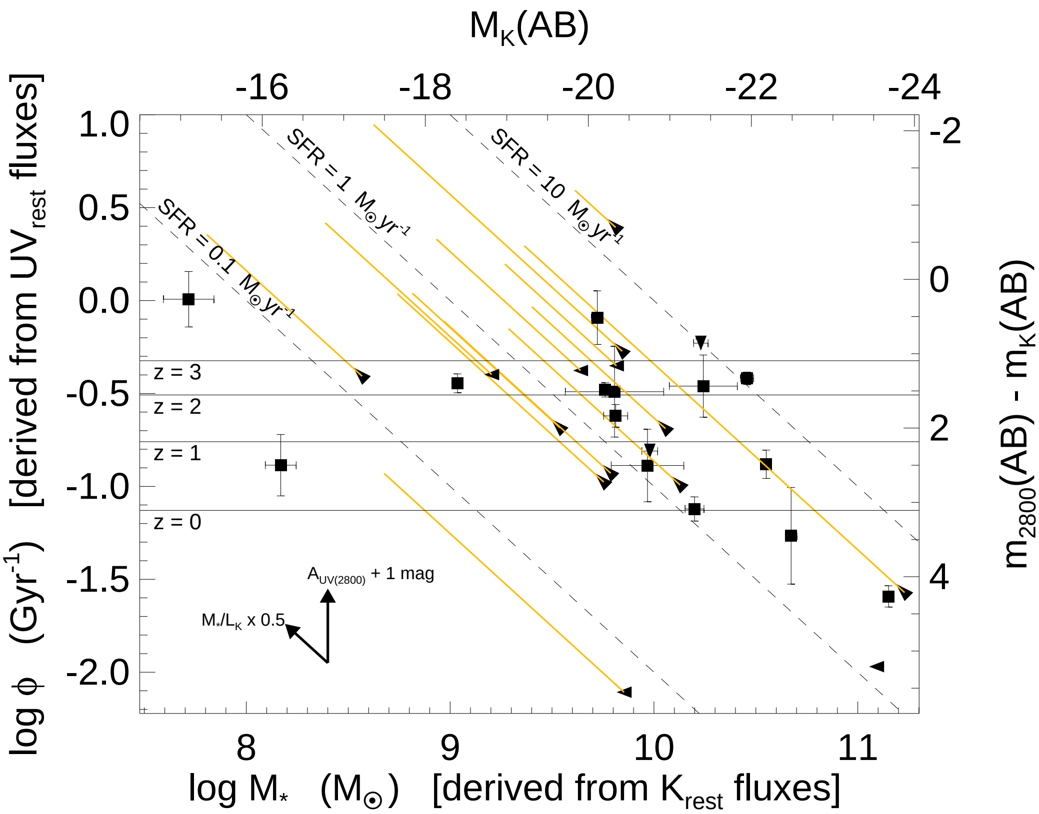

Figure 4.8: ϕ as a function of $M_\star$ for the 30 GRB host galaxy sample in CC08. Squares are detections and triangles mark upper limits for either $M_\star$, SFR, or both. *Yellow diagonals*: Distribution of the non detection measurements of $M_\star$. The lower limits of these bars were calculated by extrapolating a flat spectrum ($f_\nu \propto \nu^0$) from the NIR/optical data (references in Table 4.2, column 4. Each yellow diagonal could be displaced vertically by the size of the corresponding SFR error bar (Table 4.2, column 7). *Dashed diagonals*: Constant SFRs of 100, 10, 1, 0.1, and 0.01 $M_\odot\,\mathrm{yr}^{-1}$ respectively. *Black arrows*: Magnitudes of the displacements due to extinction by dust in the UV (e.g., 1 mag; vertical) and changes in the CC08 estimation of $M_\star/L_{K_{\mathrm{rest}}} \sim 0.4\,M_\odot/L_\odot$ (e.g., a factor of 50%; diagonal). *Right axis*: Color term equivalent to ϕ. *Top axis*: Absolute K band AB magnitude, equivalent to $M_\star$. The top/right axes represent the CC08 GRB host sample in colour magnitude space, effectively equivalent to ϕ vs. $M_\star$. (*Adapted from CC08.*)

5 mag to show in the upper right corner. Yet such dust extinction levels can be ruled out by the constraints on the SFR from the IR and the radio (§4.9).

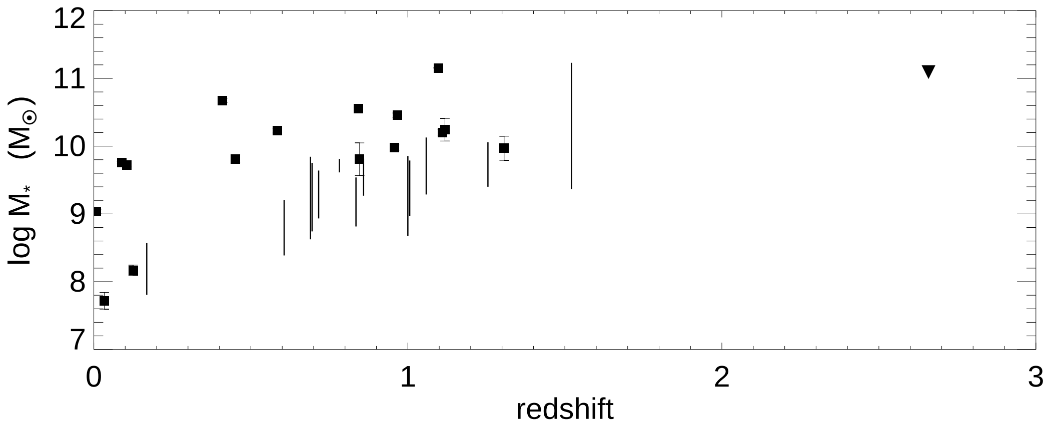

Figure 4.9: $M_\star$ as a function of redshift for the 30 GRB host galaxy sample in CC08. *Squares*: Detections. *Vertical bars*: Equivalent to the yellow bars in Figure 4.8. (*Adapted from CC08.*)

4.7 Physical evolution

I plotted $M_\star$ as a function of redshift, for my CC08 30 GRB host sample, in Figure 4.9 and found no intrinsic correlation between the two variables. The scatter of $M_\star$ is rather uniform across most of the redshift distribution. Hosts with very low $M_\star$ are only found at low redshift. For instance, the four GRB hosts (i.e., 060218, 060614, 030329 and 980425) with the lowest $M_\star$ ($< 10^9\ M_\odot$) have some of the lowest redshifts in my sample. Very low $M_\star$, high redshift hosts would have been excluded since most of these largely pre-*Swift* redshifts were measured in emission, what selects preferentially bright host galaxies. Because the redshift is a requirement for inclusion in my sample I am effectively biased against faint systems. The upper limits in the vertical bars of Figure 4.9 (i.e., the distribution for each non detection measurement of $M_\star$) mark the sensitivity limited curve for $M_\star$. Conversely, the absence of high $M_\star$, low redshift hosts suggests that such GRB host galaxies are rare.

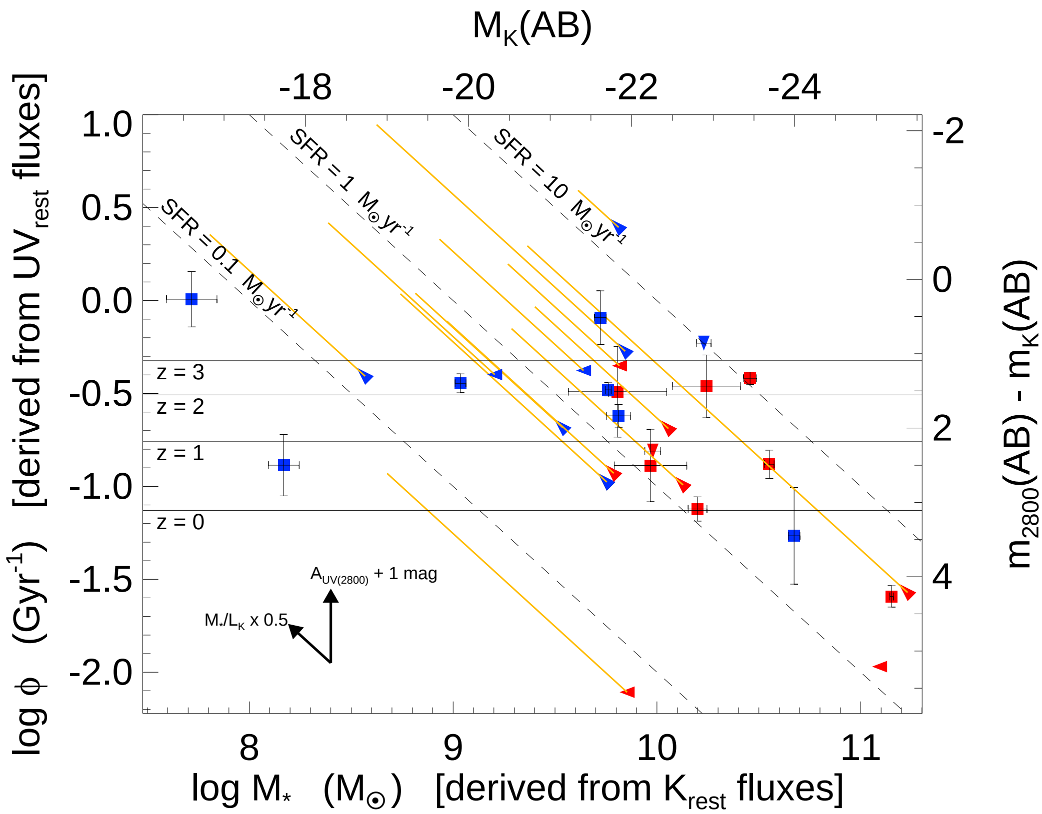

Figure 4.10: ϕ as a function of $M_\star$ for the 30 GRB host galaxy sample in CC08. This figure is identical to Figure 4.8, except that the host sample has been split in two halves by their redshifts. The splitting point is the median redshift $z = 0.84$. Blue symbols represent those galaxies that belong to the lower redshift half, while red symbols represent those galaxies that belong to the upper redshift half.

To further test this lack of physical evolution, in Figure 4.10 I replotted Figure 4.8, but split my CC08 sample in two halves, redshiftwise, at the meadian value. On a first look it seems as the lower $M_\star$ hosts have lower redshifts and the higher $M_\star$ hosts have higher redshifts. This would be indicative of physical evolution, yet it could be an artifact of small number statistics. Then my collaborators and I played a little game. Four GRB hosts were still to be added. They all had redshifts below the median value. So we made predictions about where in the plot would these last four fall. The outcome of the game was that they were evenly distributed, two on the low $M_\star$ side, two on the high $M_\star$ side, thus suggesting that the appearance of physical evolution was not real[2].

4.8 Addendum

At the time of submission of CC08 the only results available in the literature for the $M_\star$ of GRB host galaxies were the preliminary results from Savaglio et al. (2006, 2007), so I checked my results against theirs. For comparison I have plotted Figure 2 from the Savaglio et al. (2007) preliminary analysis in the background of my histogram. The two samples have a 25 object overlap. My results clearly suggest more massive hosts, about half an order of magnitude higher (median $M_\star = 10^{9.7}\,M_\odot$ in ours vs. median $M_\star = 10^{9.3}\,M_\odot$ in Savaglio et al. 2007). Savaglio et al. (2006, 2007) fitted the optical/NIR SEDs of their host galaxy sample together with a complex set of SF histories. I can reproduce the median $M_\star$ in Savaglio et al. (2007) with my dataset by applying $M_\star/L_{K_{\rm rest}} = 0.2\,M_\odot/L_\odot$. Their methodology therefore seems to implicitly contain an effective $M_\star/L_{K_{\rm rest}}$ ratio around 0.2. An adjustment by a factor of $\sim$2 to this ratio thus explains the discrepancies in $M_\star$ between my analysis and that of Savaglio et al. (2007). I note that such an adjustment is just within the spread of my calculated values (cf., $0.29\,M_\odot/L_\odot$, $0.43\,M_\odot/L_\odot$, and $0.63\,M_\odot/L_\odot$). The fact that I find larger $M_\star$ may also be indicative of underestimated dust extinction in Savaglio et al. (2007).

[2]There was even a bet between my supervisors. Unfortunately the bet involved alcohol and the winning party is abstemious so, as far as I am aware, it was never paid.

As I am nearing completion of this manuscript the final analysis has been posted in ArXiv.com (Savaglio et al. 2008). It is too late to include a detailed comparison. I will just mention few quick points: *i*) They confirmed their median $M_\star$, so my above comparison analysis holds; *ii*) Their obscured (but corrected for intrinsic extinction) SFRs are consistent with ours (only corrected for foreground Galactic extinction); *iii*) It is verified that their analysis gives a mean $M_\star/L_{K_{\rm rest}}$ ratio around 0.2, with a scatter similar to mine (§4.4); *iv*) For the seven hosts for which I have shown that there is intrinsic extinction they get significantly lower $M_\star$ and somewhat higher SFRs, thus providing additional evidence for my conclusion in §4.3.2 about estimating dust extinction in a galaxy.

4.9 Discussion

In Figure 4.11 I plotted ϕ versus $M_\star$ for my CC06 sample and five other representative galaxy samples: distant red galaxies (DRG), Lyα emitters (LAE), Lyman break galaxies (LBG), submillimitre galaxies (SMG) and an ensemble of optically selected, $z \sim 2$ galaxies from the Great Observatories Origins Deep survey-North field. GRB hosts have some of the highest ϕ values, as previously suggested by Christensen et al. (2004). ϕ^{-1} represents the SFR timescale, so high ϕ values are indicative of GRBs tracing young, starbursting galaxies. The different methods that have been used to derive the SFRs of the various samples plotted in Figure 4.11 likely introduce systematic offsets. Likewise, to determine $M_\star$, model fitting to the full SED better accounts for variations in M/L_K (e.g. CC08; Michałowski et al. 2008). For high SFR gal-

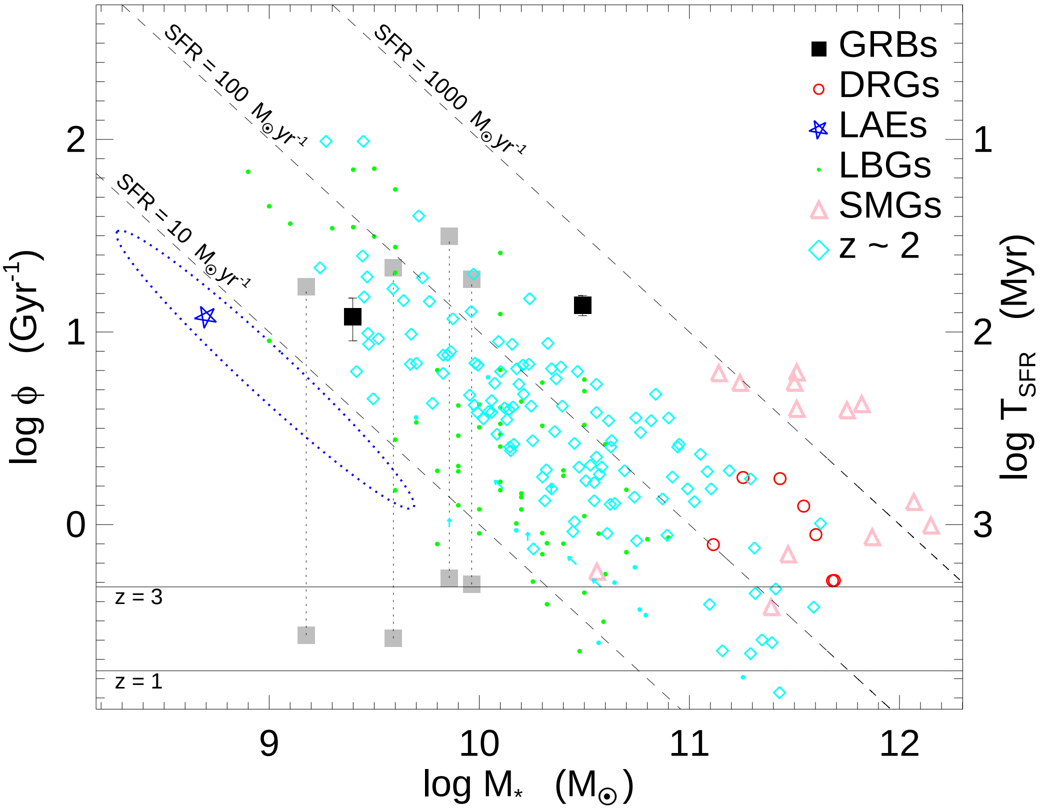

Figure 4.11: ϕ as a function of $M_\star$ for the GRB host galaxy sample in CC06 and other representative types of galaxies. *Black squares*: SFR values constrained with a best fit model. *Grey squares*: highest/lowest SFR values for those hosts for which I could not establish a best fit model. *Dashed diagonals*: SFRs of 1000, 100 and 10 $M_\odot\,\mathrm{yr}^{-1}$ respectively. *Right axis*: SFR timescale ($T_{\rm SFR} = M_\star/\mathrm{SFR}$), the inverse of ϕ. On this scale the solid horizontals represent the age of the universe for the marked redshift. The six hosts in CC06 clearly have $T_{\rm SFR} < \mathrm{t_{universe}}$, allowing for a history of constant star formation. The distribution of the CC06 sample in parameter space suggests that GRBs trace galaxies that are not selected with other techniques. *Data points*: GRBs from CC06. DRGs from van Dokkum et al. (2004). LAEs from Gawiser et al. (2006). The point plotted represents an average value of the LAE population as a whole, obtained from stacked photometry , and the dotted ellipse its uncertainty. Spectroscopically confirmed LBGs from Shapley et al. (2001) and Barmby et al. (2004). SMGs from Borys et al. (2005, $M_\star$) and Chapman et al. (2005, SFR), where I have considered $L_{\rm BOL} \simeq L_{\rm farIR}$, then applied the Kennicutt (1998) calibration. $z \sim 2$ from Erb et al. (2003) and Reddy et al. (2006). (*Adapted from CC06; for reasons of brevity and economy of space the references in this figure have not been included in the Bibliography, rather they can be found at CC06, which is included in Appendix B.*)

axies, ongoing star formation contributes to the NIR emission, especially as they lack an old stellar population. High ϕ galaxies are particularly vulnerable to this effect. Nevertheless, Figure 4.11 illustrates where, within the larger picture, my hosts fall.

In Figure 4.12 I plotted, with blue symbols, my CC08 30 host sample using a revised $M_\star/L_{K_\mathrm{rest}}$ ratio, along with the samples in CC06. In this second ϕ versus $M_\star$ plot, which is built with $\mathrm{SFR_{UV}}$, the obscuration of star formation by dust pulls the GRB data points down along a vertical line. One way to reconcile the ϕ values of host galaxies in CC06 and CC08 is to invoke extinction by dust of the order of $A_V \sim 1$–$3\,\mathrm{mag}$.

In CC06 I noted that the host sample has $T_\mathrm{SFR} < t_\mathrm{universe}$, allowing for a history of constant star formation, with a robust lower limit in $M_\star$ ($M_\star/L_{K_\mathrm{rest}}$ $\sim 0.1\,M_\odot/L_\odot$). For the sample presented in CC08, where I adopted $M_\star/L_{K_\mathrm{rest}}$ $\sim 0.4\,M_\odot/L_\odot$, clearly few GRB host galaxies are not allowed to have a history of constant star formation (i.e., young stars dominating the stellar populations of old galaxies; see the right ordinate axis in Figure 4.12). Either a starburst episode was present in the past, or a higher recent SFR is required. The latter possibility is consistent with a fraction of GRB hosts having star formation obscured by dust. The hosts of GRBs 970828 and 980613 (open blue symbols in Figure 4.12) are good examples because, under the assumption of constant star formation, major dust extinction must be invoked to account for the age differences. ϕ_UV estimates (CC08) result in $T_\mathrm{SFR} \sim 6\,\mathrm{Gyr}$ for GRB 970828 and $T_\mathrm{SFR} \sim 32\,\mathrm{Gyr}$ for GRB 980613, while ϕ_{L_K} estimates (CC06) result in $T_\mathrm{SFR} \sim 300\,\mathrm{Myr}$ for both of them. The discrepancies in T_SFR imply a dust extinction of the order of $A_V \sim 1.6\,\mathrm{mag}$ for GRB 970828

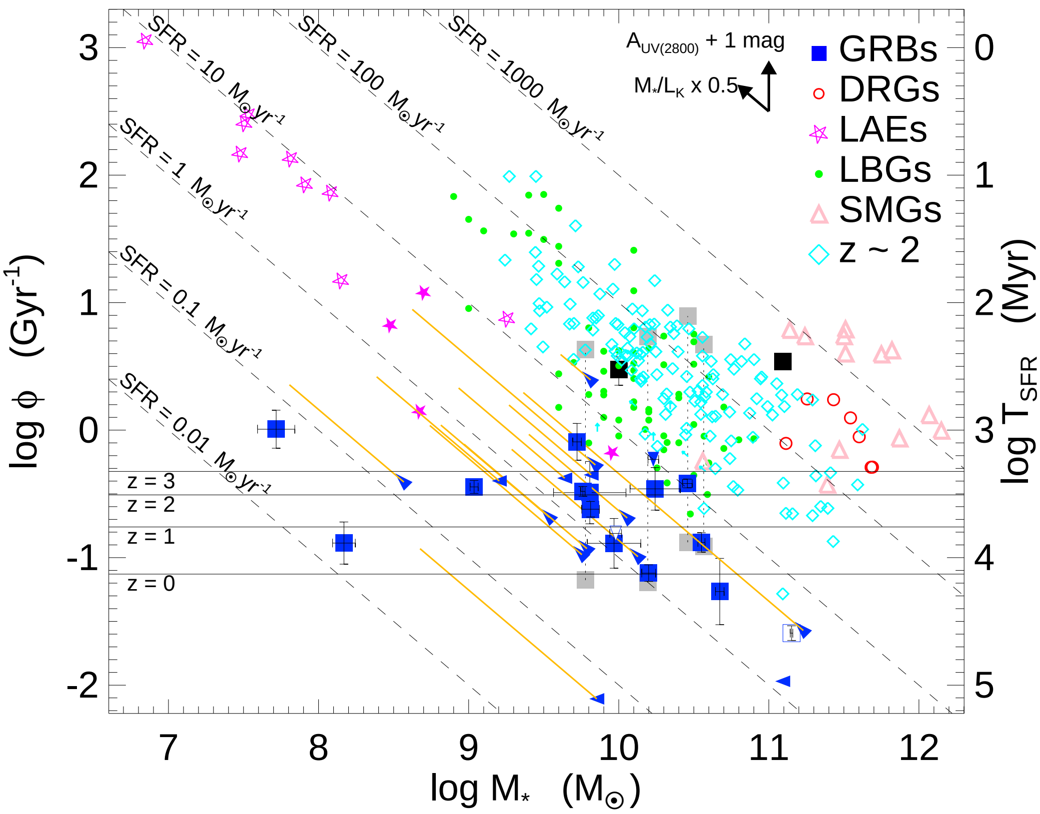

Figure 4.12: ϕ as a function of $M_\star$ for the GRB host galaxy sample in CC08, CC06 and other representative types of galaxies. *Blue squares and triangles*: Host galaxy sample from CC08, with unobscured SFRs derived from the rest frame UV continuum. Triangles mark upper limits for either $M_\star$, SFR, or both. The open blue triangle and square mark the hosts of GRBs 970828 and 980613 respectively. *Black squares*: CC06 SFR values constrained with a best fit SED model. *Grey squares*: CC06 Highest/lowest SFR values for those hosts for which I could not establish a best fit model. I have shifted here both, the black squares and the grey squares, correspondingly to compensate for the difference in $M_\star/L_{K_{\rm rest}}$ methodology (i.e., from a lower limit value of 0.1 $M_\odot/L_\odot$ in CC06 to a best estimated value of 0.4 $M_\odot/L_\odot$ in CC08). Yellow diagonals, dashed diagonals, and black arrows are as in Figure 4.8. *Right axis*: SFR timescale ($T_{\rm SFR} = M_\star/{\rm SFR}$), the inverse of ϕ. On this scale the solid horizontal lines represent the age of the universe for the marked redshift. The distribution of the CC08 and CC06 samples in parameter space suggests that GRBs trace galaxies that are not selected with other techniques. *Data points*: References from Figure 4.11. Additionally, GRBs from CC08 and LAEs from Nilsson et al. (2007), and Lai et al. (2008) (filled stars; average values of the LAE population as a whole, obtained from stacked photometry); N. Pirzkal, S. Malhotra, J. E. Rhoads, & C. Xu (2007, priv. comm.; empty stars; see Pirzkal et al. (2007) for the average values and a description of these sources). (*Adapted from CC08; for reasons of brevity and economy of space the references in this figure have not been included in the Bibliography, rather they can be found at CC08, which is included in Appendix C.*)

and $A_V \sim 2.5$ mag for GRB 980613. These discrepancies are consistent with the radio constrained SFR upper limits ($\sim$100 $M_\odot$ yr^{-1} for GRB 970828, and $\sim$500 $M_\odot$ yr^{-1} for GRB 980613; M. Michałowski 2008, priv. comm.) derived by applying the Yun & Carilli (2002) methodology to the deepest radio upper limits reported by Frail et al. (2003).

A dilution effect is present in my MIR photometry. Hosts in my current samples are not spatially resolved in the Spitzer imagery (in the case of GRB 980425 I utilize the total flux of the galaxy for consistency with the rest of the sample). To estimate their $M_\star$ I measured the total K band light. L_K traces the accumulation of $M_\star$ (Glazebrook et al. 2004) while, most commonly, the star formation is ongoing in only a small part of the host galaxy. So in normalising my samples' SFRs I did not do so with the total stellar mass of the star forming region(s), but with $M_\star$, which results in lower ϕ values. This dilution effect pulls the GRB data points in a ϕ versus $M_\star$ plot down along the diagonal (dashed) lines marking constant SFRs.

Extinction by dust, coupled with the dilution effect, could be responsible for the apparent envelope that can be visualized in Figures 4.8 and 4.12: a flat plateau with no objects above a certain ϕ value ($\sim$2.5 Gyr^{-1}), and that starts to curve down beyond a particular $M_\star$ (10^{10} $M_\odot$). Correcting for dilution and, chiefly, for dust extinction would yield a new plot where our host sample would align consistently with the results/upper limits of Figure 4.11, and provide support to the claim that GRB host galaxies are small and have some of the highest ϕ values.

Bibliography

Abraham, R. G., Glazebrook, K., McCarthy, P. J., Crampton, D., Murowinski, R., Jørgensen, I., Roth, K., Hook, I. M., Savaglio, S., Chen, H.-W., Marzke, R. O., & Carlberg, R. G. 2004, AJ, 127, 2455

Afanasiev, V., Fatkhullin, T., Dodonov, S., Sokolov, V., Castro-Tirado, A., Komarova, V., Moiseev, A., Cherepashchuk, A., & Postnov, K. 2001, GCN Circ., 1090, 1

Amati, L., Frontera, F., Castro Cerón, J. M., Costa, E., Feroci, M., Gandolfi, G., Giommi, P., Guidorzi, C., Masetti, N., Montanari, E., Piro, L., Soffitta, P., & in't Zand, J. J. M. 2003, in American Institute of Physics Conference Series, Vol. 662, Gamma-Ray Burst and Afterglow Astronomy 2001: A Workshop Celebrating the First Year of the HETE Mission, ed. G. R. Ricker & R. K. Vanderspek, 387–389

Amati, L., Frontera, F., Pian, E., Giommi, P., Capalbi, M., Costa, E., Gandolfi, G., in 't Zand, J. J. M., Guidorzi, C., Granata, S., & Paolino, A. 2000, IAU Circ., 7519, 1

Berger, E., Cowie, L. L., Kulkarni, S. R., Frail, D. A., Aussel, H., & Barger, A. J. 2003, ApJ, 588, 99

Berger, E., Kulkarni, S. R., & Frail, D. A. 2001, ApJ, 560, 652

Berger, E., Price, P. A., Cenko, S. B., Gal-Yam, A., Soderberg, A. M., Kasliwal, M., Leonard, D. C., Cameron, P. B., Frail, D. A., Kulkarni, S. R., Murphy, D. C., Krzeminski, W., Piran, T., Lee, B. L., Roth, K. C., Moon, D.-S., Fox, D. B., Harrison, F. A., Persson, S. E., Schmidt, B. P., Penprase, B. E., Rich, J., Peterson, B. A., & Cowie, L. L. 2005, Nature, 438, 988

Bertin, E. & Arnouts, S. 1996, A&AS, 117, 393

Blain, A. W., Smail, I., Ivison, R. J., Kneib, J.-P., & Frayer, D. T. 2002, Phys. Rep., 369, 111

Bloom, J. S., Kulkarni, S. R., & Djorgovski, S. G. 2002, AJ, 123, 1111

Boella, G., Butler, R. C., Perola, G. C., Piro, L., Scarsi, L., & Bleeker, J. A. M. 1997, A&AS, 122, 299

Bremer, M., Krichbaum, T. P., Galama, T. J., Castro-Tirado, A. J., Frontera, F., van Paradijs, J., Mirabel, I. F., & Costa, E. 1998, A&A, 332, L13

Bruzual, G. & Charlot, S. 2003, MNRAS, 344, 1000

Campana, S., Mangano, V., Blustin, A. J., Brown, P., Burrows, D. N., Chincarini, G., Cummings, J. R., Cusumano, G., Della Valle, M., Malesani, D., Mészáros, P., Nousek, J. A., Page, M., Sakamoto, T., Waxman, E., Zhang, B., Dai, Z. G., Gehrels, N., Immler, S., Marshall, F. E., Mason, K. O., Moretti, A., O'Brien, P. T., Osborne, J. P., Page, K. L., Romano, P., Roming, P. W. A., Tagliaferri, G., Cominsky, L. R., Giommi, P., Godet, O., Kennea, J. A., Krimm, H., Angelini, L., Barthelmy, S. D., Boyd, P. T., Palmer, D. M., Wells, A. A., & White, N. E. 2006, Nature, 442, 1008

Castro Cerón, J. M., Gorosabel, J., Castro-Tirado, A. J., Sokolov, V. V., Afanasiev, V. L., Fatkhullin, T. A., Dodonov, S. N., Komarova, V. N., Cherepashchuk, A. M., Postnov, K. A., Lisenfeld, U., Greiner, J., Klose, S., Hjorth, J., Fynbo, J. P. U., Pedersen, H., Rol, E., Fliri, J., Feldt, M., Feulner, G., Andersen, M. I., Jensen, B. L., Pérez Ramírez, M. D., Vrba, F. J., Henden, A. A., Israelian, G., & Tanvir, N. R. 2004, A&A, 424, 833

Castro Cerón, J. M., Michałowski, M. J., Hjorth, J., Malesani, D., Gorosabel, J., Watson, D., & Fynbo, J. P. U. 2008, ApJ, submitted, (arXiv:0803.2235v1 [astro.ph])

Castro Cerón, J. M., Michałowski, M. J., Hjorth, J., Watson, D., Fynbo, J. P. U., & Gorosabel, J. 2006, ApJ, 653, L85

Chapman, S. C., Blain, A. W., Smail, I., & Ivison, R. J. 2005, ApJ, 622, 772

Charmandaris, V., Le Floc'h, E., & Mirabel, I. F. 2004, ApJ, 600, L15

Chary, R., Becklin, E. E., & Armus, L. 2002, ApJ, 566, 229

Chary, R. & Elbaz, D. 2001, ApJ, 556, 562

Christensen, L., Hjorth, J., & Gorosabel, J. 2004, A&A, 425, 913

—. 2005, ApJ, 631, L29

Conselice, C. J., Vreeswijk, P. M., Fruchter, A. S., Levan, A., Kouveliotou, C., Fynbo, J. P. U., Gorosabel, J., Tanvir, N. R., & Thorsett, S. E. 2005, ApJ, 633, 29

Costa, E., Frontera, F., Heise, J., Feroci, M., in't Zand, J., Fiore, F., Cinti, M. N., Dal Fiume, D., Nicastro, L., Orlandini, M., Palazzi, E., Rapisarda#, M., Zavattini, G., Jager, R., Parmar, A., Owens, A., Molendi, S., Cusumano, G., Maccarone, M. C., Giarrusso, S., Coletta, A., Antonelli, L. A., Giommi, P., Muller, J. M., Piro, L., & Butler, R. C. 1997, Nature, 387, 783

Courty, S., Björnsson, G., & Gudmundsson, E. H. 2007, MNRAS, 376, 1375

Dale, D. A. & Helou, G. 2002, ApJ, 576, 159

Dale, D. A., Helou, G., Contursi, A., Silbermann, N. A., & Kolhatkar, S. 2001, ApJ, 549, 215

De Pasquale, M., Piro, L., Perna, R., Costa, E., Feroci, M., Gandolfi, G., Zand, J. i., Nicastro, L., Frontera, F., Antonelli, L. A., Fiore, F., & Stratta, G. 2003, ApJ, 592, 1018

Della Valle, M., Chincarini, G., Panagia, N., Tagliaferri, G., Malesani, D., Testa, V., Fugazza, D., Campana, S., Covino, S., Mangano, V., Antonelli, L. A., D'Avanzo, P., Hurley, K., Mirabel, I. F., Pellizza, L. J., Piranomonte, S., & Stella, L. 2006, Nature, 444, 1050

Djorgovski, S. G., Bloom, J. S., & Kulkarni, S. R. 2003, ApJ, 591, L13

Djorgovski, S. G., Frail, D. A., Kulkarni, S. R., Bloom, J. S., Odewahn, S. C., & Diercks, A. 2001, ApJ, 562, 654

Dutra, C. M., Ahumada, A. V., Clariá, J. J., Bica, E., & Barbuy, B. 2003, A&A, 408, 287

Erb, D. K., Steidel, C. C., Shapley, A. E., Pettini, M., Reddy, N. A., & Adelberger, K. L. 2006, ApJ, 646, 107

Fazio, G. G., Hora, J. L., Allen, L. E., Ashby, M. L. N., Barmby, P., Deutsch, L. K., Huang, J.-S., Kleiner, S., Marengo, M., Megeath, S. T., Melnick, G. J., Pahre, M. A., Patten, B. M., Polizotti, J., Smith, H. A., Taylor, R. S., Wang, Z., Willner, S. P., Hoffmann, W. F., Pipher, J. L., Forrest, W. J., McMurty, C. W., McCreight, C. R., McKelvey, M. E., McMurray, R. E., Koch, D. G., Moseley, S. H., Arendt, R. G., Mentzell, J. E., Marx, C. T., Losch, P., Mayman, P., Eichhorn, W., Krebs, D., Jhabvala, M., Gezari, D. Y., Fixsen, D. J., Flores, J., Shakoorzadeh, K., Jungo, R., Hakun, C., Workman, L., Karpati, G., Kichak, R., Whitley, R., Mann, S., Tollestrup, E. V., Eisenhardt, P., Stern, D., Gorjian, V., Bhattacharya, B., Carey, S., Nelson, B. O., Glaccum, W. J., Lacy, M., Lowrance, P. J., Laine, S., Reach, W. T., Stauffer, J. A., Surace, J. A., Wilson, G., Wright, E. L., Hoffman, A., Domingo, G., & Cohen, M. 2004, ApJS, 154, 10

Fishman, G. J. 1981, Ap&SS, 75, 125

Fomalont, E. B., Kellermann, K. I., Partridge, R. B., Windhorst, R. A., & Richards, E. A. 2002, AJ, 123, 2402

Fox, D. B., Frail, D. A., Price, P. A., Kulkarni, S. R., Berger, E., Piran, T., Soderberg, A. M., Cenko, S. B., Cameron, P. B., Gal-Yam, A., Kasliwal, M. M., Moon, D.-S., Harrison, F. A., Nakar, E., Schmidt, B. P., Penprase, B., Chevalier, R. A., Kumar, P., Roth, K., Watson, D., Lee, B. L., Shectman, S., Phillips, M. M., Roth, M., McCarthy, P. J., Rauch, M., Cowie, L., Peterson, B. A., Rich, J., Kawai, N., Aoki, K., Kosugi, G., Totani, T., Park, H.-S., MacFadyen, A., & Hurley, K. C. 2005, Nature, 437, 845

Frail, D. A., Kulkarni, S. R., Berger, E., & Wieringa, M. H. 2003, AJ, 125, 2299

Frail, D. A., Kulkarni, S. R., Nicastro, L., Feroci, M., & Taylor, G. B. 1997, Nature, 389, 261

Fruchter, A. S., Levan, A. J., Strolger, L., Vreeswijk, P. M., Thorsett, S. E., Bersier, D., Burud, I., Castro Cerón, J. M., Castro-Tirado, A. J., Conselice, C., Dahlen, T., Ferguson, H. C., Fynbo, J. P. U., Garnavich, P. M., Gibbons, R. A., Gorosabel, J., Gull, T. R., Hjorth, J., Holland, S. T., Kouveliotou, C., Levay, Z., Livio, M., Metzger, M. R., Nugent, P. E., Petro, L., Pian, E., Rhoads, J. E., Riess, A. G., Sahu, K. C., Smette, A., Tanvir, N. R., Wijers, R. A. M. J., & Woosley, S. E. 2006, Nature, 441, 463

Fruchter, A. S., Thorsett, S. E., Metzger, M. R., Sahu, K. C., Petro, L., Livio, M., Ferguson, H., Pian, E., Hogg, D. W., Galama, T., Gull, T. R., Kouveliotou, C., Macchetto, D., van Paradijs, J., Pedersen, H., & Smette, A. 1999, ApJ, 519, L13

Fynbo, J. P. U., Ledoux, C., Möller, P., Thomsen, B., & Burud, I. 2003, A&A, 407, 147

Fynbo, J. P. U., Prochaska, J. X., Sommer-Larsen, J., Dessauges-Zavadsky, M., & Moller, P. 2008, ArXiv e-prints, 801

Fynbo, J. P. U., Watson, D., Thöne, C. C., Sollerman, J., Bloom, J. S., Davis, T. M., Hjorth, J., Jakobsson, P., Jørgensen, U. G., Graham, J. F., Fruchter, A. S., Bersier, D., Kewley, L., Cassan, A., Cerón, J. M. C., Foley, S., Gorosabel, J., Hinse, T. C., Horne, K. D., Jensen, B. L., Klose, S., Kocevski, D., Marquette, J.-B., Perley, D., Ramirez-Ruiz, E., Stritzinger, M. D., Vreeswijk, P. M., Wijers, R. A. M., Woller, K. G., Xu, D., & Zub, M. 2006, Nature, 444, 1047

Fynbo, J. U., Jensen, B. L., Gorosabel, J., Hjorth, J., Pedersen, H., Møller, P., Abbott, T., Castro-Tirado, A. J., Delgado, D., Greiner, J., Henden, A., Magazzù, A., Masetti, N., Merlino, S., Masegosa, J., Østensen, R., Palazzi, E., Pian, E., Schwarz, H. E., Cline, T., Guidorzi, C., Goldsten, J., Hurley, K., Mazets, E., McClanahan, T., Montanari, E., Starr, R., & Trombka, J. 2001, A&A, 369, 373

Gal-Yam, A., Fox, D. B., Price, P. A., Ofek, E. O., Davis, M. R., Leonard, D. C., Soderberg, A. M., Schmidt, B. P., Lewis, K. M., Peterson, B. A., Kulkarni, S. R., Berger, E., Cenko, S. B., Sari, R., Sharon, K., Frail, D., Moon, D.-S., Brown, P. J., Cucchiara, A., Harrison, F., Piran, T., Persson, S. E., McCarthy, P. J., Penprase, B. E., Chevalier, R. A., & MacFadyen, A. I. 2006, Nature, 444, 1053

Galama, T. J., Vreeswijk, P. M., van Paradijs, J., Kouveliotou, C., Augusteijn, T., Böhnhardt, H., Brewer, J. P., Doublier, V., Gonzalez, J.-F., Leibundgut, B., Lidman, C., Hainaut, O. R., Patat, F., Heise, J., in't Zand, J., Hurley, K., Groot, P. J., Strom, R. G., Mazzali, P. A., Iwamoto, K., Nomoto, K., Umeda, H., Nakamura, T., Young, T. R., Suzuki, T., Shigeyama, T., Koshut, T., Kippen, M., Robinson, C., de Wildt, P., Wijers, R. A. M. J., Tanvir, N., Greiner, J., Pian, E., Palazzi, E., Frontera, F., Masetti, N., Nicastro, L., Feroci, M., Costa, E., Piro, L., Peterson, B. A., Tinney, C., Boyle, B., Cannon, R., Stathakis, R., Sadler, E., Begam, M. C., & Ianna, P. 1998, Nature, 395, 670

Gandolfi, G. 2000, GCN Circ., 879, 1

Gawiser, E., van Dokkum, P. G., Gronwall, C., Ciardullo, R., Blanc, G. A., Castander, F. J., Feldmeier, J., Francke, H., Franx, M., Haberzettl, L., Herrera, D., Hickey, T., Infante, L., Lira, P., Maza, J., Quadri, R., Richardson, A., Schawinski, K., Schirmer, M., Taylor, E. N., Treister, E., Urry, C. M., & Virani, S. N. 2006, ApJ, 642, L13

Gehrels, N., Chincarini, G., Giommi, P., Mason, K. O., Nousek, J. A., Wells, A. A., White, N. E., Barthelmy, S. D., Burrows, D. N., Cominsky, L. R., Hurley, K. C., Marshall, F. E., Mészáros, P., Roming, P. W. A., Angelini, L., Barbier, L. M., Belloni, T., Campana, S., Caraveo, P. A., Chester, M. M., Citterio, O., Cline, T. L., Cropper, M. S., Cummings, J. R., Dean, A. J., Feigelson, E. D., Fenimore, E. E., Frail, D. A., Fruchter, A. S., Garmire, G. P., Gendreau, K., Ghisellini, G., Greiner, J., Hill, J. E., Hunsberger, S. D., Krimm, H. A., Kulkarni, S. R., Kumar, P., Lebrun, F., Lloyd-Ronning, N. M., Markwardt, C. B., Mattson, B. J., Mushotzky, R. F., Norris, J. P., Osborne, J., Paczynski, B., Palmer, D. M., Park, H.-S., Parsons, A. M., Paul, J., Rees, M. J., Reynolds, C. S., Rhoads, J. E., Sasseen, T. P., Schaefer, B. E., Short, A. T., Smale, A. P., Smith, I. A., Stella, L., Tagliaferri, G., Takahashi, T., Tashiro, M., Townsley, L. K., Tueller, J., Turner, M. J. L., Vietri, M., Voges, W., Ward, M. J., Willingale, R., Zerbi, F. M., & Zhang, W. W. 2004, ApJ, 611, 1005

Gehrels, N., Norris, J. P., Barthelmy, S. D., Granot, J., Kaneko, Y., Kouveliotou, C., Markwardt, C. B., Mészáros, P., Nakar, E., Nousek, J. A., O'Brien, P. T., Page, M., Palmer, D. M., Parsons, A. M., Roming, P. W. A., Sakamoto, T., Sarazin, C. L., Schady, P., Stamatikos, M., & Woosley, S. E. 2006, Nature, 444, 1044

Gehrels, N., Sarazin, C. L., O'Brien, P. T., Zhang, B., Barbier, L., Barthelmy, S. D., Blustin, A., Burrows, D. N., Cannizzo, J., Cummings, J. R., Goad, M., Holland, S. T., Hurkett, C. P., Kennea, J. A., Levan, A., Markwardt, C. B., Mason, K. O., Meszaros, P., Page, M., Palmer, D. M., Rol, E., Sakamoto, T., Willingale, R., Angelini, L., Beardmore, A., Boyd, P. T., Breeveld, A., Campana, S., Chester, M. M., Chincarini, G., Cominsky, L. R., Cusumano, G., de Pasquale, M., Fenimore, E. E., Giommi, P., Gronwall, C., Grupe, D., Hill, J. E., Hinshaw, D., Hjorth, J., Hullinger, D., Hurley, K. C., Klose, S., Kobayashi, S., Kouveliotou, C., Krimm, H. A., Mangano, V., Marshall, F. E., McGowan, K., Moretti, A., Mushotzky, R. F., Nakazawa, K., Norris, J. P., Nousek, J. A., Osborne, J. P., Page, K., Parsons, A. M., Patel, S., Perri, M., Poole, T., Romano, P., Roming, P. W. A., Rosen, S., Sato, G., Schady, P., Smale, A. P., Sollerman, J., Starling, R., Still, M., Suzuki, M., Tagliaferri, G., Takahashi, T., Tashiro, M., Tueller, J., Wells, A. A., White, N. E., & Wijers, R. A. M. J. 2005, Nature, 437, 851

Gehrels, N. & Swift Team. 2005, in Bulletin of the American Astronomical Society, Vol. 37, Bulletin of the American Astronomical Society, 1324

Georgantopoulos, I., Stewart, G. C., Blair, A. J., Shanks, T., Griffiths, R. E., Boyle, B. J., Almaini, O., & Roche, N. 1997, MNRAS, 291, 203

Glazebrook, K., Abraham, R. G., McCarthy, P. J., Savaglio, S., Chen, H.-W., Crampton, D., Murowinski, R., Jørgensen, I., Roth, K., Hook, I., Marzke, R. O., & Carlberg, R. G. 2004, Nature, 430, 181

Gorosabel, J., Christensen, L., Hjorth, J., Fynbo, J. U., Pedersen, H., Jensen, B. L., Andersen, M. I., Lund, N., Jaunsen, A. O., Castro Cerón, J. M., Castro-Tirado, A. J., Fruchter, A., Greiner, J., Pian, E., Vreeswijk, P. M., Burud, I., Frontera, F., Kaper, L., Klose, S., Kouveliotou, C., Masetti, N., Palazzi, E., Rhoads, J., Rol, E., Salamanca, I., Tanvir, N., Wijers, R. A. M. J., & van den Heuvel, E. 2003, A&A, 400, 127

Groot, P. J., Galama, T. J., van Paradijs, J., Melnick, J., van der Steene, G., Bremer, M., Tanvir, N., Bloom, J., Strom, R., Telting, J., Rutten, R. G. M., Kouveliotou, C., in 't Zand, J., Heise, J., Costa, E., Feroci, M., Piro, L., Frontera, F., Zavattini, G., Nicastro, L., Palazzi, E., Metzger, M. R., Kulkarni, S. R., Djorgovski, S. G., Gal, R., Steidel, C. C., & Frail, D. A. 1997a, IAU Circ., 6588, 1

Groot, P. J., Galama, T. J., van Paradijs, J., Strom, R., Telting, J., Rutten, R. G. M., Pettini, M., Tanvir, N., Naber, R., Kouveliotou, C., in 't Zand, J., Heise, J., Costa, E., Feroci, M., Piro, L., Frontera, F., Zavattini, G., Nicastro, L., & Palazzi, E. 1997b, IAU Circ., 6584, 1

Heise, J., in't Zand, J., Kippen, R. M., & Woods, P. M. 2001, in Gamma-ray Bursts in the Afterglow Era, ed. E. Costa, F. Frontera, & J. Hjorth, 16

Hjorth, J., Sollerman, J., Gorosabel, J., Granot, J., Klose, S., Kouveliotou, C., Melinder, J., Ramirez-Ruiz, E., Starling, R., Thomsen, B., Andersen, M. I., Fynbo, J. P. U., Jensen, B. L., Vreeswijk, P. M., Castro Cerón, J. M., Jakobsson, P., Levan, A., Pedersen, K., Rhoads, J. E., Tanvir, N. R., Watson, D., & Wijers, R. A. M. J. 2005a, ApJ, 630, L117

Hjorth, J., Sollerman, J., Møller, P., Fynbo, J. P. U., Woosley, S. E., Kouveliotou, C., Tanvir, N. R., Greiner, J., Andersen, M. I., Castro-Tirado, A. J., Castro Cerón, J. M., Fruchter, A. S., Gorosabel, J., Jakobsson, P., Kaper, L., Klose, S., Masetti, N., Pedersen, H., Pedersen, K., Pian, E., Palazzi, E., Rhoads, J. E., Rol, E., van den Heuvel, E. P. J., Vreeswijk, P. M., Watson, D., & Wijers, R. A. M. J. 2003, Nature, 423, 847

Hjorth, J., Thomsen, B., Nielsen, S. R., Andersen, M. I., Holland, S. T., Fynbo, J. U., Pedersen, H., Jaunsen, A. O., Halpern, J. P., Fesen, R., Gorosabel, J., Castro-Tirado, A., McMahon, R. G., Hoenig, M. D., Björnsson, G., Amati, L., Tanvir, N. R., & Natarajan, P. 2002, ApJ, 576, 113

Hjorth, J., Watson, D., Fynbo, J. P. U., Price, P. A., Jensen, B. L., Jørgensen, U. G., Kubas, D., Gorosabel, J., Jakobsson, P., Sollerman, J., Pedersen, K., & Kouveliotou, C. 2005b, Nature, 437, 859

Hogg, D. W., Baldry, I. K., Blanton, M. R., & Eisenstein, D. J. 2002, ArXiv e-prints, (arXiv:astro

Holland, W. S., Robson, E. I., Gear, W. K., Cunningham, C. R., Lightfoot, J. F., Jenness, T., Ivison, R. J., Stevens, J. A., Ade, P. A. R., Griffin, M. J., Duncan, W. D., Murphy, J. A., & Naylor, D. A. 1999, MNRAS, 303, 659

Houck, J. R., Roellig, T. L., van Cleve, J., Forrest, W. J., Herter, T., Lawrence, C. R., Matthews, K., Reitsema, H. J., Soifer, B. T., Watson, D. M., Weedman, D., Huisjen, M., Troeltzsch, J., Barry, D. J., Bernard-Salas, J., Blacken, C. E., Brandl, B. R., Charmandaris, V., Devost, D., Gull, G. E., Hall, P., Henderson, C. P., Higdon, S. J. U., Pirger, B. E., Schoenwald, J., Sloan, G. C., Uchida, K. I., Appleton, P. N., Armus, L., Burgdorf, M. J., Fajardo-Acosta, S. B., Grillmair, C. J., Ingalls, J. G., Morris, P. W., & Teplitz, H. I. 2004, ApJS, 154, 18

Hurley, K. & Cline, T. 2004, in American Institute of Physics Conference Series, Vol. 727, Gamma-Ray Bursts: 30 Years of Discovery, ed. E. Fenimore & M. Galassi, 613–617

Jager, R., Mels, W. A., Brinkman, A. C., Galama, M. Y., Goulooze, H., Heise, J., Lowes, P., Muller, J. M., Naber, A., Rook, A., Schuurhof, R., Schuurmans, J. J., & Wiersma, G. 1997, A&AS, 125, 557

Jakobsson, P., Björnsson, G., Fynbo, J. P. U., Jóhannesson, G., Hjorth, J., Thomsen, B., Møller, P., Watson, D., Jensen, B. L., Östlin, G., Gorosabel, J., & Gudmundsson, E. H. 2005, MNRAS, 362, 245

Jakobsson, P., Hjorth, J., Fynbo, J. P. U., Watson, D., Pedersen, K., Björnsson, G., & Gorosabel, J. 2004, ApJ, 617, L21

Kennicutt, Jr., R. C. 1998, ARA&A, 36, 189

Klebesadel, R. W., Strong, I. B., & Olson, R. A. 1973, ApJ, 182, L85

Kouveliotou, C., Meegan, C. A., Fishman, G. J., Bhat, N. P., Briggs, M. S., Koshut, T. M., Paciesas, W. S., & Pendleton, G. N. 1993, ApJ, 413, L101

Labbé, I., Huang, J., Franx, M., Rudnick, G., Barmby, P., Daddi, E., van Dokkum, P. G., Fazio, G. G., Schreiber, N. M. F., Moorwood, A. F. M., Rix, H.-W., Röttgering, H., Trujillo, I., & van der Werf, P. 2005, ApJ, 624, L81

Lai, K., Huang, J.-S., Fazio, G., Gawiser, E., Ciardullo, R., Damen, M., Franx, M., Gronwall, C., Labbe, I., Magdis, G., & van Dokkum, P. 2008, ApJ, 674, 70

Lazzati, D., Covino, S., & Ghisellini, G. 2002, MNRAS, 330, 583

Le Floc'h, E., Charmandaris, V., Forrest, W. J., Mirabel, I. F., Armus, L., & Devost, D. 2006, ApJ, 642, 636

Le Floc'h, E., Duc, P.-A., Mirabel, I. F., Sanders, D. B., Bosch, G., Diaz, R. J., Donzelli, C. J., Rodrigues, I., Courvoisier, T. J.-L., Greiner, J., Mereghetti, S., Melnick, J., Maza, J., & Minniti, D. 2003, A&A, 400, 499

Liske, J., Lemon, D. J., Driver, S. P., Cross, N. J. G., & Couch, W. J. 2003, MNRAS, 344, 307

Lutz, D. 1999, in ESA Special Publication, Vol. 427, The Universe as Seen by ISO, ed. P. Cox & M. Kessler, 623–+

Madau, P., Pozzetti, L., & Dickinson, M. 1998, ApJ, 498, 106

Margutti, R., Chincarini, G., Covino, S., Tagliaferri, G., Campana, S., Della Valle, M., Filippenko, A. V., Fiore, F., Foley, R., Fugazza, D., Giommi, P., Malesani, D., Moretti, A., & Stella, L. 2007, A&A, 474, 815

Meegan, C. A., Fishman, G. J., Wilson, R. B., Horack, J. M., Brock, M. N., Paciesas, W. S., Pendleton, G. N., & Kouveliotou, C. 1992, Nature, 355, 143

Mészáros, P. 2002, ARA&A, 40, 137

Mészáros, P. & Rees, M. J. 1997, ApJ, 476, 232

Metzger, M. R., Djorgovski, S. G., Kulkarni, S. R., Steidel, C. C., Adelberger, K. L., Frail, D. A., Costa, E., & Frontera, F. 1997, Nature, 387, 878

Michałowski, M. J., Hjorth, J., Castro Cerón, J. M., & Watson, D. 2008, ApJ, 672, 817

Nemiroff, R. J. 1994, Comments on Astrophysics, 17, 189

Piran, T. 1999, Phys. Rep., 314, 575

Portinari, L., Sommer-Larsen, J., & Tantalo, R. 2004, MNRAS, 347, 691

Prochaska, J. X., Bloom, J. S., Chen, H.-W., Hurley, K. C., Melbourne, J., Dressler, A., Graham, J. R., Osip, D. J., & Vacca, W. D. 2004, ApJ, 611, 200

Ramirez-Ruiz, E., Trentham, N., & Blain, A. W. 2002, MNRAS, 329, 465

Real Academia Española, ed. 2001, Diccionario de la Lengua Española, 22nd edn. (Madrid: Espasa-Calpe, S.A.)

Rees, M. J. 1995, PASP, 107, 1176

Ricker, G. R., Atteia, J.-L., Crew, G. B., Doty, J. P., Fenimore, E. E., Galassi, M., Graziani, C., Hurley, K., Jernigan, J. G., Kawai, N., Lamb, D. Q., Matsuoka, M., Pizzichini, G., Shirasaki, Y., Tamagawa, T., Vanderspek, R., Vedrenne, G., Villasenor, J., Woosley, S. E., & Yoshida, A. 2003, in American Institute of Physics Conference Series, Vol. 662, Gamma-Ray Burst and Afterglow Astronomy 2001: A Workshop Celebrating the First Year of the HETE Mission, ed. G. R. Ricker & R. K. Vanderspek, 3–16

Rieke, G. H., Young, E. T., Engelbracht, C. W., Kelly, D. M., Low, F. J., Haller, E. E., Beeman, J. W., Gordon, K. D., Stansberry, J. A., Misselt, K. A., Cadien, J., Morrison, J. E., Rivlis, G., Latter, W. B., Noriega-Crespo, A., Padgett, D. L., Stapelfeldt, K. R., Hines, D. C., Egami, E., Muzerolle, J., Alonso-Herrero, A., Blaylock, M., Dole, H., Hinz, J. L., Le Floc'h, E., Papovich, C., Pérez-González, P. G., Smith, P. S., Su, K. Y. L., Bennett, L., Frayer, D. T., Henderson, D., Lu, N., Masci, F., Pesenson, M., Rebull, L., Rho, J., Keene, J., Stolovy, S., Wachter, S., Wheaton, W., Werner, M. W., & Richards, P. L. 2004, ApJS, 154, 25

Sakamoto, T., Lamb, D. Q., Kawai, N., Yoshida, A., Graziani, C., Fenimore, E. E., Donaghy, T. Q., Matsuoka, M., Suzuki, M., Ricker, G., Atteia, J.-L., Shirasaki, Y., Tamagawa, T., Torii, K., Galassi, M., Doty, J., Vanderspek, R., Crew, G. B., Villasenor, J., Butler, N., Prigozhin, G., Jernigan, J. G., Barraud, C., Boer, M., Dezalay, J.-P., Olive, J.-F., Hurley, K., Levine, A., Monnelly, G., Martel, F., Morgan, E., Woosley, S. E., Cline, T., Braga, J., Manchanda, R., Pizzichini, G., Takagishi, K., & Yamauchi, M. 2005, ApJ, 629, 311

Salpeter, E. E. 1955, ApJ, 121, 161

Sari, R., Piran, T., & Narayan, R. 1998, ApJ, 497, L17+

Savaglio, S., Budavári, T., Glazebrook, K., Le Borgne, D., Le Floc'h, E., Chen, H.-W., Greiner, J., & Yoldas, A. K. 2007, The Messenger, 128, 47

Savaglio, S., Glazebrook, K., & Le Borgne, D. 2006, in American Institute of Physics Conference Series, Vol. 836, Gamma-Ray Bursts in the Swift Era, ed. S. S. Holt, N. Gehrels, & J. A. Nousek, 540–545

Savaglio, S., Glazebrook, K., & Le Borgne, D. 2008, ArXiv e-prints, 803

Schlegel, D. J., Finkbeiner, D. P., & Davis, M. 1998, ApJ, 500, 525

Shapley, A. E., Steidel, C. C., Pettini, M., & Adelberger, K. L. 2003, ApJ, 588, 65

Silva, L., Granato, G. L., Bressan, A., & Danese, L. 1998, ApJ, 509, 103

Soderberg, A. M., Berger, E., Page, K., Schady, P., Parrent, J., Pooley, D., Wang, X. ., Ofek, E., Cucchiara, A., Rau, A., Waxman, E., Simon, J., Bock, D., Milne, P., Page, M., Barthelmy, S., Beardmore, A., Bietenholz, M., Brown, P., Burrows, A., Burrows, D. N., Byrngelson, G., Cenko, S. B., Chandra, P., Cummings, J., Fox, D. B., Gal-Yam, A., Gehrels, N., Immler, S., Kasliwal, M., Kong, A., Krimm, H., Kulkarni, S. R., Mészáros, P., Nakar, E., O'Brien, P., de Pasquale, M., Racusin, J., & Rea, N. 2008, Nature, submitted, arXiv:0802.1712v1 [astro.ph]

Spitzer Science Centre, ed. 2006, Infrared Array Camera Data Handbook, 3.0 edn. (Pasadena: California Institute of Technology)

—. 2007a, Multiband Imaging Photometer for *Spitzer* (MIPS) Data Handbook, 3.3.0 edn. (Pasadena: California Institute of Technology)

—. 2007b, *Spitzer Space Telescope* Observer's Manual, 8.0 edn. (Pasadena: California Institute of Technology)

Stanek, K. Z., Matheson, T., Garnavich, P. M., Martini, P., Berlind, P., Caldwell, N., Challis, P., Brown, W. R., Schild, R., Krisciunas, K., Calkins, M. L., Lee, J. C., Hathi, N., Jansen, R. A., Windhorst, R., Echevarria, L., Eisenstein, D. J., Pindor, B., Olszewski, E. W., Harding, P., Holland, S. T., & Bersier, D. 2003, ApJ, 591, L17

Steidel, C. C. & Hamilton, D. 1992, AJ, 104, 941

Strong, I. B. & Klebesadel, R. W. 1976, Scientific American, 235, 66

Strong, I. B., Klebesadel, R. W., & Olson, R. A. 1974, ApJ, 188, L1

Swank, J. H. 1999, Nuclear Physics B Proceedings Supplements, 69, 12

Tanvir, N. R., Barnard, V. E., Blain, A. W., Fruchter, A. S., Kouveliotou, C., Natarajan, P., Ramirez-Ruiz, E., Rol, E., Smith, I. A., Tilanus, R. P. J., & Wijers, R. A. M. J. 2004, MNRAS, 352, 1073

Taylor, G. B., Frail, D. A., & Bloom, J. S. 2000, GCN Circ., 880, 1

Terekhov, O. V., Lobachev, V. A., Syunyaev, R. A., Kovtun, A. V., Denisenko, D. V., Kuznetsov, A. V., Barat, C., Vedrenne, G., & Desaley, J.-P. 1995, Astronomy Letters, 21, 217

Terrell, J. 1989, Journal of the British Interplanetary Society, 42, 309

van der Wel, A., Franx, M., Wuyts, S., van Dokkum, P. G., Huang, J., Rix, H.-W., & Illingworth, G. D. 2006, ApJ, 652, 97

van Dokkum, P. G., Förster Schreiber, N. M., Franx, M., Daddi, E., Illingworth, G. D., Labbé, I., Moorwood, A., Rix, H.-W., Röttgering, H., Rudnick, G., van der Wel, A., van der Werf, P., & van Starkenburg, L. 2003, ApJ, 587, L83 van Dokkum, P. G., Franx, M., Förster Schreiber, N. M., Illingworth, G. D., Daddi, E., Knudsen, K. K., Labbé, I., Moorwood, A., Rix, H.-W., Röttgering, H., Rudnick, G., Trujillo, I., van der Werf, P., van der Wel, A., van Starkenburg, L., & Wuyts, S. 2004, ApJ, 611, 703

van Paradijs, J., Groot, P. J., Galama, T., Kouveliotou, C., Strom, R. G., Telting, J., Rutten, R. G. M., Fishman, G. J., Meegan, C. A., Pettini, M., Tanvir, N., Bloom, J., Pedersen, H., Nørdgaard-Nielsen, H. U., Linden-Vørnle, M., Melnick, J., van der Steene, G., Bremer, M., Naber, R., Heise, J., in't Zand, J., Costa, E., Feroci, M., Piro, L., Frontera, F., Zavattini, G., Nicastro, L., Palazzi, E., Bennet, K., Hanlon, L., & Parmar, A. 1997, Nature, 386, 686

van Paradijs, J., Kouveliotou, C., & Wijers, R. A. M. J. 2000, ARA&A, 38, 379

Villasenor, J. S., Lamb, D. Q., Ricker, G. R., Atteia, J.-L., Kawai, N., Butler, N., Nakagawa, Y., Jernigan, J. G., Boer, M., Crew, G. B., Donaghy, T. Q., Doty, J., Fenimore, E. E., Galassi, M., Graziani, C., Hurley, K., Levine, A., Martel, F., Matsuoka, M., Olive, J.-F., Prigozhin, G., Sakamoto, T., Shirasaki, Y., Suzuki, M., Tamagawa, T., Vanderspek, R., Woosley, S. E., Yoshida, A., Braga, J., Manchanda, R., Pizzichini, G., Takagishi, K., & Yamauchi, M. 2005, Nature, 437, 855

Waldron, H. 1997, SMC Astro News, February 7th

Werner, M. W., Roellig, T. L., Low, F. J., Rieke, G. H., Rieke, M., Hoffmann, W. F., Young, E., Houck, J. R., Brandl, B., Fazio, G. G., Hora, J. L., Gehrz, R. D., Helou, G., Soifer, B. T., Stauffer, J., Keene, J., Eisenhardt, P., Gallagher, D., Gautier, T. N., Irace, W., Lawrence, C. R., Simmons, L., Van Cleve, J. E., Jura, M., Wright, E. L., & Cruikshank, D. P. 2004, ApJS, 154, 1

Winkler, C., Courvoisier, T. J.-L., Di Cocco, G., Gehrels, N., Giménez, A., Grebenev, S., Hermsen, W., Mas-Hesse, J. M., Lebrun, F., Lund, N., Palumbo, G. G. C., Paul, J., Roques, J.-P., Schnopper, H., Schönfelder, V., Sunyaev, R., Teegarden, B., Ubertini, P., Vedrenne, G., & Dean, A. J. 2003, A&A, 411, L1

Yun, M. S. & Carilli, C. L. 2002, ApJ, 568, 88

Zeh, A., Klose, S., & Hartmann, D. H. 2004, ApJ, 609, 952

Zhang, B. & Mészáros, P. 2004, International Journal of Modern Physics A, 19, 2385

Appendix A

Paper I

On the constraining observations of

the dark GRB 001109 and the properties of a

$z = 0.398$ radio selected starburst galaxy
contained in its error box

by

J. M. Castro Cerón, J. Gorosabel, A. J. Castro-Tirado, V. V. Sokolov,
V. L. Afanasiev, T. A. Fatkhullin, S. N. Dodonov, V. N. Komarova,
A. M. Cherepashchuk, K. A. Postnov, U. Lisenfeld, J. Greiner, S. Klose,
J. Hjorth, J. P. U. Fynbo, H. Pedersen, E. Rol, J. Fliri, M. Feldt,
G. Feulner, M. I. Andersen, B. L. Jensen, M. D. Pérez Ramírez, F. J. Vrba,
A. A. Henden, G. Israelian & N. R. Tanvir.

Astronomy & Astrophysics, **424**, 833–839 (2004)

Statement of coauthorship

J.M. Castro Cerón wrote the paper and made Figures 1 and 3. He did most of the photometry, one of the astrometric solutions, the analysis of the afterglow SED and contributed to the analysis of the X-ray data necessary for the afterglow SED. J. Gorosabel made Figure 5, the analysis of object A's SED and contributed critical discussion for the paper. He also assisted with the photometry. V.V. Sokolov and his collaborators contributed the spectrum and its analysis, as well as the other astrometric solution. J.P.U. Fynbo made Figure 4. U. Lisenfeld contributed the analysis of the submillimetre data. Other authors contributed in various ways, including data and discussion.

José María Castro Cerón **Javier Gorosabel** **Jens Hjorth**

A&A 424, 833–839 (2004)
DOI: 10.1051/0004-6361:20035921

Astronomy & Astrophysics

On the constraining observations of the dark GRB 001109 and the properties of a z = 0.398 radio selected starburst galaxy contained in its error box*

J. M. Castro Cerón[1,2], J. Gorosabel[2,3,4], A. J. Castro-Tirado[3], V. V. Sokolov[5], V. L. Afanasiev[5], T. A. Fatkhullin[5], S. N. Dodonov[5], V. N. Komarova[5], A. M. Cherepashchuk[6], K. A. Postnov[6], U. Lisenfeld[3], J. Greiner[7], S. Klose[8], J. Hjorth[9], J. P. U. Fynbo[9,10], H. Pedersen[9], E. Rol[11], J. Fliri[12], M. Feldt[13], G. Feulner[12], M. I. Andersen[14], B. L. Jensen[9], M. D. Pérez Ramírez[15], F. J. Vrba[16], A. A. Henden[16,17], G. Israelian[18], and N. R. Tanvir[19]

1 Real Instituto y Observatorio de la Armada, Sección de Astronomía, 11.110 San Fernando-Naval (Cádiz), Spain
e-mail: josemari@alumni.nd.edu
2 Space Telescope Science Institute, 3.700 San Martín Dr., Baltimore MD 21.218–2.463, USA
e-mail: gorosabel@stsci.edu
3 Instituto de Astrofísica de Andalucía (IAA-CSIC), Camino Bajo de Huétor, 24, 18.008 Granada, Spain
e-mail: [jgu;ajct;ute]@iaa.es
4 Danish Space Research Institute, Juliane Maries Vej 30, 2100 København Ø, Denmark; e-mail: jgu@dsri.dk
5 Special Astrophysical Observatory of the Russian Academy of Sciences, Nizhnij Arkhyz, 357 147 Karachai-Cherkessia, Russia;e-mail: [sokolov;vafan;timur;dodo;vkom]@sao.ru
6 Sternberg Astronomical Institute, Mikhail Vasil'evich Lomonosov Moscow State University, Moscow, 119 899 Leninskie Gory, Russia; e-mail: [cher;moulin]@sai.msu.su
7 Max Planck Institut für extraterrestrische Physik, Giessenbachstraße, Postfach 1312, 85 741 Garching, Germany
e-mail: jcg@mpe.mpg.de
8 Thüringer Landessternwarte Tautenburg, 07 778 Tautenburg, Germany; e-mail: klose@tls-tautenburg.de
9 Astronomical Observatory, University of Copenhagen, Juliane Maries Vej 30, 2100 København Ø, Denmark
e-mail: [jgu;jens;holger;brian_j]@astro.ku.dk
10 Institute of Physics and Astronomy, University of Århus, Ny Munkegade, 8000 Århus C, Denmark
e-mail: jfynbo@phys.au.dk
11 Astronomical Institute Anton Pannekoek, University of Amsterdam, Kruislaan 403, 1098 SJ Amsterdam, The Netherlands
e-mail: evert@science.uva.nl
12 Universitäts-Sternwarte München, Scheinerstraße 1, 81 679 München, Germany
e-mail: [fliri;feulner]@usm.uni-muenchen.de
13 Max Planck Institut für Astronomie, Königstuhl 17, 69 117 Heidelberg, Germany; e-mail: mfeldt@mpia-hd.mpg.de
14 Astrophysikalisches Institut, An der Sternwarte 16, 14 482 Potsdam, Germany; e-mail: mandersen@aip.de
15 Sci-SA Department, ESTEC-ESA, Keplerlaan 1, Postbus 299, 2200 AG Noordwijk, The Netherlands
e-mail: dperez@rssd.esa.int
16 US Naval Observatory, Flagstaff Station, PO Box 1.149, Flagstaff AZ 86.002-1.149, USA
e-mail: [fjv;ahenden]@nofs.navy.mil
17 Universities Space Research Association
18 Instituto de Astrofísica de Canarias, c/. vía Láctea, s/n, 38.200 La Laguna (Tenerife), Spain
e-mail: gil@iac.es
19 Department of Physical Sciences, University of Hertfordshire, College Lane, Hatfield, Herts GB–AL10 9AB, UK
e-mail: nrt@star.herts.ac.uk

Received 20 December 2003 / Accepted 4 June 2004

* Based on observations made with telescopes at the Centro Astronómico Hispano Alemán (1.23 m + 3.50 m), at the Observatorio del Roque de los Muchachos (NOT + WHT), at the United States Naval Observatory (1.00 m) and at the Russian Academy of Sciences's Special Astrophysical Observatory (6.05 m). The NOT is operated on the island of San Miguel de la Palma jointly by Denmark, Finland, Iceland, Norway and Sweden, in Spain's Observatorio del Roque de los Muchahos of the Instituto de Astrofísica de Canarias. The Centro Astronómico Hispano Alemán is operated in Calar Alto by the Max-Planck Institut für Astronomie of Heidelberg, jointly with Spain's Comisión Nacional de Astronomía.

Abstract. We present optical and NIR (near infrared) follow up observations of the GRB 001109 from 1 to 300 days after the burst. No transient emission was found at these wavelengths within this GRB's (Gamma Ray Burst) 50″ radius BeppoSAX error box. Strong limits (3σ) are set with: $R \gtrsim 21$, 10.2 h after the GRB; $I \gtrsim 23$, 11.4 h after the GRB; $H \gtrsim 20.7$, 9.9 h after the GRB; and $K_S \gtrsim 20$, 9.6 h after the GRB. We discuss whether the radio source found in the GRB's error box (Taylor et al. 2000) might be related to the afterglow. We also present a multiwavelength study of a reddened starburst galaxy, found coincident with the potential radio and the X-ray afterglow. We show that our strong *I* band upper limit makes of the GRB 001109 the darkest one localised by the BeppoSAX's NFI (Narrow Field Instrument), and it is one of the most constraining upper limits on GRB afterglows to date. Further to it, the implications of these observations in the context of dark GRBs are considered.

Key words. gamma rays: bursts – Galaxy: fundamental parameters – techniques: photometric

1. Introduction

For the period spanning 1997–2001, approximately only one third of all GRBs (Gamma Ray Bursts) with well determined coordinates have had successful searches for optical counterparts (Greiner 2003). Several mechanisms (Lazzati et al. 2002; Ramírez-Ruíz et al. 2002) have been presented to explain the lack of optical counterparts despite the prompt/deep observations carried out for some of them (Fynbo et al. 2001; Piro et al. 2002). It is thought that extinction around the progenitor and in the host galaxy plays a role in the non detection of the optical counterpart associated with dark GRBs (Groot et al. 1998; Taylor et al. 1998).

The GRB 001109 was detected on 09.391169 UT November 2000 (t_0 hereafter) by the BeppoSAX (Boella et al. 1997) with a refined uncertainty of 2.5′ (Gandolfi et al. 2000a,b). A BeppoSAX NFI (Narrow Field Instrument) observation at t_0 + 16.5 h detected a previously unknown source inside the 2.5′ radius WFC (Wide Field Camera) error box (Amati et al. 2000). The source, designated 1SAX J1830.1+5517, had RA (J2000) = $18^{\rm h}30^{\rm m}07.8^{\rm s}$, Dec (J2000) = +55°17′56″ (error radius = 50″) and a 2–10 keV flux of $7.1 \pm 0.5 \times 10^{-13}$ erg cm^{-2} s^{-1}. See Amati et al. (2003, 2004) for a detailed discussion of the X-ray properties.

A radio source (dubbed VLA J1830+5518) was found within the NFI error box with RA (J2000) = $18^{\rm h}30^{\rm m}06.51^{\rm s}$, Dec (J2000) = +55°18′35.7″ (conservative errors of 0.1″ in each coordinate) and a flux of 236 ± 31 μJy at 8.46 GHz (Taylor et al. 2000). It seemed to decrease in brightness over a time span of 2 days (Rol et al. 2000), but further observations at the VLA for ~390 days failed to reveal a consistent decay (Berger & Frail 2001).

In this paper we report on the deep optical/NIR (near infrared) observations carried out for the GRB 001109 and their implications in the study of dark GRBs. Further we report on millimetre observations.

2. Observations

Table 1 displays the observing log. Target of Opportunity observations started at t_0 + 9.1 h (referred to the start time of the first frame reported by Greiner et al. (2000), taken with the 1.23 CAHA). We performed aperture photometry using SExtractor[1] (Bertin & Arnouts 1996) to study the contents of the BeppoSAX error box. The field was calibrated observing the Landolt field SA113 (Landolt 1992) in the *UBVRI* bands (*R* and *I* in the Cousins system), at airmasses similar to that of the GRB's field, in only one night. Table 2 shows the positions and magnitudes of several secondary standards in the GRB's field (see Fig. 1). Spectroscopic observations were made at the 6.05 SAO telescope (12 × 600 s exposures; see Fig. 2) with SCORPIO and a 300 lines/mm grating. The spectral resolution (FWHM) obtained was ~20 Å and the effective wavelength coverage was 3500−9500 Å (Afanasiev et al. 2001). Millimetre observations were carried out at the 30 m IRAM telescope (see Sect. 3.5).

[1] http://terapix.iap.fr/soft/sextractor/

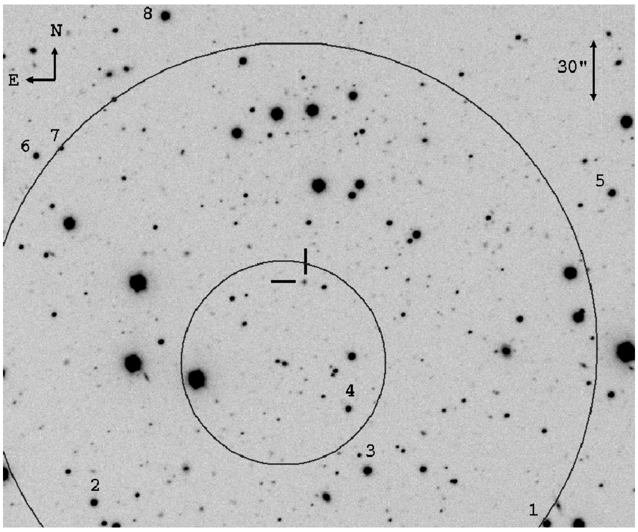

Fig. 1. The contents of the BeppoSAX error box for the GRB 001109 field. This *R* band image was taken with the 2.56 NOT (+ALFOSC) on 14.0524–14.0734 UT August 2001. The source in between ticks is the galaxy coincident with the VLA J1830+5518 and consistent with the position of the X-ray afterglow. The numbered stars are the secondary standards indicated in Table 2. The large circle represents the refined WFC error box (Gandolfi et al. 2000b) and the small one the NFI error circle (Amati et al. 2000). The field of view covered by the figure is 5.1′ × 4.3′. North is upwards and East is leftwards.

3. Results and analysis

3.1. Content of the BeppoSAX NFI error box

No optical afterglow was detected in the first 1.23 CAHA (Greiner et al. (2000); $R_{\rm lim} > 20.9$ mag at 10.2 h after the GRB)

Table 1. Journal of observations of the GRB 001109 field.

Date UT	Telescope	Filtre	Exposure time (s)	Limiting magnitude (3σ)
09.7708–09.8590/11/2000	1.23 CAHA (CCD)	R	7×500	20.9*
09.7847–09.8854/11/2000	1.23 CAHA (CCD)	B	3×600	20.3*
09.7848–09.7961/11/2000	4.20 WHT (INGRID)	K_S	750	19.9**
09.7968–09.8081/11/2000	4.20 WHT (INGRID)	H	750	21.0**
09.8083–09.8128/11/2000	4.20 WHT (INGRID)	J	300	21.3**
09.8447–09.8845/11/2000	2.56 NOT (StanCam)	I	4×600	22.9
10.0876–10.1084/11/2000	1.00 USNO (CCD)	I	1800	21.0*
10.7363–10.7883/11/2000	3.50 CAHA (OMEGA Prime)	H	10×300	20.5*
10.7618–10.8417/11/2000	1.23 CAHA (CCD)	R	9×500	20.9*
11.8191–11.8281/11/2000	4.20 WHT (INGRID)	H	600	20.7**
11.8292–11.8383/11/2000	4.20 WHT (INGRID)	K_S	600	19.4**
11.8423–11.8514/11/2000	4.20 WHT (INGRID)	J	600	21.4**
13.0560–13.0768/11/2000	1.00 USNO (CCD)	I	1800	21.0*
22.1590–22.1938/11/2000	2.56 NOT (ALFOSC)	B	600	23.0
22.8278–22.8444/11/2000	2.56 NOT (ALFOSC)	U	2×600	24.0
23.8035–22.8194/11/2000	2.56 NOT (ALFOSC)	B	2×600	23.5
26.7576–26.7618/11/2000	3.50 CAHA (MOSCA)	R	120	22.0
27.7514–27.7556/11/2000	3.50 CAHA (MOSCA)	R	180	22.3
22.1590–22.1938/05/2001	4.20 WHT (PF)	B	3×900	24.0
22.1951–22.2079/05/2001	4.20 WHT (PF)	V	3×450	23.5
29.1249–29.1795/05/2001	2.56 NOT (ALFOSC)	U	3×1500	23.5
30.1249–30.1723/05/2001	2.56 NOT (ALFOSC)	V	900 + 300	23.5
31.0468–31.0548/05/2001	2.56 NOT (ALFOSC)	V	600	22.0
18.0361–18.0924/06/2001	4.20 WHT (PF)	U	5×900	23.5
30.0583–30.1361/06/2001	3.50 CAHA (OMEGA Cass)	K'	120×60	21.0†
01.0354–01.1181/07/2001	3.50 CAHA (OMEGA Cass)	K'	120×60	21.0†
24.8655–24.8828/07/2001	6.05 SAO (SCORPIO)	R	3×180	25.5
14.0524–14.0734/08/2001	2.56 NOT (ALFOSC)	R	600 + 900	23.8
14.9983–15.0223/08/2001	2.56 NOT (ALFOSC)	R	2×900	24.0
16.0571–16.1169/08/2001	2.56 NOT (ALFOSC)	B	4×1200	25.0
16.9835–17.0570/08/2001	2.56 NOT (ALFOSC)	U	5×1500	24.1
17.0148–17.0720/08/2001	2.56 NOT (ALFOSC)	V	5×900	24.5
17.0720–17.1148/08/2001	2.56 NOT (ALFOSC)	I	6×600	23.7
05.9503–06.0220/08/2002	2.20 CAHA (BUSCA)	y	6×900	22.5

* Greiner et al. (2000). Their BRI band limiting magnitudes have been shifted to our zero point.
** Vreeswijk et al. (2000). Their JHK_S band limiting magnitudes have been shifted to our zero point.
† The images from 30/6–01/07/2001 were coadded in just a single limiting magnitude, $K' = 21.0$.

Table 2. Photometric secondary standards in the GRB 001109 field.

	RA (J2000) h m s	Dec (J2000) ° ′ ″	U	B	V	R	I
1	18 29 52.55	+55 16 37.8	18.62 ± 0.03	18.53 ± 0.08	17.95 ± 0.02	17.58 ± 0.02	17.25 ± 0.02
2	18 30 18.61	+55 16 46.6	21.02 ± 0.17	19.57 ± 0.04	18.49 ± 0.02	17.79 ± 0.02	17.16 ± 0.02
3	18 30 02.94	+55 17 03.2	19.24 ± 0.06	18.48 ± 0.07	17.55 ± 0.02	16.90 ± 0.02	16.36 ± 0.02
4	18 30 04.05	+55 17 33.7	21.31 ± 0.17	19.99 ± 0.05	18.97 ± 0.02	18.16 ± 0.02	17.52 ± 0.02
5	18 29 48.91	+55 19 20.5	20.26 ± 0.12	19.27 ± 0.06	18.33 ± 0.02	17.73 ± 0.02	17.25 ± 0.02
6	18 30 22.09	+55 19 36.9	19.16 ± 0.06	19.45 ± 0.02	19.03 ± 0.07	18.77 ± 0.02	18.45 ± 0.02
7	18 30 20.65	+55 19 40.7	20.63 ± 0.15	20.49 ± 0.08	20.05 ± 0.02	19.68 ± 0.03	19.27 ± 0.04
8	18 30 14.57	+55 20 43.3	19.54 ± 0.08	18.62 ± 0.03	17.28 ± 0.02	16.33 ± 0.02	15.30 ± 0.02

and 2.56 NOT ($I_{\rm lim} > 22.9$ mag at 11.4 h after the GRB) frames. Strong limits come from the deep NIR observations. The H and K' 3.50 CAHA images (Greiner et al. (2000) reported the value of H) have been compared to the H and K_S 4.20 WHT ones reported by Vreeswijk et al. (2000). We derived the following upper limits[2] for any NIR transient emission within the NFI error box: $K' > 19.9$, $H > 20.7$ and $J > 21.3$, ~10 h after the GRB, all of them with a 3σ confidence level.

[2] We have assumed $K' \simeq K_S$.

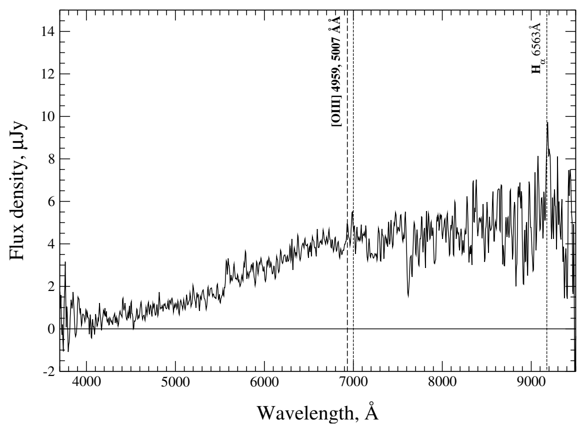

Fig. 2. Optical spectrum of the galaxy coincident with the VLA J1830+5518, obtained with the 6.05 SAO (+SCORPIO). It shows rest frame emission lines for Hα (6563 Å) and O[III] (4959 Å, 5007 Å).

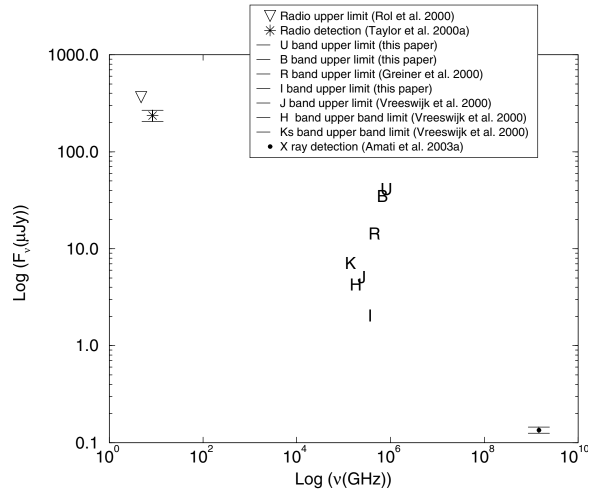

Fig. 3. Selected detections (X-ray) and upper limits ($UBVRIJHK_S$) associated with the GRB 001109. The most constraining upper limit corresponds to the 2.56 NOT I band measurement.

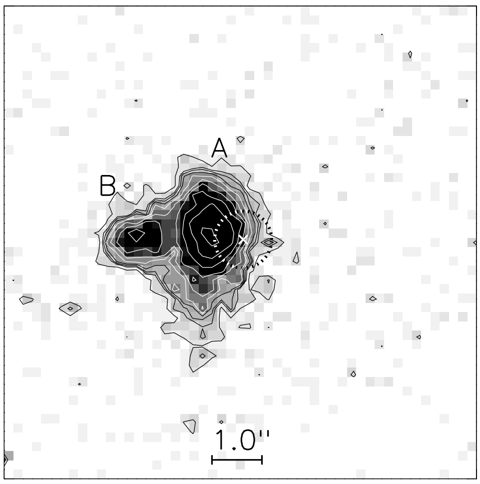

Fig. 4. Contour plot displaying the galaxy coincident with the VLA J1830+5518. The figure shows the coadded I band image taken with the 2.56 NOT (+ALFOSC) (17.0720–17.1148/08/2001) of the source coincident with the VLA J1830+5518. A seeing of 0.8″ allowed us to separate the two components, the objects A and B. The centre of the circle marks the position of the radio source (Taylor et al. 2000), RA (J2000) = $18^h30^m06.51^s$, Dec (J2000) = 55°18′35.7″. The radius of the circle is 0.57″. The contours show the detection confidence level above the background in a logarithmic scale. North is upwards and East is leftwards.

3.2. Afterglow's SED

Figure 3 displays selected detections and upper limits associated with the GRB 001109 (to keep the figure legible we have only plotted the most constraining measurement for each of the optical and NIR bands). All plotted measurements have been shifted to a common epoch ($t = t_0 + 0.4$ days; epoch of the radio detection, Taylor et al. 2000) assuming a power law decay index $\alpha = 1.27$ (suggested by the X-ray observations reported in Amati et al. 2003). As shown, the most constraining upper limit corresponds to the 2.56 NOT I band image taken on 9.8447−9.8845 UT November 2000.

This I band measurement allows us to impose an upper limit on the afterglow's optical to X-ray spectral index: $\beta_{\mathrm{optical-X-ray}} < 0.33 \pm 0.02$ (β is the power law index of the specific flux; $F_\nu \sim \nu^{-\beta}$). The corresponding optical to X-ray spectral index upper limits for the full BeppoSax's NFI dark burst sample can be worked out from the limits on the optical to X-ray flux ratio[3] ($f_{0\mathrm{X}}$ from Table 1 in de Pasquale et al. 2003):

$$f_{0\mathrm{X}} = \frac{\nu_{\mathrm{optical}}^{-\beta}}{\nu_{\mathrm{X}}^{-\beta}}.$$

The GRB 001109 has the strongest limit in this sample where the upper limits range from 0.33 to 0.55.

3.3. VLA J1830+5518

3.3.1. Astrometry

We performed astrometry on two different data sets. For the first data set, 10 USNO A2.0 stars, not saturated on the 6.05 SAO images, were used. The astrometrical uncertainty was found to be ∼0.5″, including both, statistical and systematic errors (Sokolov et al. 2001). For the second data set, an independent astrometric solution, based on 50 USNO A2.0 stars, was obtained using the coadded I band image taken at the 2.56 NOT (see the penultimate entry in Table 1). It yielded a similar uncertainty (0.57″). Both astrometric solutions showed, independently, that the position of the radio source is consistent with the brighter component ($R = 20.65 \pm 0.06$, the object A hereafter) of a complex system (see Fig. 4). The second brightest component (the object B hereafter) is located 1.25″ to the East of the object A. Strictly speaking the astrometry reveals the registration of the optical image, and has nothing to do with the location of the VLA radio source which was determined

[3] The optical to X-ray flux ratio ($f_{0\mathrm{X}}$) is defined as the R band flux (or upper limit), in units of μJy, divided by the 1.6−10 keV X-ray flux, in units of 10^{-13} cg (de Pasquale et al. 2003).

absolutely in the International Coordinate Reference Frame. These two objects were independently detected in the optical and in the NIR, so we conclude that they are real objects.

3.3.2. Spectroscopy

Spectral measurements (performed with the slit aligned in the East-West direction) detected Balmer breaks and emission lines for the sources A and B. First we divided the 2D spectra of the objects A and B using Gaussian analysis. Then we aproximated the resulting 2D spectrum across the dispersion direction by summing the two gaussians with the FWHM parametres (wavelength dependent). Finally we checked our extraction model by subtracting the model from the real data. Object A's redshift is $z = 0.398 \pm 0.002$ based on the identification of the Hα (6563 Å) and O[III] (4959 Å, 5007 Å) emission lines (see Fig. 2 and Afanasiev et al. 2001). Object B's redshift is $z = 0.3399 \pm 0.0005$ based on the identification of the Hα (6563 Å) and Hβ (4861 Å) emission lines (Afanasiev et al. 2001). The redshift difference between sources A and B corresponds to a large relative expansion velocity of $\sim$13 000 km s^{-1}. Given that velocity dispersions in galaxy clusters are, at most, $\sim$5000 km s^{-1} (Fadda et al. 1996; Girardi et al. 1993), the alignment of both sources is likely the result of a chance projection. An HST high resolution deep image that might find signs of interaction would help to clarify this issue.

If the object A were the host of the GRB 001109, then the burst redshift would be $z = 0.398 \pm 0.002$. To further constrain this suggestion we calculate the probability to find a radio source with the brightness of VLA J1830+5518 in an error box with a radius of 50″.

Following Fomalont et al. (2002) the density of radio sources detected at 8.4 GHz above a flux density S in microjanskys is given by:

$$N = (0.099 \pm 0.010) \left(\frac{S}{40}\right)^{-1.11 \pm 0.13} \quad \mathrm{arcmin}^{-2}.$$

So we conclude that the chance probability of having a source brighter than 238 ± 31 μJy inside the NFI error box is 3 ± 0.9% and thus, consider that the probability is not low enough to establish a physical relationship between the location of this radio source inside the GRB's error box and the occurrence of the γ ray event.

3.4. Object A's SED

We have determined the flux distribution of the galaxy coincident (not necessarily related) with the VLA J1830+5518 by means of our *UBVRI* broad band photometric measurements together with the JHK_{S} broad band measurements reported by Vreeswijk et al. (2000). The photometry was based on SExtractor (Bertin & Arnouts 1996), which allows to deblend entangled sources (this is specially relevant for cases like that of the objects A and B). The fluxes at the $UBVRIJHK_{\mathrm{S}}$ passband wavelengths have been dereddened of Galactic extinction using a value of $E(B-V) = 0.04$ (DIRBE/IRAS dust maps: Schlegel et al. 1998).

The $UBVRIJHK_{\mathrm{S}}$ passband fluxes (measured in units of 2×10^{-17} erg cm^{-2} s^{-1} Å^{-1}; see Fig. 5) correspond to the following values: 0.118 ± 0.014, 0.234 ± 0.007, 0.475 ± 0.012, 0.684 ± 0.034, 0.573 ± 0.030, 0.526 ± 0.023, 0.393 ± 0.018 and 0.315 ± 0.014, respectively. We have modelled the SED using stellar population synthesis techniques (Bolzonella et al. 2000) leaving the extinction and the redshift as free parametres. For the extinction law we have used the one given by Calzetti et al. (2000), which is typical for starburst galaxies. The best fit is obtained with a dusty galaxy SED at $z = 0.381$, with $A_{\mathrm{V}} = 1.4$ mag and an episode of star formation 0.25 Gyr ago (see Fig. 5). This episode of star formation dominates the optical continuum.

Although the radio emission from the object A is not related to the afterglow of the GRB, the object A could still be the host galaxy of the burst. To further constrain this suggestion we have calculated the number of galaxies, with magnitude $B < 22.96$ (reddened), to be found inside a circular area with a 50″ radius. Using the Millennium Galaxy Catalogue (Liske et al. 2003) we estimate a count of $\sim$3 galaxies (the B passband flux has been dereddened of Galactic extinction using a value of $E(B-V) = 0.04$; DIRBE/IRAS dust maps: Schlegel et al. 1998).

The estimated extinction ($A_{\mathrm{V}} = 1.4$) might explain the lack of optical emission and agree with the presence of the Hα (6563 Å) and O[III] (4959 Å, 5007 Å) emission lines (see Fig. 2 and Afanasiev et al. 2001) and the non negligible intrinsic $N_{\mathrm{H}} = 2.83 \times 10^{22} \pm {}^{4.7}_{2.83}$ cm^{-2} (de Pasquale et al. 2003). This would also be consistent with the fact that the majority of the long duration GRB afterglows located so far have been linked to actively star forming galaxies.

3.5. Results of the millimetre observations

We observed the VLA J1830+5518 with the 117 channel Max Planck Millimetre Bolometre array (MAMBO, Kreysa et al. 1998) at the IRAM's 30 m radiotelescope on Pico Veleta, Spain, between 4 Mar 2003 and 12 Mar. 2003. MAMBO has an effective centre frequency of $\sim$250 GHz (1.2 mm) and a beam size of 10.6″. The observations were done in standard on/off mode with 2 Hz chopping of the secondary mirror with a throw of 32″. The flux was calibrated by performing observations on Mars and Uranus, which yielded a conversion factor of 30 000 counts/Jy with an estimated error of 15%. We did not detect any emission from the VLA J1830+5518 down to a rms noise level of 0.5 mJy.

Further, we have estimated how "unusual" is a non detection with MAMBO in this case. This estimation is based in a correlation between the far IR and the radio. Carilli & Yun (1999) give the correlation of the far IR/radio bands as a function of the redshift. Adapting this correlation to our frequencies we expect, for $z = 0.398$, the fluxes at 8.4 GHz and 250 GHz to be aproximately equal. We have that, for 8.4 GHz, flux = 0.2 mJy, and that, for 250 GHz, flux < 1.5 mJy (3σ), so our results agree with the expected ones. With a higher redshift the flux at 250 GHz is expected to rise as a function of the flux in radio. Our upper limit at 250 GHz and

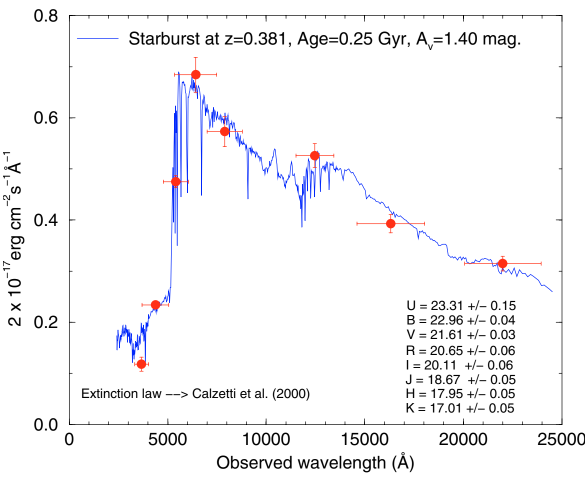

Fig. 5. SED of the galaxy coincident with the VLA J1830+5518. The solid line is the SED of a dusty galaxy at $z = 0.381$, with $A_V = 1.4$ mag and an episode of star formation 0.25 Gyr ago. This episode of star formation dominates the optical continuum. The SED has been constructed with homogeneous data taken with the 2.56 NOT (+ALFOSC) for the optical and with the 4.20 WHT (+INGRID) for the NIR.

Table 3. The object A's magnitudes.

Band	Magnitude
U	23.31 ± 0.15
B	22.96 ± 0.04
V	21.61 ± 0.03
R	20.65 ± 0.06
I	20.11 ± 0.06
J	18.67 ± 0.05
H	17.95 ± 0.05
K	17.01 ± 0.05

the correlation from Carilli & Yun (1999) give us an estimate of $z = 1$ as the maximum redshift allowed for the VLA source (taking the flux at 250 GHz to be less than 1.5 mJy at 3σ). This consistency with the far IR/radio correlation implies that the radio emission probably originates from star formation and not from an AGN. Such conclusion can be accomodated by our *UBVRIJHK* band SED of the object A (see Table 3 and Fig. 5). Additionally, the $z = 1$ upper limit for the VLA J1830+5518 is consistent with the object A's redshift.

Barnard et al. (2003) observed the VLA J1830+5518 with the ~350 GHz photometry pixel on the Submillimetre Common User Bolometre Array (SCUBA, Holland et al. 1999), at the James Clerk Maxwell Telescope on Mauna Kea, United States. Their measurement yielded a flux of 1.89 ± 1.4 mJy, consistent with our upper limit at 250 GHz since the flux at 350 GHz is larger by a factor of 3–4 (considering a rms noise level of 0.5 mJy).

4. Discussion and conclusions

Our optical/NIR/millimetre observations are consistent with a connection between the VLA J1830+5518 and the object A. On the other hand, a connection between the object A and the GRB 001109 can not be established.

If we define a dark GRB as one with no counterpart brighter than $R < 23$ at 24 h from the onset, then the GRB 001109 is clearly a dark GRB, given the $I > 22.9$ limit imposed by the 2.56 NOT 0.47 days after the γ ray event. We have used our 2.56 NOT $I > 22.9$ upper limit (9.8447–9.8845/11/2000 UT) to further constrain the luminosity of the GRB 001109 within the context of the BeppoSAX's NFI dark burst sample (see upper limits for dark bursts in Table 1 of de Pasquale et al. 2003). To do so we have (following the methodology described in de Pasquale et al. 2003) calculated the R band upper limit 11 h after the GRB, from the 2.56 NOT I band constraint. First, we calculated the R band flux associated with the I band limit using the spectral index $\beta_{\mathrm{optical-X\text{-}ray}} = 0.33 \pm 0.02$ (see Sect. 3.2). Then, the R band flux was rescaled from $t - t_0 =$ 11.3624 h (9.8646 UT November 2000; mean 2.56 NOT observing time) to $t - t_0 = 11$ h (assuming a power law decay index $\alpha = 1.15$, adopted by de Pasquale et al. 2003). Further, the R band flux upper limit was corrected for Galactic extinction using a $E(B - V) = 0.04$ value (Schlegel et al. 1998). As a result we derived an unextincted R band flux upper limit of 1.80 μJy 11 h after the γ ray event. This new R band flux upper limit is approximately 7 times deeper than the one reported previously (11.81 μJy in de Pasquale et al. 2003). Moreover, our I band image lowers the f_{0X} from 0.59 to 0.09, making the GRB 001109, by far, the darkest BeppoSAX NFI GRB. Consequently, the 2.56 NOT I band measurement has impossed one of the most constraining upper limits on GRB afterglows to date.

The GRB 001109 belongs to the subsample of darkest BeppoSAX NFI bursts (~25% of the total BeppoSAX NFI dark GRB sample) which show f_{0X} values incompatible (at a 2.6σ level) with GRBs with detected optical transients (de Pasquale et al. 2003). For those objects the spectral index $\beta_{\mathrm{optical-X\text{-}ray}} \leq 0.62$, so the GRB 001109 is clearly in this group, which is composed by the GRBs 981226, 990704, 990806 and 000210.

It is important to highlight that the GRB 001109 exhibited the brightest X-ray afteglow among the dark BeppoSAX NFI bursts (de Pasquale et al. 2003). On the other hand it showed the lowest N_H reported for the dark BeppoSAX NFI GRBs (de Pasquale et al. 2003). In fact, the GRB 001109 N_H value is consistent with the ones measured for GRBs with detected optical transients. Thus, the bright X-ray afterglow of the GRB 001109, its low N_H value (in comparison to the rest of the dark BeppoSAX NFI GRB sample) and the constraining optical limits imposed in the present work, might indicate that the GRB 001109 showed a spectrum intrinsically different from GRBs with detected optical transients.

Acknowledgements. For their assistance during the observations we are grateful to, L. Montoya and A. Aguirre at the CAHA, A. A. Kass at the NOT and, I. Skillen, C. Benn, T. Augusteijn and C. Zurita at the WHT. Some images were taken under the auspices of the Isaac Newton Group's Service Observation Programme. Some of the data presented here have been taken using ALFOSC, which is owned by the Instituto de Astrofísica de Andalucía (IAA-CSIC) an operated at the Nordic Optical Telescope under agreement between the IAA-CSIC and the NBIfAFG of the Astronomical Observatory of Copenhagen. We thank E. Pérez Jiménez and M. A. Cerviño Saavedra for fruitful discussions. J.M.C.C. and J.G. acknowledge a FPI doctoral fellowship from Spain's Ministerio de Ciencia y Tecnología and a Marie Curie Research Grant from the European Commission respectively. J.M.C.C. is grateful for the hospitality extended by the Danish Space Research Institute (DSRI), the Instituto de Astrofísica de Andalucía (IAA-CSIC) and the Astronomical Observatory of the University of Copenhagen, where parts of this work were carried out. This research has been partially supported by Spain's Ministerio de Ciencia y Tecnología under programme AYA2 002-082 (which includes FEDER funds). The work of the SAO team was supported by the Russian Astronomy Foundation and RFBR grant N01-02-17 106a. K.A.P. acknowledges partial support by RFBR grants 00-02-17 164 and 99-02-16 205. U.L. acknowledges partial support from Spain's Ministerio de Ciencia y Tecnología, under grant AYA 2 002-03 338, and Junta de Andalucía. J.P.U.F. gratefully acknowledges support from the Carlsberg Foundation. This work was supported by the Danish Natural Science Research Council. This research has made use of NASA's Astrophysics Data System. The authors wish to thank Dr. G. B. Taylor for helpful comments during the refereeing process.

References

Afanasiev, V., Fatkhullin, T., Dodonov, S., et al. 2001, GCN, 1090
Amati, L., Frontera, F., Pian, E., et al. 2000, IAU Circ., 7519
Amati, L., Frontera, F., Castro Cerón, J. M., et al. 2003, The Prompt and Afterglow Emission of GRB 001109 Measured by BeppoSAX, in Gamma-Ray Bursts and Afterglow Astronomy 2001: A Workshop Celebrating the First Year of the HETE Mission, ed. G. R. Ricker, & R. K. Vanderspek, Melville, AIP Conf. Proc., 662, 387
Amati, L., Frontera, F., Castro Cerón, J. M., et al. 2004, A&A, in preparation
Barnard, V. E., Blain, A. W., Tanvir, N. R., et al. 2003, MNRAS, 338, 1
Berger, E., & Frail, D. A. 2001, GCN, 1168
Bertin, E., & Arnouts, S. 1996, A&AS, 117, 393
Boella, G., Chiappetti, L., Conti, G., et al. 1997, A&AS, 122, 327
Bolzonella, M., Miralles, J. M., & Pelló, R. 2000, A&A, 363, 476
Calzetti, D., Armus, L., Bohlin, R. C., et al. 2000, ApJ, 533, 682
Carilli, C. L., & Yun, M. S. 1999, ApJ, 513, L13
de Pasquale, M., Piro, L., Perna, R., et al. 2003, ApJ, 592, 1018
Fadda, D., Girardi, M., Giuricin, G., Mardirossian, F., & Mezzetti, M. 1996, ApJ, 473, 670
Fomalont, E. B., Kellermann, K. J., Partridge, R. B., Windhorst, R. A., & Richards, E. A. 2002, AJ, 123, 2402
Fynbo, J. U., Jensen, B. L., Gorosabel, J., et al. 2001, A&A, 369, 373
Gandolfi, G., & Piro, L. 2000a, GCN, 878
Gandolfi, G., & Piro, P. 2000b, GCN, 879
Girardi, M., Biviano, A., Giuricin, G., et al. 1993, ApJ, 404, 38
Greiner, J., Stecklum, B., Klose, S., et al. 2000, GCN, 887
Greiner, J. 2003, `http://www.mpe.mpg.de/~jcg/grb.html`
Groot, P. J., Galama, T. J., van Paradijs, J., et al. 1998, ApJ, 493, L27
Holland, W. S., Robson, E. I., Gear, W. K., et al. 1999, MNRAS, 303, 659
Kreysa, E., Gemuend, H. P., Gromke, J., et al. 1998, Bolometre array development at the Max Planck Institut für Radioastronomie, in Advanced Technology MMW, Radio, and Terahertz Telescopes, ed. T. G. Phillips, Bellingham, Proc. of the SPIE, 3357, 319
Lazzati, D., Covino, S., & Ghisellini, G. 2002, A&A, 330, 583
Landolt, A. U. 1992, AJ, 104, 340
Liske, J., Lemon, D. J., Driver, S. P., Cross, N. J. G., & Couch, W. J. 2003, MNRAS, 344, 307
Piro, L., Frail, D. A., Gorosabel, J., et al. 2002, ApJ, 577, 680
Ramírez-Ruíz, E., Trentham, N., & Blain, A. W. 2002, MNRAS, 329, 465
Rol, E., Vreeswijk, P. M., Strom, R., et al. 2000, GCN, 889
Schlegel, D. J., Finkbeiner, D. P., & Davis, M. 1998, ApJ, 500, 525
Sokolov, V., Fatkhullin, T., & Komarova, V. 2001, GCN, 1092
Taylor, G. B., Frail, D. A., & Kulkarni, S. R. 1998, ApJ, 502, L115
Taylor, G. B., Frail, D. A., & Bloom, J. S. 2000, GCN, 880
Vreeswijk, P. M., Rol, E., Packham, C., et al. 2000, GCN, 886

Appendix B

Paper II

Star formation rates and stellar masses in $z \sim 1$ γ-ray burst hosts

by

J. M. Castro Cerón, M. J. Michałowski, J. Hjorth, D. Watson, J. P. U. Fynbo & J. Gorosabel.

The Astrophysical Journal, **653**, L85–L88 (2006)

Statement of coauthorship

J.M. Castro Cerón wrote the paper, checked the MIR data reduction and did the MIR photometry. He also made Figure 2 and calculated the SFRs and the $M_\star$. M.J. Michałowski performed the SED fits and calculated the SFRs and the dust masses; he also made Figure 1. The idea for this paper was provided by J. Hjorth and D. Watson. Other authors contributed in various ways, including discussion.

José María Castro Cerón **Michał Jerzy Michałowski**

Jens Hjorth **Darach Watson** **Javier Gorosabel**

The Astrophysical Journal, 653: L85–L88, 2006 December 20

STAR FORMATION RATES AND STELLAR MASSES IN $z \sim 1$ GAMMA-RAY BURST HOSTS[1]

J. M. Castro Cerón,[2] M. J. Michałowski,[2] J. Hjorth,[2] D. Watson,[2] J. P. U. Fynbo,[2] and J. Gorosabel[3]
Received 2006 August 9; accepted 2006 November 6; published 2006 December 4

ABSTRACT

We analyze 4.5, 8, and 24 μm band *Spitzer* images of six gamma-ray burst host galaxies at redshifts close to 1. We constrain their star formation rates (SFRs) based on the entire available spectral energy distribution rather than the 24 μm band only. Further, we estimate their stellar masses ($M_\star$) based on rest-frame *K*-band luminosities. Our sample spans a wide range of galaxy properties: derived SFRs range from less than 10 to a few hundred solar masses per year; values of $M_\star$ range from 10^9 to $10^{10}\ M_\odot$ with a median of $5.6 \times 10^9\ M_\odot$. Comparing the specific star formation rate ($\phi \equiv \mathrm{SFR}/M_\star$) of our sample as a function of $M_\star$ to other representative types of galaxies (distant red galaxies, Lyα emitters, Lyman break galaxies, submillimeter galaxies, and $z \sim 2$ galaxies from the Great Observatories Origins Deep Survey–North field), we find that gamma-ray burst hosts are among those with the highest ϕ.

Subject headings: cosmology: observations — dust, extinction — galaxies: high-redshift — galaxies: ISM — gamma rays: bursts — infrared: galaxies

1. INTRODUCTION

A canonical model is well established for long-duration gamma-ray bursts (GRBs): association with stellar core-collapse events and hence with high-mass star formation (e.g., Hjorth et al. 2003; Stanek et al. 2003; Zeh et al. 2004; Campana et al. 2006). The emerging picture, however, is complex. Most GRB host galaxies are faint and blue (Fruchter et al. 1999; Le Floc'h et al. 2003). A few hosts show tentative evidence of very high star formation rates (SFRs; Chary et al. 2002; Berger et al. 2003), but their optical properties do not appear typical of the galaxies found in blind submillimeter galaxy surveys (Tanvir et al. 2004; Christensen et al. 2004; Fruchter et al. 2006).

The *Spitzer* (Werner et al. 2004) IRAC (Infrared Array Camera; Fazio et al. 2004) and MIPS (Multiband Imaging Photometer for *Spitzer*; Rieke et al. 2004) photometry, together with optical, near-IR, submillimeter, and radio observations, can help establish how GRB hosts relate to other high-redshift galaxy populations. This is essential if we are to understand the full range of properties of star-forming galaxies at high redshifts and exploit the potential of GRBs as more general probes of cosmic star formation.

In this Letter we study a subsample of the 16 GRB hosts observed with *Spitzer* by Le Floc'h et al. (2006). We compute SFRs, dust masses (M_dust), and stellar masses ($M_\star$) for hosts at redshifts close to 1. This redshift is particularly relevant because it has been argued that the global SFR peaks there (Madau et al. 1998). To determine SFRs we fit full (optical to radio) spectral energy distributions (SEDs), which allows us to calculate the most accurate and robust values for the SFR in a sample of GRB host galaxies to date. At $z \sim 1$ M_dust is constrained by 850 μm SCUBA observations. To determine $M_\star$ we fit observed 4.5 μm fluxes. The $M_\star$ estimator is well calibrated for $z \sim 1$ (Labbé et al. 2005) since the 4.5 μm observed wavelength corresponds to the rest-frame *K* band. This gives us, for the first time, an accurate value of the stellar mass in those hosts. We assume an $\Omega_m = 0.3$, $\Omega_\Lambda = 0.7$ cosmology with $H_0 = 70$ km s^{-1} Mpc^{-1}.

2. DATA

From the sample of 16 GRB hosts (GTO program 76) we selected six that have $z \sim 1$ ($1^{+0.11}_{-0.17}$). The reader is referred to Le Floc'h et al. (2006) for a detailed description of the full data set. Each host has been imaged with IRAC and MIPS. IRAC observations were 4.5 μm (300 s per host; scale = 1″.220 pixel^{-1}; field of view [FOV] = 5.21 × 5.21 arcmin^2; instrumental point-spread function [PSF] FWHM = 1″.98) and 8.0 μm (300 s per host; scale = 1″.213 pixel^{-1}; FOV = 5.18 × 5.18 arcmin^2; instrumental PSF FWHM = 1″.72). MIPS observations were 24 μm (420 s per host; scale = 2″.45 pixel^{-1}; FOV = 5.23 × 5.23 arcmin^2; instrumental PSF FWHM ~6″).

We used official *Spitzer* post–Basic Calibrated Data products (carefully verified with our own reductions). Host extraction was based on archival imagery world coordinate system calibration and visually confirmed with optical comparison images from the literature. The median separation between the host centroid in each *Spitzer* image and the best set of coordinates published was about 1″. We measured the flux densities over a circled area of radius 2 pixels in IRAC and 3 pixels in MIPS. Aperture corrections were then applied to account for the extended size of the PSF. Our photometry, presented in Table 1, is consistent with Le Floc'h et al. (2006).

3. SPECTRAL ENERGY DISTRIBUTION FITS

Photometry available for our sample includes our *Spitzer* flux densities and data points from the literature, spanning from optical to radio wavelengths. We scaled a set of SED templates to fit these data: Arp 220, an archetypal ultraluminous IR galaxy (ULIRG); NGC 6946, a well-characterized, blue, star-forming galaxy (both Silva et al. 1998); and 64 SED templates ranging from starbursts to quiescent ones (Dale et al. 2001; Dale & Helou 2002). The spectral width of the different bandpass filters was taken into account. Fitting was evaluated by means of a weighted least-squares method.

[1] This work is based in part on observations made with the *Spitzer Space Telescope*, which is operated by the Jet Propulsion Laboratory, California Institute of Technology, under a contract with NASA.

[2] Dark Cosmology Centre, Niels Bohr Institute, University of Copenhagen, Juliane Maries Vej 30, DK-2100 Copenhagen Ø, Denmark; josemari@dark-cosmology.dk, michal@dark-cosmology.dk, jens@dark-cosmology.dk, darach@dark-cosmology.dk, jfynbo@dark-cosmology.dk.

[3] Instituto de Astrofísica de Andalucía (CSIC), c/. Camino Bajo de Huétor, 50, E-18.008 Granada, Spain; jgu@iaa.es.

TABLE 1

HOSTS: FLUX DENSITIES, STAR FORMATION RATES, DUST, AND STELLAR MASSES

GRB HOST	REDSHIFT z	REDSHIFT Ref.	$f_{4.5\,\mu m}$[a] (μJy)	$f_{8.0\,\mu m}$[a] (μJy)	$f_{24\,\mu m}$[a] (μJy)	SFR[b] ($M_\odot$ yr^{-1}) UV$_{cont}$	SFR Ref.	SFR L_{8-1000}	M_{dust} ($10^7\,M_\odot$)	$M_\star$ ($10^9\,M_\odot$)
970508	0.83	1	<3.1	<17	<82	2.5[c]	7	0.4–26	0.3–1.1	1.5
970828	0.96	2	3.9 ± 1.1	<18	94 ± 17	1.1[d]	2	30 ± 8	1.3	2.5
980613	1.10	3	37 ± 1	33 ± 8	169 ± 36	70[c]	7	428 ± 51	19	31
980703	0.97	4	11 ± 2	<24	<85	30[c]	7	3.8–226	2.7–10	7.2
981226	1.11	5	4.5 ± 1.4	<31	<87	1.2[d]	5	1.0–84	0.7–3.7	3.9
990705	0.84	6	19 ± 1	<18	159 ± 31	~5[d]	6	4.5–173	3.2–7.7	9.2

[a] Upper limits are quoted at the 3 σ level, while errors are 1 σ.

[b] We have corrected all the SFRs quoted to account for differences in their IMF scales with respect to our choice of a Salpeter IMF (0.1–100 $M_\odot$; Salpeter 1955).

[c] Corrected using the β-slope technique (Chary et al. 2002 and references therein), typically larger than the Balmer lines decrement correction.

[d] Uncorrected for internal extinction; Christensen et al. (2005) argue for no extinction in the host of GRB 981226.

REFERENCES.—(1) Bloom et al. 1998; (2) Djorgovski et al. 2001; (3) Djorgovski et al. 2003; (4) Djorgovski et al. 1998; (5) Christensen et al. 2005; (6) Le Floc'h et al. 2002; (7) Chary et al. 2002

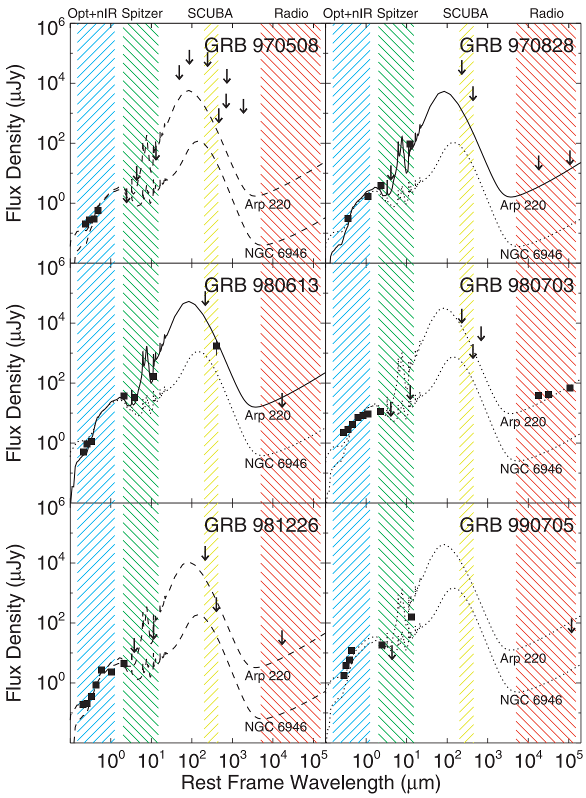

FIG. 1.—SED fits of the six GRB host galaxies. *Filled squares*: Detections (*error bars within the squares*). *Arrows*: 3 σ upper limits (value marked by the base of the arrow). For each host in our sample we plotted the fit to the template that yielded the highest (Arp 220) and the lowest (NGC 6949) SFR value. *Solid lines*: Best fit. *Dashed lines*: Fits we could not discriminate between. *Dotted lines*: Fits inconsistent with the data, shown for illustrative purposes. *Data points*: Optical/near-IR from Vreeswijk et al. (1999), Sokolov et al. (2001), Djorgovski et al. (2001), Le Floc'h et al. (2002), and Christensen et al. (2005). Thermal IR from our photometry of *Spitzer* archival data. Far-IR from Hanlon et al. (2000). Submillimeter from Smith et al. (1999), Tanvir et al. (2004), and our photometry of SCUBA archival data. Radio from Bremer et al. (1998), Shepherd et al. (1998), Berger et al. (2001), Djorgovski et al. (2001), and Berger et al. (2003).

Figure 1 shows our models. The Arp 220 template best fits the hosts of GRBs 970828 and 980613. For these two hosts the data rule out the other SED templates; we have plotted the NGC 6946 template for comparison. For the hosts of GRBs 970508 and 981226 we could not unambiguously discriminate a best-fitting SED template, so we plotted those models yielding the highest and lowest values for the SFR (see § 3.1 and Table 1). Model degeneracy was expected in these two cases because we only have optical-IR data. For the remaining two hosts we also plotted those models yielding the highest and lowest values for the SFR. For GRB 980703, the Arp 220 template approximately reproduced the radio flux densities but was inconsistent with the 24 μm upper limit, while the NGC 6946 template was consistent with the 24 μm upper limit but underestimated the radio flux densities. For GRB 990705, the Arp 220 template overestimated the 24 μm flux density and was marginally inconsistent with the 8 μm upper limit, while the NGC 6946 template underestimated the 24 μm flux density. Reproducing the SEDs of these two galaxies is problematic and may require dust with properties different from those in our templates. The Dale et al. (2001) and Dale & Helou (2002) templates yielded SFR values between those of the Arp 220 and NGC 6946 models for all the hosts in our sample.

For each host we may be fitting subcomponents that differ in their properties (Charmandaris et al. 2004). For instance, for GRB 980613 some components detected in the optical/near-IR bands (Hjorth et al. 2002; Djorgovski et al. 2003) are offset by >2″.5 from the *Spitzer* centroid (Le Floc'h et al. 2006). While such effects might induce some scatter in the SEDs, we can still utilize the SED templates as powerful diagnostic tools for the SFRs of the sample.

3.1. *Star Formation Rates*

Using our SED fitting models, we calculated the SFR for each host using IR luminosities. We converted flux densities into luminosity densities using $L_\nu(\nu_{rest}) = 4\pi D_L^2 f_\nu(\nu_{observed})/(1+z)$ (Hogg et al. 2002), where D_L is the luminosity distance, and scaled the SED templates to match the data points. IR luminosities (L_{8-1000}) were obtained integrating under the scaled SED templates from 8 to 1000 μm (rest frame). This wavelength range was chosen so the SFRs could be computed using SFR($M_\odot$ yr^{-1}) = 4.5 ×

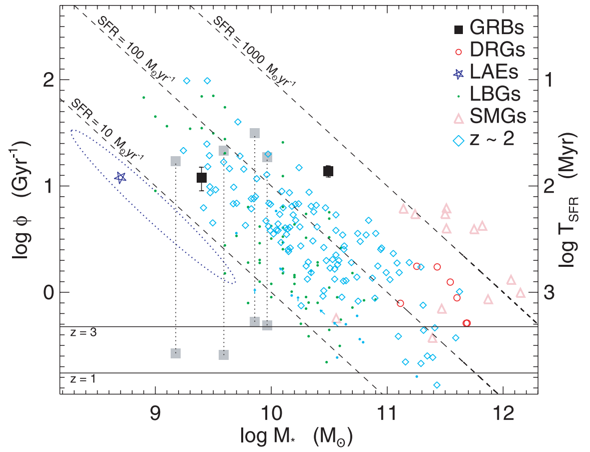

FIG. 2.—ϕ as a function of $M_\star$ for our GRB host galaxy sample and other representative types of galaxies (for a similar plot see Erb et al. 2006b). *Black squares*: SFR values constrained with a best-fit model. *Gray squares*: highest/lowest SFR values for those hosts for which a best-fit model could not be established. *Dashed diagonals*: SFRs of 1000, 100, and 10 $M_\odot$ yr^{-1}, respectively. *Right axis*: SFR timescale ($T_{\rm SFR} = M_\star$/SFR), the inverse of ϕ. On this scale the solid horizontals represent the age of the universe for the marked redshift. Our six hosts clearly have $T_{\rm SFR} < t_{\rm universe}$, allowing for a history of constant star formation. The distribution of our sample in parameter space suggests that GRBs trace galaxies that are not selected with other techniques. *Data points*: GRBs from this Letter. DRGs from van Dokkum et al. (2004). LAEs from Gawiser et al. (2006). The point plotted represents an average value of the LAE population as a whole, obtained from stacked photometry, and the dotted ellipse its uncertainty. Spectroscopically confirmed LBGs from Shapley et al. (2001) and Barmby et al. (2004). SMGs from Chapman et al. (2005; $M_\star$) and Borys et al. (2005; SFR), where we have considered $L_{\rm BOL} \simeq L_{\rm far\text{-}IR}$ and then applied the Kennicutt (1998) calibration. $z \sim 2$ from Erb et al. (2003) and Reddy et al. (2006).

$10^{-44} L_{\rm IR}$ ergs s^{-1} (Kennicutt 1998). The results are summarized in Table 1. Errors quoted are statistical and assume the template is a good representation of the data. In addition there may be significant systematic errors related, for example, to how well the template represents the actual SED (Michałowski 2006), the $L_{8\text{–}1000}$ to SFR conversion (Kennicutt 1998) (both of the same order, ~30%), or a factor of 2 from the choice of initial mass function (IMF; Erb et al. 2006a).

For the hosts of GRBs 970508 , 980703, 981226 and 990705, the lower end of their SFR ranges indicates low star formation, consistent with the estimates from the UV continuum and, in GRB 981226, with no internal extinction (Christensen et al. 2005). The host of GRB 970828 is a moderately star-forming galaxy, in good agreement with Le Floc'h et al. (2006). The host of GRB 980613 is characterized by high star formation activity. Our SFR value for this host is ~5 times higher than the one obtained by Le Floc'h et al. (2006) with a lower uncertainty, because we have fitted the entire SED, as opposed to only the flux density at 24 μm. We verified that if we base our calculations exclusively on the 24 μm flux densities we reproduce the results in Le Floc'h et al. (2006) for all hosts.

3.2. *Dust Masses*

Dust emission dominates submillimeter wavelengths. The total $M_{\rm dust}$ in a galaxy can be estimated from its rest-frame 450 μm flux density: $M_{\rm dust} = S_\nu D_L^2/(1+z)\kappa(\nu)B(\nu,T)$; where S_ν is the flux density at an observed wavelength corresponding to the rest frame wavelength of 450 μm at $z = 1$, interpolated from the fitted SED templates; ν is the frequency (666.21 GHz) corresponding to a wavelength of 450 μm; $\kappa \propto \nu^\beta$ is the mass absorption coefficient with β being the dust emissivity index; and $B(\nu, T)$ is the Planck function (Taylor et al. 2005). We assumed optically thin dust emitting a gray spectrum. This method yields statistical errors of ~25% (Taylor et al. 2005). The ranges in $M_{\rm dust}$ are estimates of the systematic, model-dependent error. Our results are listed in Table 1. The derived median, $M_{\rm dust} = 8 \times 10^6\ M_\odot$ (calculated from the lowest $M_{\rm dust}$ value for each host), is consistent with the distribution for starburst galaxies (4×10^5 to $7 \times 10^8\ M_\odot$) found by Taylor et al. (2005).

4. STELLAR MASSES

We estimated $M_\star$ from rest-frame K-band fluxes (e.g., Glazebrook et al. 2004). M/L_K depends to some extent on the composition of the stellar population (Portinari et al. 2004) or, according to Labbé et al. (2005) who used Bruzual & Charlot (2003) with a Salpeter IMF, on the rest-frame $U - V$ color, age, and $M_\star$. GRB hosts are blue, young, and faint (e.g., Le Floc'h et al. 2003; Berger et al. 2003; Christensen et al. 2004); thus, we assume $M/L_K \sim 0.1$ (lowest detection in Labbé et al. 2005 is 0.16), obtaining a robust lower limit. Table 1 summarizes our $M_\star$ estimates. Van der Wel et al. (2006) examined redshift-dependent systematics in determining $M_\star$ from broadband SEDs. They found no significant bias for Bruzual & Charlot (2003) models with a Salpeter IMF (Salpeter 1955).

5. DISCUSSION

We have found the hosts in our sample to span a wide range of properties. Their SEDs are fitted with templates that vary from a blue, star-forming galaxy to a ULIRG. Their SFRs and $M_\star$ are quite different, ranging from the host of GRB 980613, which is forming a few hundred solar masses a year with $M_\star = 3 \times 10^{10}\ M_\odot$, to the host of GRB 970508, which is forming of the order of 10 $M_\odot$ yr^{-1} with $M_\star = 1.5 \times 10^9\ M_\odot$.

We find that our SFR values are significantly higher (up to a factor of 30) than the lower limits from the rest-frame UV continuum emission ($L_{\rm UV}$; see Table 1) and higher (by a factor of 6) than those corrected with the β-slope technique (Chary et al. 2002). GRBs 970828, 980613, and 980703 illustrate how even the best estimates of dust extinction in a galaxy from the UV slope may fall short, not only for ULIRGs (Chary & Elbaz 2001), but also for LIRGs (i.e., $10^{12}\ L_\odot > L_{8\text{–}1000} \geq 10^{11}\ L_\odot$). Our SFR value for GRB 981226 is consistent with no internal extinction (Christensen et al. 2005).

The specific star formation rate ($\phi \equiv {\rm SFR}/M_\star$) gives an indication of how intensely star-forming a galaxy is. In Figure 2 we have plotted ϕ versus $M_\star$ for ours and five other representative galaxy samples: distant red galaxies (DRGs), Lyα emitters (LAEs), Lyman break galaxies (LBGs), submillimeter galaxies (SMGs), and an ensemble of optically selected, $z \sim 2$ galaxies from the Great Observatories Origins Deep Survey–North field. GRB hosts have some of the highest ϕ values, as previously suggested by Christensen et al. (2004). ϕ^{-1} represents the SFR timescale, so high ϕ values are indicative of GRBs tracing young, starbursting galaxies.

The different methods that have been used to derive the SFRs of the various samples plotted in Figure 2 likely introduce systematic offsets. Likewise, to determine $M_\star$, model fitting to the full SED could better account for variations in M/L_K. For high SFR galaxies, ongoing star formation contributes to the near-IR emission, especially as they lack an old stellar population. High ϕ galaxies are particularly vulnerable to this effect.

Nevertheless, Figure 2 illustrates where, within the larger picture, our hosts fall.

We have shown the capabilities of IR observations to characterize GRB host galaxies and have compared values of ϕ for different types of galaxies irrespective of their redshift. Unfortunately, the selection effects are difficult to quantify for the present small sample, which therefore does not allow a robust statistical analysis. The next step to increase our understanding of GRB hosts will be to extend our mid- and far-IR observed sample, as a larger, well-selected one will tell us more about the span of host properties (i.e., SFR, $M_{\rm dust}$, and $M_\star$). Future work should include full population synthesis modeling and address the redshift dependence of ϕ.

We thank J. Baradziej, B. Cavanagh, F. Economou, Á. Elíasdóttir, E. Gawiser, T. R. Greve, T. Jenness, K. Nilsson, R. Priddey, E. Ramirez-Ruiz, and S. Toft for insightful comments, and our anonymous referee for genuinely helping us to improve the manuscript. The Dark Cosmology Centre is funded by the Danish National Research Foundation. J. M. C. C. gratefully acknowledges support from the Instrument center for Dansk Astrofysik and the Niels Bohr Instituttet's International Ph.D. School of Excellence. J. G. was funded in part by Spain's AyA 2.004-01515 and ESP 2.002-04124-C03-01 grants. The authors acknowledge benefits from collaboration within EU's FP5 RTN "GRBs: an enigma and a tool" (HPRN-CT-2002-00294). This research has made use of NASA's Astrophysics Data System.

Facilities: Spitzer (IRAC, MIPS).

REFERENCES

Barmby, P., et al. 2004, ApJS, 154, 97
Berger, E., Cowie, L. L., Kulkarni, S. R., Frail, D. A., Aussel, H., & Barger, A. J. 2003, ApJ, 588, 99
Berger, E., Kulkarni, S. R., & Frail, D. A. 2001, ApJ, 560, 652
Bloom, J. S., Djorgovski, S. G., Kulkarni, S. R., & Frail, D. A. 1998, ApJ, 507, L25
Borys, C., Smail, I., Chapman, S. C., Blain, A. W., Alexander, D. M., & Ivison, R. J. 2005, ApJ, 635, 853
Bremer, M., Krichbaum, T. P., Galama, T. J., Castro-Tirado, A. J., Frontera, F., van Paradijs, J., Mirabel, I. F., & Costa, E. 1998, A&A, 332, L13
Bruzual, G., & Charlot, S. 2003, MNRAS, 344, 1000
Campana, S., et al. 2006, Nature, 442, 1008
Chapman, S. C., Blain, A. W., Smail, I., & Ivison, R. J. 2005, ApJ, 622, 772
Charmandaris, V., Le Floc'h, E., & Mirabel, I. F. 2004, ApJ, 600, L15
Chary, R., Becklin, E. E., & Armus, L. 2002, ApJ, 566, 229
Chary, R., & Elbaz, D. 2001, ApJ, 556, 562
Christensen, L., Hjorth, J., & Gorosabel, J. 2004, A&A, 425, 913
———. 2005, ApJ, 631, L29
Dale, D. A., & Helou, G. 2002, ApJ, 576, 159
Dale, D. A., Helou, G., Contursi, A., Silbermann, N. A., & Kolhatkar, S. 2001, ApJ, 549, 215
Djorgovski, S. G., Bloom, J. S., & Kulkarni, S. R. 2003, ApJ, 591, L13
Djorgovski, S. G., Frail, D. A., Kulkarni, S. R., Bloom, J. S., Odewahn, S. C., & Diercks, A. 2001, ApJ, 562, 654
Djorgovski, S. G., Kulkarni, S. R., Bloom, J. S., Goodrich, R., Frail, D. A., Piro, L., & Palazzi, P. 1998, ApJ, 508, L17
Erb, D. K., Shapley, A. E., Steidel, C. C., Pettini, M., Adelberger, K. L., Hunt, M. P., Moorwood, A. F. M., & Cuby, J.-G. 2003, ApJ, 591, 101
Erb, D. K., Steidel, C. C., Shapley, A. E., Pettini, M., Reddy, N. A., & Adelberger, K. L. 2006a, ApJ, 646, 107
———. 2006b, ApJ, 647, 128
Fazio, G., et al. 2004, ApJS, 154, 10
Fruchter, A. S., et al. 1999, ApJ, 519, L13
———. 2006, Nature, 441, 463
Gawiser, E., et al. 2006, ApJ, 642, L13
Glazebrook, K., et al. 2004, Nature, 430, 181
Hanlon, L., et al. 2000, A&A, 359, 941
Hjorth, J., et al. 2002, ApJ, 576, 113
———. 2003, Nature, 423, 847
Hogg, D. W., Baldry, I. K., Blanton, M. R., & Eisenstein, D. J. 2002, preprint (astro-ph/0210394)
Kennicutt, R. C., Jr. 1998, ARA&A, 36, 189
Labbé, I., et al. 2005, ApJ, 624, L81
Le Floc'h, E., Charmandaris, V., Forrest, W. J., Mirabel, I. F., Armus, L., & Devost, D. 2006, ApJ, 642, 636
Le Floc'h, E., et al. 2002, ApJ, 581, L81
———. 2003, A&A, 400, 499
Madau, P., Pozzetti, L., & Dickinson, M. 1998, ApJ, 498, 106
Michałowski, M. J. 2006, Master's thesis, Univ. Denmark
Portinari, L., Sommer-Larsen, J., & Tantalo, R. 2004, MNRAS, 347, 691
Reddy, N. A., Steidel, C. C., Fadda, D., Yan, L., Pettini, M., Shapley, A. E., Erb, D. K., & Adelberger, K. L. 2006, ApJ, 644, 792
Rieke, G., et al. 2004, ApJS, 154, 25
Salpeter, E. E. 1955, ApJ, 121, 161
Shapley, A. E., Steidel, C. C., Adelberger, K. L., Dickinson, M., Giavalisco, M., & Pettini, M. 2001, ApJ, 562, 95
Shepherd, D. S., Frail, D. A., Kulkarni, S. R., & Metzger, M. R. 1998, ApJ, 497, 859
Silva, L., Granato, G. L., Bressan, A., & Danese, L. 1998, ApJ, 509, 103
Smith, I. A., et al. 1999, A&A, 347, 92
Sokolov, V. V., et al. 2001, A&A, 372, 438
Stanek, K. Z., et al. 2003, ApJ, 591, L17
Tanvir, N. R., et al. 2004, MNRAS, 352, 1073
Taylor, E. L., et al. 2005, MNRAS, 361, 1352
van der Wel, A., Franx, M., Wuyts, S., van Dokkum, P. G., Huang, J., Rix, H.-W., & Illingworth, G. D. 2006, ApJ, 652, 97
van Dokkum, P. G., et al. 2004, ApJ, 611, 703
Vreeswijk, P. M., et al. 1999, ApJ, 523, 171
Werner, M., et al. 2004, ApJS, 154, 1
Zeh, A., Klose, S., & Hartmann, D. H. 2004, ApJ, 609, 952

Appendix C

Paper III

On the distribution of stellar masses in
γ-ray burst host galaxies

by

J. M. Castro Cerón, M. J. Michałowski, J. Hjorth, D. Malesani,
J. Gorosabel, D. Watson & J. P. U. Fynbo.

The Astrophysical Journal, submitted (2006)

(arXiv:0803.2235v1 [astro-ph])

Statement of coauthorship

J.M. Castro Cerón wrote the paper. He defined the sample and did all the MIR photometry, as well as all the figures. He calculated the $M_\star$ and SFRs. D. Malesani did the 2MASS and *GALEX* photometry. M.J. Michałowski, D. Malesani, D. Watson, J. Hjorth and J. Gorosabel contributed critical discussion in various issues, specially to the photometric and error analyses. The idea for this paper was provided by J. Hjorth. Other authors contributed in various ways.

José María Castro Cerón | **Michał Jerzy Michałowski**

Jens Hjorth | **Javier Gorosabel** | **Darach Watson**

The Astrophysical Journal, xxx: xxx–xxx, 2008 XXX xx

ON THE DISTRIBUTION OF STELLAR MASSES IN GAMMA-RAY BURST HOST GALAXIES[1]

J. M. Castro Cerón[2], M. J. Michałowski[2], J. Hjorth[2], D. Malesani[2],
J. Gorosabel[3], D. Watson[2], and J. P. U. Fynbo[2]
Received 2008 March 12; accepted 2008 XXX xx; published 2008 XXX xx

ABSTRACT

We analyse *Spitzer* images of 30 long-duration gamma-ray burst (GRB) host galaxies. We estimate their total stellar masses ($M_\star$) based on the rest-frame K-band luminosities and constrain their unobscured star-formation rates (SFR) based on the rest-frame UV continuua. Further, we compute a mean $M_\star/L_{K_{\rm rest}} = 0.45\,M_\odot/L_\odot$. We find that the hosts are low $M_\star$, star-forming systems. The median $M_\star$ in our sample ($\langle M_\star \rangle = 10^{9.7}\,M_\odot$) is lower than that of "field" galaxies (e.g., Gemini Deep Deep Survey). The range spanned by $M_\star$ is $10^7\,M_\odot < M_\star < 10^{11}\,M_\odot$, while the range spanned by the unobscured SFR is $10^{-2}\,M_\odot\,{\rm yr}^{-1} < {\rm SFR} < 10\,M_\odot\,{\rm yr}^{-1}$. There is no evidence for intrinsic evolution in the distribution of $M_\star$ with redshift. We show that extinction by dust must be present in at least 25% of the GRB hosts in our sample, and suggest that this is a way to reconcile our lower, UV-based, specific SFR ($\phi \equiv {\rm SFR}/M_\star$) with previous claims that GRBs have some of the highest ϕ values. We also examine the effect that the inability to resolve the star-forming regions in the hosts has on ϕ.

Subject headings: cosmology: observations — dust, extinction — galaxies: fundamental parameters — galaxies: ISM — gamma rays: bursts — infrared: galaxies

1. INTRODUCTION

It is central to contemporary cosmology to map the build-up of cosmic structure and star-formation (SF); and we know that the detection of a gamma-ray burst (GRB) is an indication that its host galaxy harbors massive SF. GRBs are pulses of γ-rays from sources of cosmological origins, and are the most luminous, photon-emitting events in the universe. As tracers of SF they have fundamental advantages: dust extinction has essentially no effect in their detection at γ-ray and X-ray wavelengths; GRBs can be observed to very high redshifts; these redshifts can be measured from afterglow spectroscopy independently of the host magnitudes; and the selection of GRBs is independent of the host galaxy luminosity at any wavelength. That is to say that GRBs are unique eyes to gainfully look at the star-forming universe. But the following critical questions should be answered in order to use GRBs as tracers of SF: What is the level of bias in optically-selected GRB host samples? And what is the intrinsic bias in the GRB-SF rate?

A canonical model is well established for long-duration GRBs: they occur in star-forming regions in star-forming galaxies (Bloom et al. 2002; Gorosabel et al. 2003a; Christensen et al. 2004; Fruchter et al. 2006) and are associated with stellar core collapse events and hence with high-mass SF (e.g. Galama et al. 1998; Hjorth et al. 2003; Stanek et al. 2003; Zeh et al. 2004; Campana et al. 2006). The emerging picture, however, is complex. Most GRB host galaxies are faint and blue (Fruchter et al. 1999; Le Floc'h et al. 2003). A few hosts show tentative evidence of very high star-formation rates (SFRs; Chary et al. 2002; Berger et al. 2003), but their optical properties do not appear typical of the galaxies found in blind submillimeter galaxy surveys (Tanvir et al. 2004; Fruchter et al. 2006).

It is currently debated how GRB hosts relate to other known populations of star-forming galaxies. At redshifts around 3 the UV luminosities of host galaxies and the metallicities of GRB sightlines are consistent with the expectation if hosts are drawn from the underlying population of all star-forming galaxies weighted with the total SF density per luminosity bin (Jakobsson et al. 2005a; Fynbo et al. 2008). With *Spitzer*'s (Werner et al. 2004) IRAC (Infrared Array Camera; Fazio et al. 2004) mid-infrared (MIR) photometry, together with optical and near-infrared (NIR) data, we can establish how the host galaxies relate to other star-forming populations in terms of total stellar mass ($M_\star$). This is essential if we are to understand the full range of properties of star-forming galaxies at high redshifts and fully exploit the potential of GRBs as probes of cosmic SF.

Castro Cerón et al. (2006) studied a sample of 6 long-duration GRB host galaxies observed with IRAC and MIPS (Multiband Imager Photometer for *Spitzer*; Rieke et al. 2004). They estimated their $M_\star$ based on rest-frame K-band luminosity densities and constrained their SFRs based on the entire available spectral energy distribution (SED). In this work we extend the computations to a sample of 30, but constrain only the unobscured SFRs with the rest-frame UV continuum. This larger sample ought to allow for a more robust statistical analysis, as well as to probe the distribution of $M_\star$ in redshift space. To determine $M_\star$ we utilize rest-frame K flux densities (interpolated from observed IRAC and NIR fluxes). This extends the data set presented by Castro Cerón et al. (2006), yielding accurate values of $M_\star$ in a large host galaxy sample. To determine the unobscured SFRs we use rest-frame UV flux densities (interpolated from ob-

[1] This work is based in part on observations made with the *Spitzer Space Telescope*, which is operated by the Jet Propulsion Laboratory, California Institute of Technology, under a contract with NASA.

[2] Dark Cosmology Centre, Niels Bohr Institute, University of Copenhagen, Juliane Maries Vej 30, DK-2100 Copenhagen Ø, Denmark; josemari@dark-cosmology.dk, michal@dark-cosmology.dk, malesani@dark-cosmology.dk, darach@dark-cosmology.dk, jens@dark-cosmology.dk, jfynbo@dark-cosmology.dk.

[3] Instituto de Astrofísica de Andalucía (CSIC), c/. Camino Bajo de Huétor, 50, E-18.008 Granada, Spain; jgu@iaa.es.

served optical fluxes). These unobscured SFRs are lower limits to the total SFR of a galaxy due to the possible extinction by dust, and we compare them with those of Castro Cerón et al. (2006). Our paper is organized as follows: An overview of the sample selection is given in §2; The analytic methodology is described in §3. $M_\star$ for the sample are derived in §4, and §5 sees the computation of the unobscured SFRs. We conclude in §6 with analysis and discussion. We assume an $\Omega_m = 0.3$, $\Omega_\Lambda = 0.7$ cosmology with $H_0 = 70\,\mathrm{km\ s^{-1}\ Mpc^{-1}}$.

2. DATA

Our current sample is composed of 30 long-duration GRB host galaxies, three of them within the X-ray flash category (Heise 2003). We made the selection by requiring each host to have rest-frame K-band data available (for the purposes of this work we define $K \equiv 2.2\,\mu\mathrm{m} \pm 0.3\,\mu\mathrm{m}$); thus the $M_\star$ estimator is well calibrated (Glazebrook et al. 2004). An additional requirement for inclusion in the sample was the availability of the redshift.

This 30 GRB host galaxy sample spans a redshift interval $0 < z < 2.7$, with a median value $z \simeq 0.84$. For comparison, the median redshift[4] of those GRBs detected prior to the start of operations of the *Swift* satellite (Gehrels et al. 2004) is $\langle z \rangle \simeq 1.0$, and that of those GRBs detected afterwards is $\langle z \rangle \simeq 2.3$; i.e., in this work we are chiefly looking at the lower end of the GRB redshift distribution. Given the redshifts sampled, the rest-frame K-band data for 24 of the 30 host galaxies were obtained from the *Spitzer* Science Archive, where we examined all publicly available hosts up to (and including) October 2007. The remaining 6 GRB hosts (980425, 030329, 031203, 060218, 060505, and 060614) in the sample have very low redshifts ($z \lesssim 0.1$), so in those cases $K_{\lambda_{\mathrm{obs}}} \sim K_{\lambda_{\mathrm{rest}}}$ (i.e., $K_{\lambda_{\mathrm{rest}}}$ falls within the nominal width of $K_{\lambda_{\mathrm{obs}}}$). The sample is presented in Table 1.

Each host (except GRBs 060218, 060505, and 060614) were imaged with IRAC. Detectors are 256×256 squared pixel arrays (scale = $1''\!.2\,\mathrm{pixel}^{-1} \times 1''\!.2\,\mathrm{pixel}^{-1}$; field of view = 5.21 arcmin × 5.21 arcmin). The instrumental PSFs (FWHM) are: channel 1 = $1''\!.66$; channel 2 = $1''\!.72$; channel 3 = $1''\!.88$; channel 4 = $1''\!.98$. The optical and NIR data complementing IRAC in Table 1 were obtained from the literature. Two UV data points (GRBs 980425 and 060505) come from our analysis of *GALEX* (Galaxy Evolution Explorer; Martin et al. 2003, 2005) data.

3. METHODOLOGY

For the MIR photometry we use official *Spitzer* Post Basic Calibrated Data (Post-BCD) products (in Castro Cerón et al. 2006 we carefully verified the Post-BCD with our own reductions). Host extraction is based on the archival imagery world coordinate system calibration and visually confirmed with optical and/or NIR comparison images from the literature. The median separation between the host centroid in each IRAC image and the best set of coordinates published is well below $1''$. GRB 980425 is the only host galaxy resolved in the IRAC images and we have obtained its photometry from the literature (Le Floc'h et al. 2006). None of the other GRB host galaxies of our sample are spatially resolved in the IRAC images, and their flux densities can be estimated using small circular aperture photometry. We measure the flux densities over a circled area of radius 2 pixels. In most cases this allows us to recover the emission of the host while avoiding contamination from other field sources located nearby. But in a few instances there was suspicion that the nearby field sources might be contaminating our host galaxy photometry. As a sanity check we subtracted those field sources and redid the photometry. Field-source subtraction was performed using the detection output image given by the Source Extractor software package (SExtractor; Bertin & Arnouts 1996), where the detected sources were replaced by background noise. The photometry on the field-source-subtracted images was always consistent with the original aperture photometry. Aperture corrections have been applied to account for the extended size of the PSF. Based on the *Spitzer* Science Center recipe for *Estimating Signal-To-Noise Ratio of a Point Source Measurement for IRAC*[5] we calculate conservative errors, including both statistical and systematic estimates. Our flux density measurements and upper limits are given in Table 1, column (3). We find that, of those hosts in our sample observed with channel 1, about 36% are detected. For channel 2 the rate is about 64%. This is roughly of the same order as the detection rate by Le Floc'h et al. (2006) with IRAC channel 2 (44%), though we caution that both samples are incomplete and suffer from selection biases.

For each GRB host we compute the flux density at the central wavelength of the rest-frame K-band by means

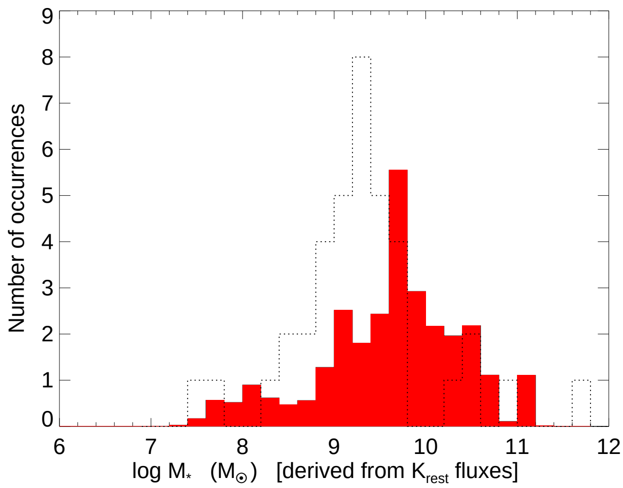

FIG. 1.— Distribution of the total stellar mass ($M_\star$) in GRB host galaxies. *Filled histogram*: 29 out of the 30 hosts in our sample, spanning a redshift interval $0 < z < 1.5$. We note that GRB 030429 has been excluded from the histogram above and the calculation of the median $M_\star$. This is because its host was never detected at any wavelength and, consequently, no lower limit to $M_\star$ can be estimated. The horizontal axis shows the inferred host $M_\star$, derived from interpolated rest-frame K-band flux densities. The median $M_\star$ of the sample is $\langle M_\star \rangle = 10^{9.7}\,M_\odot$. For those host galaxies for which we have upper limits we estimate a conservative lower limit by extrapolating a flat spectrum ($f_\nu \propto \nu^0$) from the reddest NIR/optical detection (references in Table 1, column 4); then we split an area normalized to unit among the bins bracketed by the limits. For each GRB host for which we have detections we assume a normalized Gaussian distribution of the error bars in linear space. Then we allocate $M_\star$ in proportion to the area of the Gaussian in each bin. *Open histogram*: Figure 2 from Savaglio et al. (2007) is shown for comparison.

[4] http://astro.ku.dk/~pallja/GRBsample.html

[5] http://ssc.spitzer.caltech.edu/documents/irac_memo.txt

TABLE 1
Hosts: flux densities, total stellar masses, and star-formation rates

	Redshift		IRAC		$K_{\rm rest}$ (21 980 Å)			$\rm UV_{rest}$ (2 800 Å)		
GRB Host (1)	z (2)	Ref.	f_ν (μJy) (3)	Ch.	f_ν (μJy) (4)	Refs.	$M_{\star(K)}$ ($10^9\,M_\odot$) (5)	f_ν (μJy) (6)	Refs.	$\rm SFR_{(UV)}$ ($M_\odot\,\rm yr^{-1}$) (7)
970228	0.70	1	<3.7	1	<4.2	‡, 30	<5.7	0.34 ± 0.16	48	0.60 ± 0.28
970508	0.83	2	<2.1[a]	2	<1.8	31, 30	<3.5	0.28 ± 0.15	48	0.71 ± 0.38
970828	0.96	3	3.9 ± 0.3[a]	2	3.7 ± 0.3	31, 3	9.5 ± 0.9	<0.44	34	<1.5
980326	∼1.0	4	<2.7	2	<2.6	‡, 30	<7.1	<0.015	49	<0.056
980425	0.0085	5	2 977 ± 101	2	6 389 ± 395	‡[b], 32	1.1 ± 0.1	1 748 ± 173	‡[c], 50	0.39 ± 0.04
980613	1.10	6	38 ± 1[a]	2	42 ± 1	31, 6	142 ± 3	0.83 ± 0.11	6, 30	3.6 ± 0.5
980703	0.97	7	11 ± 1[a]	2	11 ± 1	31, 33	29 ± 2	3.2 ± 0.1	48	10.9 ± 0.3
981226	1.11	8	4.5 ± 0.5[a]	2	4.6 ± 0.5	31, 8	16 ± 2	0.27 ± 0.03	8	1.2 ± 0.1
990506	1.31	9	2.0 ± 0.7	2	2.0 ± 0.8	‡, 34	9.3 ± 3.8	0.20 ± 0.04	34	1.2 ± 0.2
990705	0.84	10	19 ± 1[a]	2	18 ± 1	31, 10	36 ± 2	∼1.8 ± 0.3	10	∼4.7 ± 0.8
000210	0.85	11	3.3 ± 2.0	2	3.2 ± 1.8	‡, 35	6.4 ± 3.6	0.79 ± 0.07	48	2.1 ± 0.2
000418	1.12	9	4.8 ± 1.8	2	5.0 ± 1.9	‡, 36	17 ± 7	1.33 ± 0.04	48	6.1 ± 0.2
000911	1.06	12	<4.3	2	<4.3	‡, 37	<13	0.33 ± 0.08	37	1.4 ± 0.3
010921	0.45	13	11 ± 2	1	12 ± 2	‡, 13	6.5 ± 0.9	2.2 ± 0.1	48	1.6 ± 0.1
020405	0.69	14	<5.4	1	<5.3	‡, 38	<7.0	2.1 ± 0.1	38	3.7 ± 0.2
020813	1.26	15	<2.5	2	<2.6	‡, 38	<11	0.41 ± 0.08	34, 38	2.3 ± 0.5
020819B	0.41	16	97 ± 2	1	104 ± 7	‡, 16	47 ± 3	4.3 ± 2.6	16	2.6 ± 1.5
021211	1.01	17	<2.2	2	<2.2	‡, 38	<6.1	0.20 ± 0.04	38	0.72 ± 0.15
030328	1.52	18	<29	3	<27	‡, 39	<170	0.56 ± 0.08	39	4.6 ± 0.6
030329	0.17	19	<4.9	1	<5.1	‡, 40[d]	<0.37	1.5 ± 0.2	40	0.14 ± 0.02
030429[e]	2.66	20	<7.0	4	<7.3	‡, 20	<124	<0.060	20	<1.3
030528[e]	0.78	21	<4.6	1	<3.8	‡, 41	<6.5	7.2 ± 1.4	41	16 ± 3
031203	0.11	22	216 ± 3[f]	1	192 ± 13[f]	‡, 42	5.3 ± 0.4	119 ± 39[f]	51	4.3 ± 1.4
040924	0.86	23	<2.9	1	<3.2	‡, 38	<6.5	<1.1	38	<2.9
041006	0.72	24	<2.9	1	<3.1	‡, 38	<4.4	<0.98	38	<1.8
050223	0.58	25	18 ± 2	1	18 ± 2	‡, 25	17 ± 1	<8.1	25	<10
050525A	0.61	26	<1.6	1	<1.6	‡, 43	<1.6	<0.48	43	<0.64
060218[e]	0.03	27	...	...	20 ± 6	44	0.052 ± 0.015	15 ± 3	52	0.053 ± 0.010
060505	0.09[g]	28	...	...	298 ± 10	45	5.8 ± 0.2	75 ± 6	‡[c], 45	1.9 ± 0.2
060614	0.13	29	...	...	3.8 ± 0.7	46, 47	0.15 ± 0.03	0.37 ± 0.13	53	0.019 ± 0.006

References. — ‡ This work; (1) Bloom et al. 2001; (2) Bloom et al. 1998; (3) Djorgovski et al. 2001; (4) Bloom et al. 1999; (5) Tinney et al. 1998; (6) Djorgovski et al. 2003; (7) Djorgovski et al. 1998; (8) Christensen et al. 2005; (9) Bloom et al. 2003; (10) Le Floc'h et al. 2002; (11) Piro et al. 2002; (12) Price et al. 2002a; (13) Price et al. 2002b; (14) Price et al. 2003; (15) Barth et al. 2003; (16) Jakobsson et al. 2005b; (17) Vreeswijk et al. 2003; (18) Maiorano et al. 2006; (19) Hjorth et al. 2003; (20) Jakobsson et al. 2004; (21) Rau et al. 2005; (22) Prochaska et al. 2004; (23) Wiersema et al. 2004; (24) Soderberg et al. 2006; (25) Pellizza et al. 2006; (26) Foley et al. 2005; (27) Pian et al. 2006; (28) Colless et al. 2001; (29) Della Valle et al. 2006a; (30) Chary et al. 2002; (31) Castro Cerón et al. 2006; (32) Le Floc'h et al. 2006; (33) Vreeswijk et al. 1999; (34) Le Floc'h et al. 2003; (35) Gorosabel et al. 2003a; (36) Gorosabel et al. 2003b; (37) Masetti et al. 2005; (38) Wainwright et al. 2007; (39) Gorosabel et al. 2005a; (40) Gorosabel et al. 2005b; (41) Rau et al. 2004; (42) Malesani et al. 2004; (43) Della Valle et al. 2006b; (44) Kocevski et al. 2007; (45) Thöne et al. 2008; (46) J. Hjorth 2008, priv. comm.; (47) Cobb et al. 2006; (48) Christensen et al. 2004; (49) Bloom et al. 2002; (50) Michałowski et al. 2008, in prep.; (51) Margutti et al. 2007; (52) Sollerman et al. 2006; (53) Mangano et al. 2007.

Note. — Because host positions are well determined from previous broadband imaging, upper limits are quoted at the 2σ level, while errors are 1σ. All (UV, optical, NIR, and MIR) flux densities and magnitudes in this table (including those in the table notes) are corrected for foreground Galactic dust-extinction. Corrections to the IRAC wavebands follow Lutz (1999). For the UV, optical and NIR passbands we use the DIRBE/IRAS dust maps (Schlegel et al. 1998). We adopt a Galactic dust-extinction curve A_λ/A_V, parameterized by $R_V \equiv A_V/E(B-V)$, with $R_V = 3.1$ (Cardelli et al. 1989). Col. (3): Our photometry of *Spitzer*'s IRAC, publicly available, archival data (§3). Channel 1 = 3.6 μm; channel 2 = 4.5 μm; channel 3 = 5.8 μm; channel 4 = 8.0 μm. Col. (4): Interpolated flux densities for the rest-frame K-band (§3). The data used were obtained from these references. Col. (5): $M_\star$ derived (§4) from the rest-frame K-band flux densities listed in column (4), with $M_\star/L_{K_{\rm rest}} = 0.4\,M_\odot/L_\odot$. Col. (6): Interpolated flux densities for the rest-frame UV continuum (§3). The data used were obtained from these references. Col. (7): Unobscured SFRs derived (§5) from the rest-frame UV continuum flux densities listed in column (6).

[a] Flux density values are taken from Castro Cerón et al. (2006); we refine their error estimates.

[b] Our photometry of 2MASS XSC Final Release (Two Micron All Sky Survey Extended Source Catalog; released 25 March 2003; Jarrett et al. 2000; `http://www.ipac.caltech.edu/2mass/`), NIR ($K_{\rm S}$-band) archival data for galaxy ESO 184-G082 ($f_{21\,739\,\text{Å}} = 6\,510\,\mu$Jy ± 406 μJy).

[c] Our photometry of *GALEX* (Galaxy Evolution Explorer; Martin et al. 2003, 2005; `http://galex.stsci.edu/`), UV archival data for the host galaxies of GRBs 980425 ($f_{2\,267\,\text{Å}} = 1\,592\,\mu$Jy ± 162 μJy) and 060505 ($f_{2\,267\,\text{Å}} = 72\,\mu$Jy ± 10 μJy).

[d] K-band is the closest passband, blueward of IRAC, for which this host has data available in the literature. It is a poorly constrained upper limit. We make use of it nevertheless, for methodological consistency (see §3). But we note that in this particular case, given the low redshift of the host, a much closer representation of reality is provided by the lower limit $M_\star = 6.4 \times 10^7\,M_\odot$ (extrapolated from J-band and H-band data). This value is fully consistent with those cited by Thöne et al. (2007) and references therein.

[e] X-ray flash.

[f] Because of the low Galactic latitude ($b = -4.6°$) of this host we correct for dust-extinction overestimates. Following the recommendation by Dutra et al. (2003) we scale the Schlegel et al. (1998) reddening value multiplying by 0.75 and adopt $E_{\rm MW}(B-V) = 0.78$ mag. The UV flux density error (column 6) contains the additional 25% uncertainty estimated by Margutti et al. (2007).

[g] Redshift of the 2dFGRS Public Database (Two Degree Field Galaxy Redshift Survey; `http://magnum.anu.edu.au/∼TDFgg/`), archival data for galaxy TGS173Z112.

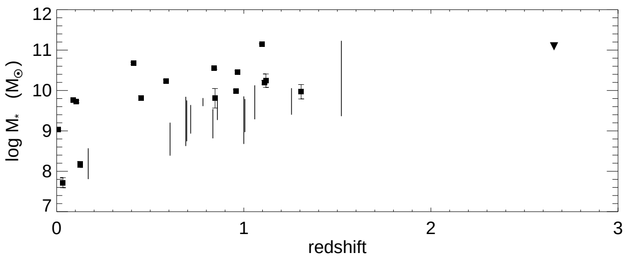

FIG. 2.— Total stellar mass ($M_\star$) as a function of redshift for our 30 GRB host galaxy sample. *Squares*: Detections. *Vertical bars*: Distribution of the non-detection measurements of $M_\star$. The lower limits of these bars were calculated by extrapolating a flat spectrum ($f_\nu \propto \nu^0$) from the NIR/optical data (references in Table 1, column 4).

of a linear interpolation in log space. We interpolate between the IRAC channel and the closest passband, blueward of IRAC, for which data are available in the literature. In a few cases the IRAC waveband corresponds to a rest-frame wavelength shorter than K-band, thus we extrapolate. The rest-frame K-band flux densities are shown in Table 1, column (4), along with the appropriate references. In the same fashion we compute, for each host, the rest-frame UV continuum (2 800 Å; Kennicutt 1998) flux density. We either interpolate between the two closest passbands, with data available from the literature, that bracket the rest-frame UV continuum or, when all available data falls redward of 2 800 Å, we extrapolate. These results are shown in Table 1, column (6). In those cases for which only an upper limit to $M_\star$ can be computed we also estimate a conservative lower limit. We do so by extrapolating a flat spectrum ($f_\nu \propto \nu^0$) from the reddest NIR/optical detection available (references in Table 1, column 4). These lower limits are presented as solid bars in Figures 2, 3, and 4.

All flux densities listed in Table 1 are corrected for foreground Galactic dust-extinction (see Table 1 notes for the details). Conversion of the magnitudes obtained from the literature to flux densities is based on Fukugita et al. (1995) for the optical passbands and on Tokunaga & Vacca (2005) and Cohen et al. (2003) for the NIR passbands. The error introduced by the assumption of these photometric systems never dominates over the photometric uncertainties themselves and was safely neglected.

4. TOTAL STELLAR MASSES

We infer $M_\star$ for our sample from rest-frame K-band flux densities. The light emitted by a galaxy in the K-band (e.g., the MIR photometry analyzed in this work) is closely related to its $M_\star$ and thus it is a reliable estimator (Glazebrook et al. 2004). It has little sensitivity to dust since the majority of a galaxy's stellar population has moved away from the birth clouds, and because the NIR bands are virtually unaffected by dust extinction. Such derivation of $M_\star$ is more physically meaningful than an optical/UV luminosity; it effectively integrates over the accumulated $M_\star$ and merger history and can only increase with time, in contrast, for instance, to UV light.

In order to obtain $M_\star$ we apply:

$$M_\star(M_\odot) = 3.74 \times 10^{-11} \times \frac{4\pi D_L^2 f_\nu(\nu_{\rm obs})}{1+z} \times \frac{M_\star}{L_{K_{\rm rest}}}, \quad (1)$$

where for any given object, D_L is its luminosity distance in cm; $f_\nu(\nu_{\rm obs})$ is its flux density at the observed wavelength in μJy; observations should have been made at wavelengths $1.9\,\mu$m $< \nu_{\rm obs}/(1+z) <$ $2.5\,\mu$m (e.g., this work); and the factor of 3.74×10^{-11} converts the first term in equation 1 to units of solar luminosity density. The second term in equation 1, $M_\star/L_{K_{\rm rest}}$, also in solar units, must be estimated for each object.

$M_\star/L_{K_{\rm rest}}$ depends to some extent on the composition of the stellar population (Portinari et al. 2004) or, according to Labbé et al. (2005) who used Bruzual & Charlot (2003) with a Salpeter IMF (Salpeter 1955), on the rest frame $U-V$ colour, age, and $M_\star$. GRB host galaxies are blue, young, and faint (e.g. Le Floc'h et al. 2003; Berger et al. 2003; Christensen et al. 2004). In Castro Cerón et al. (2006) $M_\star/L_{K_{\rm rest}}$ was assumed to be $\sim$0.1 $M_\odot/L_\odot$ to obtain robust lower limits. For this work we compute $M_\star/L_{K_{\rm rest}}$ for GRBs 980703, 000210, and 000418 with the rest-frame K-band flux densities from Table 1, column (4), and $M_\star$ values derived from stellar population model SED fitting (Michałowski et al. 2008), and obtain the following results: 0.29 $M_\odot/L_\odot$ for GRB 980703, 0.63 $M_\odot/L_\odot$ for GRB 000210, and 0.43 $M_\odot/L_\odot$ for GRB 000418. These results yield a mean $M_\star/L_{K_{\rm rest}}$ = 0.45 $M_\odot/L_\odot$, fully consistent with the average value in Courty et al. (2007), and among the lowest ratios presented by Portinari et al. (2004) for a Salpeter IMF (Salpeter 1955). It is sensible to calculate an average $M_\star/L_{K_{\rm rest}}$ because this ratio is nearly constant, with little dependence on the previous SF history. In fact, $M_\star/L_{K_{\rm rest}}$ varies only by a factor of two between extremely young and extremely old galaxy stellar populations (Glazebrook et al. 2004). So we estimate a conservative 0.4 $M_\odot/L_\odot$ in the calculations of $M_\star$ for our host sample. Table 1, column (5) summarises our $M_\star$ estimates. Errors quoted are statistical. We present a histogram of the distribution of $M_\star$ in log space for our GRB host sample in Figure 1. Van der Wel et al. (2006) examined redshift dependent systematics in determining $M_\star$ from broad band SEDs. They found no significant bias for Bruzual & Charlot (2003) models with a Salpeter IMF (Salpeter 1955).

For comparison we plot Figure 2 from the Savaglio et al. (2007) preliminary analysis in the background of our histogram. The two samples have a 25 object overlap. Our results clearly suggest more massive hosts, about half an order of magnitude higher (median $M_\star$ = $10^{9.7}\,M_\odot$ in ours vs. median $M_\star = 10^{9.3}\,M_\odot$ in Savaglio et al. 2007; both distributions have a 1σ dispersion of 0.8 dex, and in both cases the average has the same value as the median). Savaglio et al. (2006, 2007) fit the optical-NIR SEDs of their host galaxy sample together with a complex set of SF histories. We can reproduce the median and average $M_\star$ in Savaglio et al. (2007) with our dataset by applying $M_\star/L_{K_{\rm rest}} = 0.2\,M_\odot/L_\odot$ (The Kolmogorov-Smirnov test indicates to a high probability, $p \sim 0.99$ likely because of the 25 object overlap, that our data set and that of Savaglio et al. 2007 come from a population with the same specific disctribution). Their methodology therefore seems to contain an effective $M_\star/L_{K_{\rm rest}}$ ratio around 0.2. An adjustment by a factor of $\sim$2 to this ratio thus explains the discrepancies in $M_\star$ between our work and that of Savaglio et al. (2007). We note that such an adjustment is within the spread of our calculated values (cf., 0.29 $M_\odot/L_\odot$, 0.43 $M_\odot/L_\odot$, and $0.63\,M_\odot/L_\odot$). The fact that we find larger $M_\star$ may also be indicative of underestimated dust extinction in Savaglio et al. (2007) (see §6).

Our $M_\star$ are always lower than those of the normal $0.4 < z < 2$ galaxies from the Gemini Deep Deep Survey (GDDS; Abraham et al. 2004; Savaglio et al. 2006). The GDDS is a deep optical-NIR ($K < 20.6$) survey complete, for the already mentioned redshift range, down to $M_\star = 10^{10.8}\,M_\odot$ for all galaxies and to $M_\star = 10^{10.1}\,M_\odot$ for star-forming galaxies. In our host sample at least 70% of the galaxies have $M_\star < 10^{10.1}\,M_\odot$. This comparison clearly highlights the efficiency of the GRB selection technique, against that of traditional high-redshift surveys, to pick low-$M_\star$ galaxies at high redshifts.

We plot $M_\star$ as a function of the redshifts for our 30 GRB host galaxy sample in Figure 2 and find no intrinsic correlation between the two variables. The scatter of $M_\star$ is rather uniform across most of the redshift distribution. Hosts with very low $M_\star$ are only found at low redshift. For instance, the four GRB hosts (i.e., 060218, 060614, 030329, and 980425) with the lowest $M_\star$ ($< 10^9\,M_\odot$) have some of the lowest redshift values in our sample. Very low-$M_\star$, high-redshift hosts would have been excluded since most of our largely pre-*Swift* redshifts were measured in emission, what selects preferentially bright host galaxies. Because the redshift is a requirement for inclusion in our sample we are effectively biased against faint systems. This situation has now been corrected in the *Swift* era when most redshifts are secured via afterglow absorption spectroscopy. The upper limits in the vertical bars of Figure 2 (i.e., the distribution for each non-detection measurement of $M_\star$) mark the sensitivity-limited curve for $M_\star$. Conversely, the absence of high-$M_\star$, low-redshift hosts suggests that such GRB host galaxies are rare.

5. STAR-FORMATION RATES

We compute the unobscured SFR for each host by means of their UV continuum luminosity. We convert flux densities into luminosity densities using $L_\nu(\nu_{\rm rest}) = 4\pi D_L^2 f_\nu(\nu_{\rm observed})/(1+z)$ (Hogg et al. 2002). Then we can calculate the unobscured SFRs by applying ${\rm SFR}(M_\odot\,{\rm yr}^{-1}) = 1.4\times10^{-28} L_{\rm UV}\,({\rm erg\,s^{-1}})$ to the rest-frame $\lambda = 2\,800$ Å flux densities (Kennicutt 1998). The results are summarised in Table 1, column (7). Errors quoted are statistical. In addition there are systematic errors of order 30% (Kennicutt 1998).

The specific SFR $\phi \equiv {\rm SFR}/M_\star$ gives an indication of how intensely star-forming a galaxy is. In Figure 3 we plot ϕ versus $M_\star$ for our GRB host sample. The absence of hosts in the lower-left corner is explained as a combination of selection effects and low-number statistics. A host galaxy in this region of the plot has both low $M_\star$ and low SFR, making its detection difficult unless at very low redshifts. As the sampled comoving volume becomes smaller because of the lower redshift required to make a detection, the chance of finding a host decreases accordingly. Given the size of our sample, it is reasonable to expect no detections in this area of the plot. The four GRB host galaxies with the lowest $M_\star$ (GRBs 060218, 060614, 030329, and 980425) are all at very low redshifts and UV bright. We also note that our sample may be biased against low-SFR hosts, since many redshifts have been measured from emission lines. On the other hand,

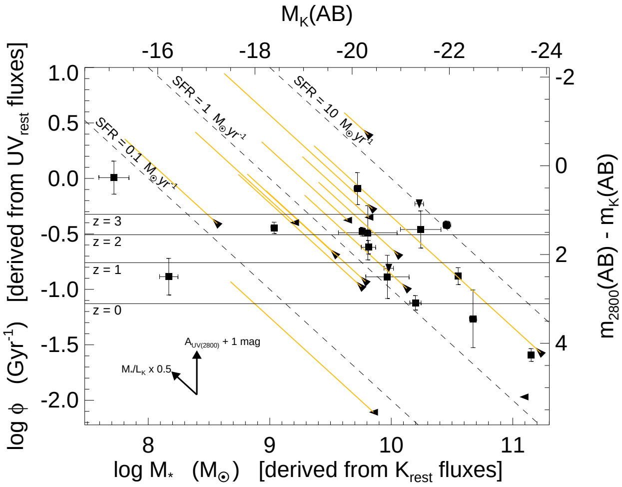

FIG. 3.— Specific SFR (ϕ) as a function of total stellar mass ($M_\star$) for our 30 GRB host galaxy sample. Squares are detections and triangles mark upper limits for either $M_\star$, SFR, or both. *Yellow diagonals*: Equivalent to the vertical bars in Figure 2. Each yellow diagonal could be displaced vertically by the size of the corresponding SFR error bar (Table 1, column 7). *Dashed diagonals*: Constant SFRs of 100, 10, 1, 0.1, and 0.01 $M_\odot\,{\rm yr}^{-1}$ respectively. *Black arrows*: Magnitudes of the displacements due to extinction by dust in the UV (e.g., 1 mag; vertical) and changes in our estimation of $M_\star/L_{K_{\rm rest}} \sim 0.4\,M_\odot/L_\odot$ (e.g., a factor of 50%; diagonal). *Right axis*: Color term equivalent to ϕ. *Top axis*: Absolute K-band AB magnitude, equivalent to $M_\star$. The top/right axes represent our GRB host sample in color-magnitude space, effectively equivalent to ϕ vs. $M_\star$.

the non-detection of any GRB host in the upper-right corner of Figure 3 should not be due to a selection effect. Such hosts either do not exist or their afterglows were obscured by dust, thus preventing their localization. The sample at hand offers some indication as to the former posibility. Our two host galaxies with the highest $M_\star$ (GRBs 030328 and 980613) would require a dust extinction of $A_V \sim 5$ mag to show there. Yet such dust-extinction levels can be ruled out by the constraints on the SFR from the IR and the radio (see §6 below).

To exemplify how the estimation of $M_\star/L_{K_{\rm rest}} \sim 0.4\,M_\odot/L_\odot$ affects the location of our hosts in the plot we suppose a 50% uncertainty. We repeat the exercise for an UV-continuum dust-extinction of 1 magnitude. The corresponding displacements are plotted in Figures 3 and 4 with black arrows. The magnitude of these displacements is limited enough not to affect our analysis.

6. ANALYSIS AND DISCUSSION

We find the GRB host galaxies in our current sample possess a wide range of properties; with $10^7\,M_\odot < M_\star < 10^{11}\,M_\odot$; and $10^{-2}\,M_\odot\,{\rm yr}^{-1} <$ unobscured SFR $< 10\,M_\odot\,{\rm yr}^{-1}$. Yet this diversity points towards low $M_\star$, star-forming systems.

Part of our host sample is extinguished by dust. GRB hosts 970828, 980613, and 990705 (Le Floc'h et al. 2006, 24 μm flux densities; Castro Cerón et al. 2006, SED fitting), as well as 980703, 000210, and 000418 (Castro Cerón et al. 2006, SED fitting for GRB 980307; Michałowski et al. 2008, SED modelling), have highly obscured SFRs. Additionally several authors argued for dust extinction in the host of GRB 031203 (e.g., Prochaska et al. 2004; Margutti et al. 2007). Applying the recipe in Castro Cerón et al. (2006) to this

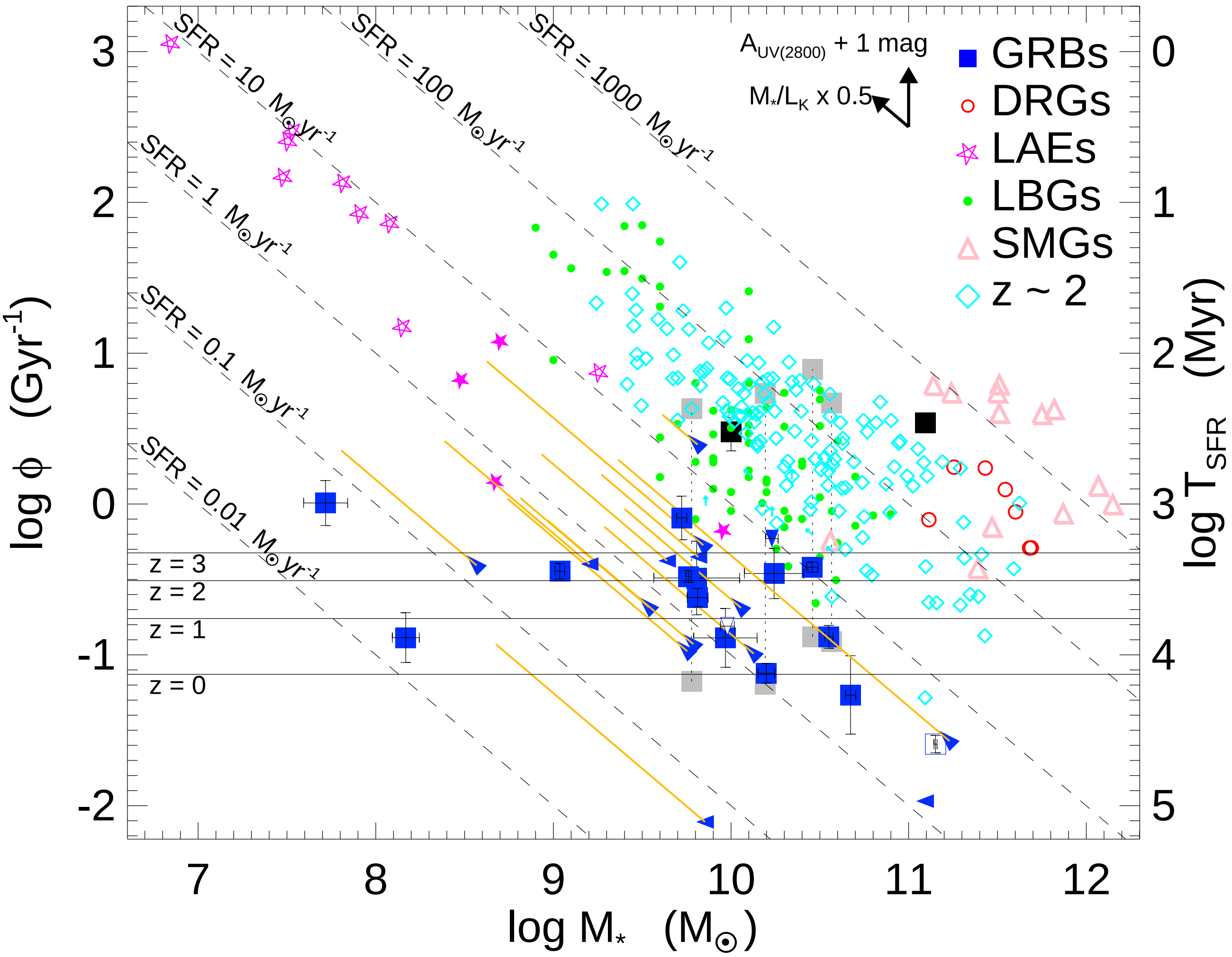

FIG. 4.— Specific SFR (ϕ) as a function of total stellar mass ($M_\star$) for our GRB host galaxy sample and other representative types of galaxies (for a similar plot see Erb et al. 2006; Castro Cerón et al. 2006). *Blue squares and triangles*: Host galaxy sample from this work, with unobscured SFRs derived from the rest-frame UV continuum. Triangles mark upper limits for either $M_\star$, SFR, or both. The open blue triangle and square mark the hosts of GRBs 970828 and 980613 respectively (see §6). *Black squares*: SFR values constrained with a best fit SED model (Castro Cerón et al. 2006). *Grey squares*: Highest/lowest SFR values for those hosts for which a best fit model could not be established (Castro Cerón et al. 2006). Both the black squares and the grey squares have been shifted here correspondingly to compensate for the difference in $M_\star/L_{K_{\rm rest}}$ methodology (i.e., from a lower limit value of $0.1\,M_\odot/L_\odot$ in Castro Cerón et al. 2006 to a best estimated value of $0.4\,M_\odot/L_\odot$ in this work). Yellow diagonals, dashed diagonals, and black arrows are as in Figure 2. *Right axis*: SFR timescale ($T_{\rm SFR} = M_\star/{\rm SFR}$), the inverse of ϕ. On this scale the solid horizontal lines represent the age of the universe for the marked redshift. The distribution of our sample in parameter space suggests that GRBs trace galaxies that are not selected with other techniques. *Data points*: GRBs from this work and Castro Cerón et al. (2006). DRGs from van Dokkum et al. (2004). LAEs from Gawiser et al. (2006), Nilsson et al. (2007), and Lai et al. (2008) (filled stars; average values of the LAE population as a whole, obtained from stacked photometry); N. Pirzkal, S. Malhotra, J. E. Rhoads, & C. Xu (2007, priv. comm.; empty stars; see Pirzkal et al. (2007) for the average values and a description of these sources). Spectroscopically confirmed LBGs from Shapley et al. (2001) and Barmby et al. (2004). SMGs from Borys et al. (2005, $M_\star$) and Chapman et al. (2005, SFR), where we have considered $L_{\rm BOL} \simeq L_{\rm farIR}$, then applied the Kennicutt (1998) calibration. $z \sim 2$ from Erb et al. (2003) and Reddy et al. (2006).

host galaxy's MIR photometry ($f_{3.6\,\mu{\rm m}} = 216\,\mu$Jy $\pm$ $3\,\mu$Jy; $f_{5.8\,\mu{\rm m}} = 390\,\mu$Jy $\pm$ $16\,\mu$Jy; $f_{24\,\mu{\rm m}} = 13\,103\,\mu$Jy $\pm$ $41\,\mu$Jy; flux densities corrected for foreground Galactic dust-extinction, Lutz 1999; Dutra et al. 2003) we obtain a ${\rm SFR}_{L_{8-1000}} = 13\,M_\odot\,{\rm yr}^{-1}$. That brings the total number of extinguished hosts to at least 7 out of 30, and allows us to crudely estimate that >25% of the sample in this work suffer significant dust extinction ($A_V \gtrsim 1$ mag). Neither our host galaxy sample, nor those others cited in this work, are bias-free. The searches for the GRBs in such samples have been carried out mostly following the localization of an optical afterglow, implicitly biasing the sample against dust-extincted systems. Such potential bias strengthens our statement on dust extinction in GRB host galaxies. Parenthetically, we note that GRBs 970828, 980613, 980703, and 990705 make up two-thirds of a redshift-z~1-selected, small subsample (Castro Cerón et al. 2006; Le Floc'h et al. 2006). They hint at the possibility that even a higher fraction of hosts are affected by dust extinction, though with the caveat of low-number statistics.

Castro Cerón et al. (2006) plotted ϕ versus $M_\star$ for six GRB hosts and samples of five other representative types of galaxies: distant red galaxies (DRGs), Lyα emitters (LAEs), Lyman break galaxies (LBGs), submillimeter galaxies (SMGs) and an ensemble of optically-selected, z

~ 2 galaxies from the Great Observatories Origins Deep Survey-North field. In Figure 4 we plot, with blue symbols, our 30 host sample using a revised $M_\star/L_{K_\mathrm{rest}}$ ratio, along with the samples in Castro Cerón et al. (2006). In our ϕ versus $M_\star$ plot (i.e., Figure 4; we use $\mathrm{SFR_{UV}}$) the obscuration of SF by dust pulls the GRB data points down along a vertical line. One way to reconcile the ϕ values of host galaxies in Castro Cerón et al. (2006) and this work is to invoke extinction by dust of the order of $A_V \sim$ 1–3 mag (see below). The conversion from A_UV to A_V follows Cardelli et al. (1989).

A primary scientific goal in the quantification of galactic evolution is the derivation of the SF histories, as described by the temporal evolution of the star-formation rate, SFR(t). Castro Cerón et al. (2006) noted that their sample had $T_\mathrm{SFR} < t_\mathrm{universe}$, allowing for a history of constant SF, with a robust lower limit in $M_\star$ ($M_\star/L_{K_\mathrm{rest}} \sim 0.1\,M_\odot/L_\odot$). For the sample we present in this work, where we adopt $M_\star/L_{K_\mathrm{rest}} \sim 0.4\,M_\odot/L_\odot$, clearly few GRB host galaxies are not allowed to have a history of constant SF (i.e., young stars dominating the stellar populations of old galaxies; see the right ordinate axis in Figure 4). Either a starburst episode was present in the past, or a higher recent SFR is required. The latter possibility is consistent with a fraction of GRB hosts having SF obscured by dust. The hosts of GRBs 970828 and 980613 (open blue symbols in Figure 4) are good examples because, under the assumption of constant SF, major dust-extinction must be invoked to account for the age differences. ϕ_UV estimates result in $T_\mathrm{SFR} \sim 6$ Gyr for GRB 970828 and $T_\mathrm{SFR} \sim 32$ Gyr for GRB 980613, while ϕ_{L_K} estimates (see Castro Cerón et al. 2006) result in $T_\mathrm{SFR} \sim 300$ Myr for both of them. The discrepancies in T_SFR imply a dust extinction of the order of $A_V \sim 1.6$ mag for GRB 970828 and $A_V \sim 2.5$ mag for GRB 980613. These discrepancies are consistent with the radio-constrained SFR upper limits ($\sim$100 $M_\odot\,\mathrm{yr}^{-1}$ for GRB 970828, and $\sim$500 $M_\odot\,\mathrm{yr}^{-1}$ for GRB 980613) derived by applying the Yun & Carilli (2002) methodology to the deepest radio upper limits reported by Frail et al. (2003).

A dilution effect is present in our MIR photometry. Hosts in our current sample are not spatially resolved in the Spitzer imagery (in the case of GRB 980425 we utilize the total flux of the galaxy for consistency with the rest of the sample). To estimate their $M_\star$ we measure the total K-band light. L_K traces the accumulation of $M_\star$ (Glazebrook et al. 2004) while, most commonly, the SF is ongoing in only a small part of the host galaxy. So we do not normalize our sample's unobscured SFRs by the total stellar mass of the star-forming region(s), rather by $M_\star$, which results in lower ϕ values. This dilution effect pulls the GRB data points in a ϕ versus $M_\star$ plot down along the diagonal (dashed) lines marking constant SFRs.

Extinction by dust, coupled with the dilution effect, could be responsible for the apparent envelope that can be visualized in Figures 3 and 4: a flat plateau with no objects above a certain ϕ value ($\sim$2.5 Gyr^{-1}), and that starts to curve down beyond a particular $M_\star$ ($10^{10}\,M_\odot$). Correcting for dilution and, chiefly, for dust extinction would yield a new plot where our host sample would align consistently with the results/upper limits of Castro Cerón et al. (2006), and provide support to the claim that GRB host galaxies are small and have some of the highest ϕ values.

We conclude by putting forward a simple idea for GRB hosts based on the data analyzed here. As a working hypothesis we suggest that, while low $M_\star$ hosts might contain no dust (i.e., host galaxies with a low $M_\star$ and a low SFR are rare; see §5), progressing upwards in the $M_\star$ distribution of host galaxies will yield significant dust extinction, as well as the already mentioned dilution effect (i.e., the apparent envelope described above for Figures 3 and 4). Our suggestion is consistent with the theoretical predictions presented in Lapi et al. (2008). They further predict that GRB host galaxies trace the faint end of the luminosity function of LBGs and LAEs. Future work (i.e., Herschel observations) on a complete host sample will allow us to test this by quantifying dust extinction and the dilution effect.

The nature of GRBs 060505 and 060614 is strongly debated as no supernova was associated with these long-duration GRBs to deep limits (Fynbo et al. 2006; Gehrels et al. 2006; Della Valle et al. 2006a; Gal-Yam et al. 2006). GRB 060505 falls within the distribution of other long-duration GRB hosts in our sample, whereas GRB 060614 seems to be an outlier. Though this may indirectly suggest that the progenitor of GRB 060614 is different from other typical long-duration GRBs, we note that its SFR is in range with that of the bulk of the sample; and as for $M_\star$, its properties are not very different from some of our other low-redshift host galaxies (e.g., GRBs 060218, 030329, and 980425).

We thank Árdís Elíasdóttir, Peter Laursen, Bo Milvang-Jensen, and Paul M. Vreeswijk for insightful comments. The Dark Cosmology Centre is funded by the Danish National Research Foundation. J. M. C. C. gratefully acknowledges support from the Instrumentcenter for Dansk Astrofysik and the Niels Bohr Institutet's International PhD School of Excellence. J. G. was funded in part by Spain's AyA 2.004-01.515 and ESP 2.005-07.714-C03-03 grants. The authors acknowledge the data analysis facilities provided by the Starlink Project which is run by CCLRC on behalf of PPARC. This research has made use of: the NASA's Astrophysics Data System; the GHostS database (`http://www.grbhosts.org/`), which is partly funded by Spitzer/NASA grant RSA Agreement No. 1287913; the Gamma-Ray Burst Afterglows site (`http://www.mpe.mpg.de/~jcg/grb.html`), which is maintained by Jochen Greiner; IRAF, distributed by the National Optical Astronomy Observatories, which are operated by the Association of Universities for Research in Astronomy, Inc., under cooperative agreement with the National Science Foundation; the NASA/IPAC Extragalactic Database (NED) which is operated by the Jet Propulsion Laboratory, California Institute of Technology, under contract with the National Aeronautics and Space Administration; and SAOImage DS9, developed by Smithsonian Astrophysical Observatory. *GALEX* (*Galaxy Evolution Explorer*) is a NASA Small Explorer, launched in April 2003. We gratefully acknowledge NASA's support for construction, operation, and science analysis for the *GALEX* mission, developed in cooperation with the Centre National d'Etudes Spatiales of France and the Korean Ministry of Science and Technology.

Facilities: Spitzer (IRAC) and *GALEX* (NUV).

REFERENCES

Abraham, R. G., et al. 2004, AJ, 127, 2455
Barmby, P., et al. 2004, ApJS, 154, 97
Barth, A. J., et al. 2003, ApJ, 584, L47
Berger, E., Cowie, L. L., Kulkarni, S. R., Frail, D. A., Aussel, H., & Barger, A. J. 2003, ApJ, 588, 99
Bertin, E., & Arnouts, S. 1996, A&AS, 117, 393
Bloom, J. S., Berger, E., Kulkarni, S. R., Djorgovski, S. G., & Frail, D. A. 2003, AJ, 125, 999
Bloom, J. S., Djorgovski, S. G., & Kulkarni, S. R. 2001, ApJ, 554, 678
Bloom, J. S., Djorgovski, S. G., Kulkarni, S. R., & Frail, D. A. 1998, ApJ, 507, L25
Bloom, J. S., Kulkarni, S. R., & Djorgovski, S. G. 2002, AJ, 123, 1111
Bloom, J. S., et al. 1999, Nature, 401, 453
Borys, C., Smail, I., Chapman, S. C., Blain, A. W., Alexander, D. M., & Ivison, R. J. 2005, ApJ, 635, 853
Bruzual, G., & Charlot, S. 2003, MNRAS, 344, 1000
Campana, S., et al. 2006, Nature, 442, 1008
Cardelli, J. A., Clayton, G. C., & Mathis, J. S. 1989, ApJ, 345, 245
Castro Cerón, J. M., Michałowski, M. J., Hjorth, J., Watson, D., Fynbo, J. P. U., & Gorosabel, J. 2006, ApJ, 653, L85
Chapman, S. C., Blain, A. W., Smail, I., & Ivison, R. J. 2005, ApJ, 622, 772
Chary, R., Becklin, E. E., & Armus, L. 2002, ApJ, 566, 229
Christensen, L., Hjorth, J., & Gorosabel, J. 2004, A&A, 425, 913
———. 2005, ApJ, 631, L29
Cobb, B. E., Bailyn, C. D., van Dokkum, P. G., & Natarajan, P. 2006, ApJ, 651, L85
Cohen, M., Wheaton, Wm. A., & Megeath, S. T. 2003, AJ, 126, 1090
Colless, M., et al. 2001, MNRAS, 328, 1039
Courty, S., Björnsson, G., & Gudmundsson, E. H. 2007, MNRAS, 376, 1375
Della Valle, M., et al. 2006a, Nature, 444, 1050
———. 2006b, ApJ, 642, L103
Djorgovski, S. G., Bloom, J. S., & Kulkarni, S. R. 2003, ApJ, 591, L13
Djorgovski, S. G., Frail, D. A., Kulkarni, S. R., Bloom, J. S., Odewahn, S. C., & Diercks, A. 2001, ApJ, 562, 654
Djorgovski, S. G., Kulkarni, S. R., Bloom, J. S., Goodrich, R., Frail, D. A., Piro, L., & Palazzi, P. 1998, ApJ, 508, L17
Dutra, C. M., Ahumada, A. V., Clariá, J. J., Bica, E., & Barbuy, B. 2003, A&A, 408, 287
Erb, D. K., Shapley, A. E., Steidel, C. C., Pettini, M., Adelberger, K. L., Hunt, M. P., Moorwood, A. F. M., & Cuby, J. G. 2003, ApJ, 591, 101
Erb, D. K., Steidel, C. C., Shapley, A. E., Pettini, M., Reddy, N. A., & Adelberger, K. L. 2006, ApJ, 647, 128
Fazio, G., et al. 2004, ApJS, 154, 10
Foley, R. J., Chen, H.-W., Bloom, J., & Prochaska, J. X. 2005, GCN Circular, 3483
Frail, D. A., Kulkarni, S. R., Berger, E., & Wieringa, M. H. 2003, AJ, 125, 2299
Fruchter, A. S., et al. 1999, ApJ, 519, L13
———. 2006, Nature, 441, 463
Fukugita, M., Shimasaku, K., & Ichikawa, T. 1995, PASP, 107, 945
Fynbo, J. P. U., Prochaska, J. X., Sommer-Larsen, J., Dessauges-Zavadsky, M., & Møller, P. 2008, ApJ, submitted (arXiv:0801.3273v1 [astro-ph])
Fynbo, J. P. U., et al. 2006, Nature, 444, 1047
Galama, T. J., et al. 1998, Nature, 395, 670
Gal-Yam, A., et al. 2006, Nature, 444, 1053
Gawiser, E., et al. 2006, ApJ, 642, L13
Gehrels, N., et al. 2004, ApJ, 611, 1005
———. 2006, Nature, 444, 1044
Glazebrook, K., et al. 2004, Nature, 430, 181
Gorosabel, J., Jelínek, M., de Ugarte Postigo, A., Guziy, S., & Castro-Tirado, A. J. 2005a, Il Nuovo Cimento C, 28, 677
Gorosabel, J., et al. 2003a, A&A, 400, 127
———. 2003b, A&A, 409, 123
———. 2005b, A&A, 444, 711
Heise, J. 2003, in AIP Conf. Proc. 662, Gamma-Ray Burst and Afterglow Astronomy 2001, ed. G. R. Ricker, & R. K. Vanderspek (Melville: AIP), 229
Hjorth, J., et al. 2003, Nature, 423, 847
Hogg, D. W., Baldry, I. K., Blanton, M. R., & Eisenstein D. J. 2002, e-print (arXiv:astro-ph/0210394v1)
Jakobsson, P., et al. 2004, A&A, 427, 785
———. 2005a, MNRAS, 362, 245
———. 2005b, ApJ, 629, 45
Jarrett, T. H., Chester, T., Cutri, R., Schneider, S., Skrutskie, M., & Huchra, J. P. 2000, AJ, 119, 2498
Kennicutt, Jr., R. C. 1998, ARA&A, 36, 189
Kocevski, D., et al. 2007, ApJ, 663, 1180
Labbé, I., et al. 2005, ApJ, 624, L81
Lai, K., et al. 2008, ApJ, 674, 70
Lapi, A., Kawakatu, N., Bosnjak, Z., Celotti, A., Bressan, A., Granato, G. L., & Danese, L. 2008, MNRAS, in press (arXiv:0802.0787v1 [astro-ph])
Le Floc'h, E., Charmandaris, V., Forrest, W. J., Mirabel, I. F., Armus, L., & Devost, D. 2006, ApJ, 642, 636
Le Floc'h, E., et al. 2002, ApJ, 581, L81
———. 2003, A&A, 400, 499
Lutz, D. 1999, in ESA SP-427, The Universe as Seen by ISO, ed. P. Cox & M. F. Kessler (Noordwijk: ESA), 623
Maiorano, E., et al. 2006, A&A, 455, 423
Malesani, D., et al. 2004, ApJ, 609, L5
Mangano, V., et al. 2007, A&A, 470, 105
Margutti, R., et al. 2007, A&A, 474, 815
Martin, D. C., et al. 2003, in Proc. SPIE 4854, Future EUV/UV and Visible Space Astrophysics Missions and Instrumentation, ed. J. C. Blades, &, O. H. W. Siegmund (Bellingham: SPIE), 336
———. 2005, ApJ, 619, L1
Masetti, N., et al. 2005, A&A, 438, 841
Michałowski, M. J., Hjorth, J., Castro Cerón, J. M., & Watson, D. 2008, ApJ, 672, 817
Nilsson, K. K., et al. 2007, A&A, 471, 71
Pellizza, L. J., et al. 2006, A&A, 459, L5
Pian, E., et al. 2006, Nature, 442, 1011
Piro, L., et al. 2002, ApJ, 577, 680
Pirzkal, N., Malhotra, S., Rhoads, J. E., & Xu, C. 2007, ApJ, 667, 49
Price, P. A., et al. 2002a, ApJ, 573, 85
———. 2002b, ApJ, 571, L121
———. 2003, ApJ, 589, 838
Prochaska, J. X., et al. 2004, ApJ, 611, 200
Portinari, L., Sommer-Larsen, J., & Tantalo, R. 2004, MNRAS, 347, 691
Rau, A., Salvato, M., & Greiner, J. 2005, A&A, 444, 425
Rau, A., et al. 2004, A&A, 427, 815
Reddy, N. A., Steidel, C. C., Fadda, D., Yan, L., Pettini, M., Shapley, A. E., Erb, D. K., & Adelberger, K. L. 2006, ApJ, 644, 792
Rieke, G., et al. 2004, ApJS, 154, 25
Salpeter, E. E. 1955, ApJ, 121, 161
Savaglio, S., Budavári, T., Glazebrook, K., Le Borgne, D., Le Floc'h, E., Chen, H.-W., Greiner, J., & Yoldaş, A. K. 2007, The Messenger, 128, 47
Savaglio, S., Glazebrook, K., & Le Borgne, D. 2006, in AIP Conf. Proc. 836, Gamma-Ray Bursts in the Swift Era, ed. S. S. Holt, N. Gehrels, & J. A. Nousek (Melville: AIP), 540
Schlegel, D. J., Finkbeiner, D. P., & Davis, M. 1998, ApJ, 500, 525
Shapley, A. E., Steidel, C. C., Adelberger, K. L., Dickinson, M., Giavalisco, M., & Pettini, M. 2001, ApJ, 562, 95
Soderberg, A. M., et al. 2006, ApJ, 636, 391
Sollerman, J., et al. 2006, A&A, 454, 503
Stanek, K. Z., et al. 2003, ApJ, 591, L17
Tanvir, N. R., et al. 2004, MNRAS, 352, 1073
Thöne, C. C., Greiner, J., Savaglio, S., & Jehin, E. 2007, ApJ, 671, 628
Thöne, C. C., et al. 2008, ApJ, 677, in press (arXiv:astro-ph/0703407v3)
Tinney, C., et al. 1998, IAU Circ., 6896
Tokunaga, A. T., & Vacca, W. D. 2005, PASP, 117, 421
van der Wel, A., Franx, M., Wuyts, S., van Dokkum, P. G., Huang, J., Rix, H. W., & Illingworth, G. D. 2006, ApJ, 652, 97
van Dokkum, P. G., et al. 2004, ApJ, 611, 703
Vreeswijk, P. M., Møller, P., & Fynbo, J. P. U. 2003, A&A, 447, 145
Vreeswijk, P. M., et al. 1999, ApJ, 523, 171
Wainwright, C., Berger, E., & Penprase, B. E. 2007, ApJ, 657, 367
Werner, M., et al. 2004, ApJS, 154, 1
Wiersema, K., Starling, R. L. C., Rol, E., Vreeswijk, P., & Wijers, R. A. M. J. 2004, GCN Circular, 2800
Yun, M. S., & Carilli, C. L. 2002, ApJ, 568, 88
Zeh, A., Klose, S., & Hartmann, D. H. 2004, ApJ, 609, 952